Los Alamos Environmental Restoration Records Processing Facility

ER Record I.D.# 63082

LOS ALAMOS NATIONAL LABORATORY
ENVIRONMENTAL RESTORATION
Records Processing Facility
ER Records Index Form

ER ID NO. 63082 *Date Received:* 4/30/99 *Processor:* YCA *Page Count:* 129

Privileged: (Y/N) N *Record Category:* P

FileFolder: N/A

Correction: (Y/N) N *Corrected No.* 0 *Corrected By Number:* 0

Administrative Record: (Y/N) Y

Refilmed: (Y/N) N *Old ER ID Number:* 0 *New ER ID Number:* 0

Miscellaneous Comments:

REFERENCES CITED FOR FY99 PERFORMANCE MEASURES, RECORDS PACKAGE #325 SUBMITTAL #12

14040

THIS FORM IS SUBJECT TO CHANGE. CONTACT THE RPF FOR LATEST VERSION. (JUNE 1997)

63082

Los Alamos National Laboratory

UNIVERSITY OF CALIFORNIA

Environmental Restoration

Environmental Science and Waste Technology (E)
Environmental Restoration, MS M992
Los Alamos, New Mexico 87545
505-667-0808/FAX 505-665-4747

Date: September 1, 1999
Refer to: E/ER:99-250

99 SEP -1 PM 4:58

Mr. Ted Taylor
Department of Energy
Los Alamos Area Office, MS A316
Los Alamos, NM 87545

SUBJECT: INTEGRATED MODELING DELIVERABLES IN SUPPORT OF PERFORMANCE MEASURE B.3.2

Performance Measure B.3.2, Integrated Modeling, for Fiscal Year 1998 requires that these elements be delivered to DOE-LAAO by September 1, 1999:

- Letter-report summarizing the parameters and results of Los Alamos Canyon subsurface water flow and contaminant transport, and document
- Documentation of R-well data and modeling integration, specifying modeling input to siting of characterization borehole and decisions regarding which water-bearing zones to monitor
- A memo to support FY00 baseline assumptions and resources, reflecting the integration of modeling results into baseline planning.
- The initial version of Hydrogeologic Atlas for the Pajarito Plateau,

The first three elements are attached to this transmittal letter. The Hydrogeologic Atlas was delivered to DOE-LAAO August 31, 1999, (E/ER:99-248). The Los Alamos Canyon modeling is a brief report. The documentation referred to in the 2nd and 3rd bullet is provided in an internal Laboratory memorandum from Alison Dorries to Karen West (E/ER:99:251)

As always, we are confident that that the documents submitted under this transmittal meet the specifications of the performance measure. We are hopeful that they meet your expectations, and look forward to receiving your comments within 10 days of receipt. If you have any questions or comments please provide them to Alison Dorries at (505) 665-6952 no later than September 16, 1999.

Sincerely,

for Julie A. Canepa, Program Manager
Environmental Restoration

Received by ER-RPF
OCT 0 8 1999

An Equal Opportunity Employer/Operated by the University of California

JC/DH/AD/eim

Enclosure: 1) Los Alamos Canyon Subsurface Water Flow and Contaminant Transport, and Document
2) Documentation of R-Well Data and Modeling Integration
3) Memo to Support FY00 Baseline Assumptions and Resources

Cy (w/enc.):
RPF, Records Package 325, MS M707
ER Catalog # 199900106

Cy (w/o enc.):
D. Armijo, E-PPC, MS J552
T. Baca, E-DO, MS J591
D. Boak, TSA-10, MS M992
M. Buksa, E/ER, MS M992
J. Canepa, E/ER, MS M992
A. Dorries, EES-13, MS M992
B. Martin, E/ER, MS M992
R. Notini, University of California
G. Rael, DOE-AL, MS A906
T. Trujillo, DOE-AL, MS A906
E/ER File, MS M992
Tracker, RM 604, MS M992

Finally, a model was successfully developed to visualize field data in three dimensions, specifically to graphically describe the nature and extent of the volatile-organic compound (VOC) plume at MDA L. The use of data in each modeling activity, specifically, is summarized here.

2.1 Los Alamos Canyon Groundwater Model

The FEHM model that was developed by EES-5 to calculate the flow of water from alluvial systems through the vadose zone and into the regional aquifer utilized the following data:

- PRS data from FIMAD and the ER contaminant database,
- stratigraphic contacts from regional groundwater wells R-9, R-12, R-25, and R-15
- hydrogeologic data from R-9, R-12, R-25, and R-15,
- alluvial well contamination data from FIMAD and ESH-18 and ESH-19,
- streamflow data from CST-7.

Los Alamos canyon results suggest that contaminant migration in the vadose zone may require decades or more to travel time. This information is key to the long-term monitoring strategy for Los Alamos Canyon, which is a planned FY00 activity. Ultimately, the groundwater flow and transport model developed for Los Alamos Canyon will provide a standard, or reference, model that will be used as appropriate for modeling (or scaling) groundwater transport in other canyons and watersheds.

The Los Alamos canyon modeling is detailed in a letter report submitted to the DOE on September 1, 1999.

2.2 North Ancho Canyon Surface Water Model

The SPLASH model is an event-based surface water flow model. Eventually, this process model will be used to support cumulative-risk calculations for multiple sources of soluble contaminants within a watershed. In FY99, the ER Project supported a successful pilot application of SPLAH, focusing on the North Ancho Canyon aggregate. The SPLASH model of North Ancho Canyon was developed using data directly from FIMAD. The FIMAD data included:

- Digital elevation maps,
- Soil distribution maps, and
- Vegetation coverage maps.

In addition, ESH-18 and EES-15 provided precipitation data.

Based on SPLASH modeling of runoff and interflow in the North Ancho canyon area, PRS's that are vulnerable to runoff and interflow can be identified and ranked. This will be important the future CMS activities for that area conducted by the Remedial Actions Focus Area, and in assessing cumulative impacts on watersheds across the Pajarito Plateau. The pilot application of SPLASH to the North Ancho Canyon watershed aggregate is detailed in a report from EES-15 to the Analysis and Assessment Focus Area.

Los Alamos
NATIONAL LABORATORY
Memorandum
Environmental Science and Waste Technology (E)
Environmental Restoration
E/ER

To/MS: Karen West, E/PPC, MS J552
From/MS: Alison Dorries, EES-13, MS M992 for AML
Phone/FAX: 7-0808/5-4747
Symbol: E/ER:99-251
Date: August 31, 1999

SUBJECT: INTEGRATION OF MODELING INTO WORK ELEMENTS IN THE FY00 BASELINE

1.0 Purpose

The purpose of this memorandum is to document how:

- existing corrective-actions data were used to develop computational models of contaminant flow and contaminant transport in FY99, and
- model results were used to support decisions for corrective-action activities in FY99 and FY00.

This report fulfills partial completion of Performance Measure B.3.2, Integrated Modeling, for Fiscal Year 1999, by meeting the requirement for documentation of the integration of deep-well data and modeling, and documentation of input to siting of characterization boreholes and decisions regarding which water-bearing zones to monitor. This document also reports on other accomplishments of FY99, which reflect further integration of modeling, data, and decisions.

Section 2 (below) summarizes data use in models and progress through FY99, and Section 3 summarizes how model results has influenced ER baseline planning decisions.

2.0 Use of Data in Models

There were three activities completed in FY99 that successfully integrated existing field data into mathematical models of water flow and contaminant transport. These were:

- Subsurface groundwater modeling of Los Alamos Canyon, using the FEHM
- Surface water modeling of North Ancho Canyon, using the SPLASH code
- Surface water erosion modeling of the main drainage off of Mesita del Buey (at MDA G) into Pajarito Canyon

The models, data, and results for each of these activities are detailed in final retained by the ER Project.

Three other modeling activities that were initiated but not completed in FY99 (and have therefore not been fully documented yet) are indicative of the successful integration of field data into contaminant fate and transport models. These are:

- Preliminary subsurface groundwater modeling of MDA AB,
- Preliminary subsurface vapor diffusion modeling of MDA L, and
- Preliminary sediment-reach erosion and contaminant transport modeling of Los Alamos Canyon.

2.3 Mesita del Buey Surface-Water Erosion Model

The KINEROS model is a process model that simulates erosion resulting from surface water runoff. This model can be used to integrate the erosion caused by multiple sequential runoff events, storing moisture between events in near-surface soils. Eventually, this model will be used to support decisions regarding corrective actions in the context of their impact on site erodability, and to couple mesa-top and hillside PRSs with canyon reaches to investigate cumulative effects of particulate (sediment-bound) contamination within an aggregate. In addition, this model may be used to couple surface and groundwater models.

The ER Project funded a successful pilot application of the KINEROS in FY99. The model was calibrated using data from the EES-15 surface-process pilot studies funded by the Analysis and Assessment and MDA Focus Areas. The calibrated model was applied at the major drainage from MDA G to Lower Pajarito Canyon. The results of the pilot application of KINEROS are included in a final report from EES-15 to the project.

2.4 MDA AB Groundwater Model

In early FY99, the project was considering implementing Phase 2 RFI sampling at TA-49. The purpose of the Phase 2 sampling was to characterize the hydrogeologic setting and to bound the extent of subsurface contamination. These objectives were to be met by the drilling, coring, and sampling of one or more boreholes around Area 2 of MDA AB. In keeping with the evolving MDA Core Document strategy, preliminary groundwater transport modeling of contaminants in the MDA AB inventory was initiated by EES-5 under the support of the ER Project. The objectives of integration of data and modeling are:

- Development of a 2-D numerical grid and flow model for the Area 2 subsurface, calibrated to in situ moisture data from 3 boreholes and core data from existing boreholes.
- Calculation of expected transport of plutonium, uranium and cesium (from the tracer shot), using the calibrated flow model.
- Interpretation of results of the transport calculations in determining depth of vertical borehole through shaft 2A-0.
- Revision of the flow and transport model as necessary to reflect core and moisture data from borehole through shaft 2A-0.
- Interpretation of results for siting directionally-drilled horizontal borehole(s) to bind contaminant extent, and to preserve the basal surge deposit at the base of Unit 4.

This work will be completed in accordance with the priority-driven schedule and baseline. To date, preliminary flow and transport calculations have been conducted for cesium, uranium, and plutonium.

2.5 MDA L Vapor Diffusion Model

To complete the corrective action process at MDA L, it will be necessary to understand the nature, extent, and environmental fate of the VOC plume beneath MDA L. While the existing groundwater flow and contaminant transport model (FEHM based) of MDA G is sufficient to model the environmental fate of soluble contaminants, at MDA L, it cannot model the environmental fate of volatile contaminants. To develop a full multi-phase transport model for mesa-top MDAs, the

MDA Focus Area supported the development of a vapor-diffusion model for Mesita del Buey. Once completed, the multi-phase subsurface transport model developed for Mesita del Buey will provide the standard framework for modeling or scaling subsurface contaminant fate and transport at other mesa-top MDAs.

The data from MDA L used to develop the model are reported in an attachment to the RFI Report for MDAs G, H, and L, and the conceptual model interpreting the data as a basis for numerical modeling is described in a report prepared by ESH-18 for under support from the ER Project.

2.6 Los Alamos Canyon Sediment-Reach Erosion Model

The SPLASH model (discussed above) is used to simulate water flow at large (i.e., watershed) scales, and will be useful in calculating cumulative risk from soluble contaminants within a watershed. The KINEROS model (also discussed above) is used to simulate surface-water erosion over a relatively small scale (i.e., aggregate or subaggregate), and will be useful in coupling particulate contaminants from mesa-top and hillside PRSs to canyon reaches. A different model is needed to calculate the long-term effects of erosion on a watershed scale, which is needed to calculate cumulative risk from contaminated reaches within watersheds. Such a model is currently under development by EES-1. The model is using data from the ER Project surface investigations that support surface aggregate characterization. These data provide a calibration of the model under development.

2.7 MDA L VOC Plume Visualization

The Laboratory (including the ER Project) has been monitoring the subsurface contaminant plume beneath MDA L at TA-54 since the late 1980s. Sufficient data now exist to demonstrate that the nature and extent of contamination have been characterized, as necessary to complete the RFI for that site in FY99. In addition, the Citizens Advisory Board (CAB) made two inquiries regarding the MDA L VOC plume in FY99. The ER Project developed a three-dimensional model of the MDA L plume to meet the requirements for the RFI, and to provide accessible information to the CAB. A summary of the data used to develop the visualization model is included as an attachment to the RFI Report of MDAs G, H, and L (under development).

3.0 Use of Model Results in planned activities

There were three activities completed in FY99 that successfully integrated model results into the decision-making regarding future activities in the corrective-action process. These were:

- Preliminary regional groundwater results used in siting and/or completing R-6, R-24, and R-26.
- Los Alamos Canyon groundwater results used in developing the tracer test in DP canyon
- Groundwater transport models of MDA G used to support recommendations for CMS at MDAs G, H, and L.

3.1 R-Well Siting and Data Needs

Groundwater transport modeling supported by the ER Project has identified several data needs for the conceptual hydrogeologic model of the Pajarito Plateau. Ultimately, design, implementation, prioritization, and scheduling of data collection activities will be determined by the Groundwater Integration Team (GIT) in accordance

with the Hydrogeologic Work Plan. These issues have been put forth to the GIT for consideration:

- Regional aquifer modeling conducted by EES-5 using FEHM reinforced the need for R-wells (24 and 26) in the vicinity of the Pajarito fault. The lack of field data on hydrologic conditions imposes a large uncertainty on a potentially important flow path in the model.

- Modeling of Los Alamos canyon indicates that R-6 should be drilled on the up-thrown side of the Pajarito fault to evaluate recharge on the western portion of the Laboratory.

- FEHM modeling of transient flow in the regional aquifer system was found to be quite sensitive to porosity data for the sedimentary units. Few data are currently available, and the modeling supports collection of facies-based porosity information.

- Regional aquifer modeling has also shown the need for better vertical resolution of hydraulic head data. In addition, the need for large-scale hydraulic properties was identified. To address this data need, the GIT has planned for multiple screens in future R-wells to make multiple water-level measurements, at various depths, which will be used to construct vertical hydraulic head distributions.

- FEHM modeling also suggests the need for improved groundwater dating to provide for better testing of results and improved model calibration.

The documentation of discussions of modeling results and their interpretation in the context of data needs from the Monitoring Well Installation Program is contained in GIT meeting minutes, which are prepared and retained by ESH-18.

3.2 DP Tracer Test

A tracer test is designed to confirm conceptual model for fate and transport of contaminated alluvial groundwater within the DP/LA canyon aggregate. This alluvial system is considered to be representative of other alluvial systems under investigation by the ER Project, therefore data from this test will support development of a standard alluvial groundwater model. In particular, the tracer test will provide data on water residence time, dispersivity, conductivity, etc., which are necessary parameters for groundwater flow models.

3.3 MDA G, MDA H, and MDA L RFI Recommendations

The draft RFI Report for MDAs G, H, and L completed in FY99 by the ER Project and submitted to DOE-LAAO fully documents the data and information used to model features, events, and processes related to contaminant fate in environmental media. Using the RIP computer code, a systems model was developed to calculate contaminant concentrations in soil, biota, and groundwater over a period of 10,000 years, which were the basis of future risk assessments conducted for the RFI. The

results of the RIP calculations and risk assessments were used to support a recommendation for a streamlined CMS at MDAs G, H, and L.

The RIP model was parameterized using field data from MDA G, and using results of the process models developed for the MDA G performance assessment. The details of the RIP model application and results are reported in Appendix F of the RFI Report for MDAs G, H, and L.

AD/DH/eim

Cy
E/ER, MS M992

Numerical Model of Flow and Transport for Los Alamos Canyon

Bruce A. Robinson, EES-5

Marc Witkowski, EES-5

C. James Elliott, EES-5

Leslie Dale, SIAC

Richard Koch, SAIC

Abstract

In this study we report the results of the development of a flow and transport model for the vadose zone beneath Los Alamos canyon. This model supports the Laboratory's Hydrogeologic Workplan and Environmental Restoration Project's goals by providing a synthesis of the available information on deep subsurface flow for Los Alamos canyon, a site containing several potential contaminant sources and several locations where contaminants have been detected in vadose-zone water samples. The model is developed by first building numerical grids in two and three dimensions that honor the available models for stratigraphy at this site. Hydrologic property data, recharge studies, compilations of known contaminant releases, measurements of water contents in characterization wells, and observations of perched water are all considered. For many of these data, adequate matches to the observations are obtained using base-case hydrologic properties and recharge estimates, but sensitivity analyses indicate that uncertainties in recharge and hydrologic parameter values remain, and these uncertainties influence the model results. A new technique is developed to incorporate perched water scenarios into the model through the use of a permeability reduction factor applied at unit interfaces where barriers to downward flow are suspected. The interface of the Guaje Pumice bed and Puye formation was selected for this feature to explain the presence of perched water at that location. Three-dimensional effects of varying recharge (canyon versus mesa) captured in the three-dimensional model allow water content profiles in wells LADP-3 and LADP-4 to be matched. Finally, a tritium transport model was developed by combining the historic information of tritium concentrations in the shallow alluvial groundwater with the estimates of recharge along the canyon. The model is in qualitative agreement with observations of tritium concentrations in perched water. The model result indicates that most of the tritium introduced since the 1960's has either remained in the vadose zone or has decayed. However, a relatively small amount reaches the regional aquifer. Future concentrations are predicted to decline over the next 50 to 100 years due to further radioactive decay and changes in Laboratory practices resulting in lower input concentrations.

1.0 Introduction and motivation

Los Alamos National Laboratory (LANL, or the Laboratory) has performed research and development in nuclear weapons technologies and other national defense activities for over fifty years, beginning with the Manhattan Project in the 1940's. During this time, Laboratory operations have resulted in accidental or intentional emissions of chemical contaminants into the environment at a variety of sites. Contamination with possible negative impacts to groundwater include radionuclides, chemical solvents, and metals. Today, the Laboratory is responsible for ensuring that none of its past or present contaminant releases pose a threat to human health now or in the future, and to carry out remedial activities to clean up contaminated sites. One of the key elements of that process is potential groundwater contamination, possibly affecting drinking water quality in municipal or private wells.

To confront this potential problem, the Department of Energy (DOE) and the Laboratory have, through the development of the Hydrogeologic Workplan (LANL, 1996) and other Environmental Restoration (ER) Project activities, laid out the priorities for characterization and remediation activities. The ER Project has set priorities for clean-up of areas of known contamination to mitigate future migration of contaminants, while at the same time supporting efforts to characterize and model sites of known or suspected releases. In collaboration with Defense Programs (DP), the Project is also engaged in a program of drilling characterization wells to characterize the vadose zone and regional aquifer and to measure contaminant concentrations in the subsurface.

The present study examines, through a synthesis of available data and the development of numerical models, fluid flow and contaminant transport in the vadose zone beneath Los Alamos canyon. Los Alamos canyon is one of the most complex sites at the Laboratory. A host of Technical Areas have been or are currently located in or adjacent to the canyon, resulting in multiple release locations along the canyon. The subsurface hydrology and transport in the vadose zone is also a challenging activity, given the wide range of recharge rates, the presence of perched water, and the introduction of a host of contaminants of different chemical properties. Because the canyon serves as a collector of a wide range of contaminants, we decided that it was necessary to develop a model at the scale of the canyon, rather than at a smaller scale.

The work reported here focuses on the hydrology beneath Los Alamos canyon, as a first step toward developing a predictive tool that can be used to simulate contaminant migration in the canyon. Since water is the carrier fluid for the contaminants of interest, constructing a realistic flow model that captures the most important hydrologic processes of the vadose zone is an essential first step in the development of a reliable model. Although we primarily restrict attention to flow issues, tritium transport in the vadose zone is also modeled here. Tritium, in the form of tritiated water, is an excellent tracer for groundwater, and hence is included in this modeling study as a constraint on the flow model. Although the work here is restricted to Los Alamos canyon, we anticipate that the methodology and approach applied in this study can be used to develop models at other sites at the Laboratory.

The conceptual model for vadose zone flow and transport at this site is based on the model outlined qualitatively in the Hydrogeologic Workplan (LANL, 1996) and shown

schematically in Figure 1. The Pajarito Plateau on which the Laboratory is located can

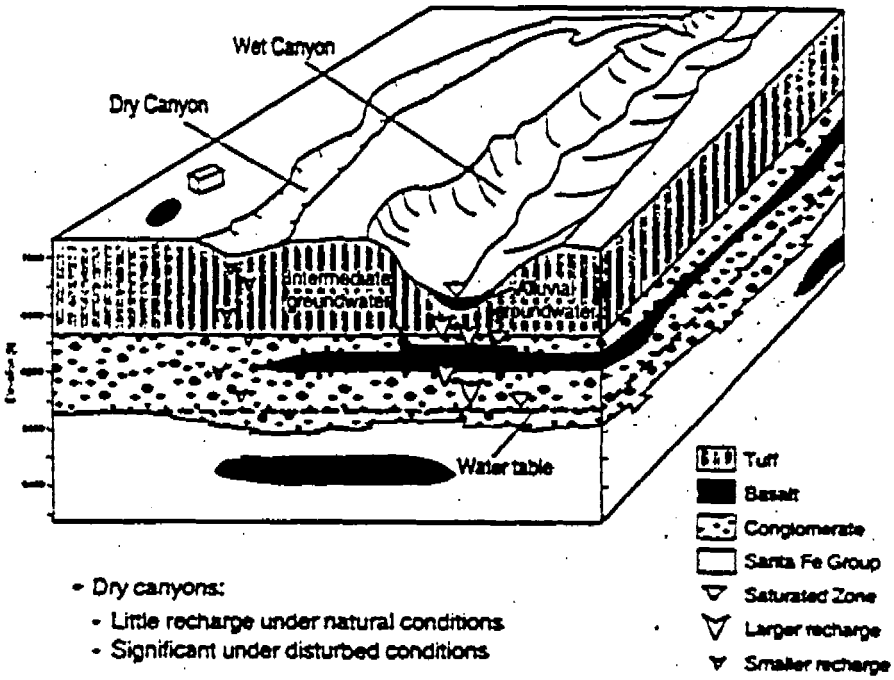

FIGURE 1. Schematic of the conceptual model for flow and transport in the vadose zone (reproduced from the Hydrogeologic Workplan, LANL, 1996)

be view as a relatively dry site with low recharge of fluids over most of the study area. However, there are known to be locations where focused recharge takes place. Most notably, canyons such as Los Alamos canyon are watersheds that provide focused flow paths for surface water flow; perennial or ephemeral streams are common in the canyons that cut through the Plateau. Therefore, in its simplest form, the conceptual model divides the Plateau into dry mesas (and in some cases, dry canyons) and wetter canyons. Contaminant travel times are anticipated to be long for sources emitted on mesas, but may be significantly shorter for contaminants in canyons.

Another commonly occurring observation is the presence of small bodies of subsurface water at the contact between canyon-bottom alluvial deposits and the underlying bedrock. These water bodies, which we call shallow alluvial groundwater, are not sufficiently extensive to be suitable for mining of the water for domestic use. Nevertheless, this water is an important component of the subsurface hydrologic system because recharge occurs from this system to the underlying rock strata. Furthermore, Laboratory

2.0 Site-wide examination of hydrologic properties and recharge through the Otowi member

Our current modeling approach in support of Environmental Restoration and Hydrogeologic Workplan activities calls for first constructing numerical models of key contamination sites or watersheds where deep subsurface transport has been observed or is considered likely. Then, other sites will be treated on an "as needed" basis, factoring in considerations such as the hydrogeologic setting and the transport characteristics of the site in question. Our approach is to construct the minimum suite of numerical models needed to cover the Pajarito Plateau adequately, and to rely on analogies to well-studied sites when treating the remaining study areas.

For such an approach to be comprehensive and complete, a firm scientific justification for the comparisons among sites must be established by performing Plateau-wide analyses of available data and observations. Therefore, although the goal of the present modeling study is to simulate the flow and transport for Los Alamos canyon, there is an interest in extending the results of the Los Alamos canyon study to the Pajarito Plateau, thereby placing the results in context. Two flow-related characteristics, the recharge rate and the hydrologic parameters of the unsaturated tuffs, are available for Los Alamos canyon and need to be assimilated into a larger picture.

To this end, in this Section we perform a site-wide examination of the vadose-zone hydrologic system through two analyses. First, we examine the spatial variability of hydrologic properties of the Otowi member of the Bandelier tuff. The goal of this analysis is to determine if there are significant differences in the hydrologic properties of the Otowi member across the Pajarito Plateau. This study could and should be extended to other hydrogeologic units as well, but we chose the Otowi member first because of its ubiquitous presence across the plateau, even in deep canyons such as Los Alamos canyon. Younger tuff units, such as the Tshirege member, are not encountered directly beneath Los Alamos canyon, and thus were not as desirable to examine in the present study. The second analysis provides estimates of local recharge through coupling of measured water content and unsaturated characteristic curves in a manner similar to that of Rogers et al. (1995). The present study augments and updates the Rogers et al. study by examining additional well data not available at that time. Again we focus our attention on the Otowi member because of its relevance to the Los Alamos canyon model.

2.1 Spatial variability on the Pajarito Plateau

The name Otowi Formation suggests a common origin of the generic Bandelier Tuff of which it is comprised. Geological history (Abeele, 1981) suggests that the Otowi Member occurred by pyroclastic flow of volcanic origin. The material is generally poorly fused and correspondingly less dense than highly fused tuff would be. The consolidation of samples from well LAOI-1.1 were so poor that they had to be repacked. One sample included in the Otowi member from a well LADP-3, has a very high bulk density of 1.69. It is at the upper extreme of the analyzed data set, but in the middle of the Otowi strata. This value contrasts with the mean bulk density of 1.20. Such variations in properties also applies to others of those based on core samples. Of the 40 core samples that have been used to obtain reported and complete properties of the Otowi Member, ten are

from CDBM-1, two from CDBM-2, five from MCM-5.9A, four from PC-4, six from LADP-3, and thirteen form LADP-4. Minimum-maximum pairs are given in Table 1 for the 40 samples , and Table 2 lists the plotting symbols and the data sources.

TABLE 1. Ranges of parameter values for the Otowi data set

Variable id	Variable (units)	Minimum	Maximum
Var. 1	Well designation		
Var. 2	Bulk density (gm/cm**3)	1.04	1.69
Var. 3	Saturated moisture (%)	24%	54%
Var. 4	Saturated Conductivity (cm/sec)	1.4E-7	7.8E-3
Var. 5	Residual moisture (%)	0%	12%
Var. 6	N (dimensionless)	1.388	3.45
Var. 7	alpha (1/cm)	5.7E-4	1.85E-2

TABLE 2. Plotting symbols and data references used in this section for the Otowi data set

Well designation	plot symbol	source
CDBM-1	X	Rogers and Gallaher (1995) LA-12968-MS
CDBM-2	x	Rogers and Gallaher (1995) LA-12968-MS
MCM-5.9	+	Rogers and Gallaher (1995) LA-12968-MS
PC-4	□	Rogers and Gallaher (1995) LA-12968-MS
LADP-3	o	Springer et al. (1999)
LADP-4	O	Springer et al. (1999)

Here the last five parameters are elements of the van Genuchten fit [Klute et al, 1986, Rogers and Gallaher, 1995, van Genuchten, 1980, Mualem, 1976] to water retention data and permit calculation of two properties, the matric potential and the relative permeability, the ratio of the unsaturated conductivity to the saturated conductivity. Correlations of these parameters do exist and they are not independent statistical parameters for the core samples analyzed. In particular, wells LADP-3 & LADP-4 have values of residual moisture equal to zero for all samples; all other wells from the forty core samples with complete data have at least 70% of their residual moistures non-zero. We have not investigated the errors associated with the reported parameters. Our subsequent conclusions could be modified if, for instance, all wells could be fit reasonably well with zero residual moisture. In that case, assuming the errors were large enough for each of

the six parameters to be fit by a single value throughout the Otowi Member, the results described below, which are based on negligible error would need substantial revising. Furthermore, if water retention curves can be fit within error by several sets of hydrological parameters, our subsequent work would want to take this feature into account.

An explanation for the variations and correlations of the parameters is of prime interest. Furthermore, the assumption that the core parameters are all equally likely, irrespective of the site of origin, needs to be examined. A van Genuchten parameter plot of the residual moisture, θ_r, vs. N shows three classes of wells, each of which fall on its own fuzzy line. However, working in the space of all six variables, we show below that we can construct an algorithm for identifying all the well sites uniquely for the forty cases at hand.

2.1.1 Summary of the analysis technique

Because the analytical methods employed to examine and correlate the hydrologic property data have not, to our knowledge, previously been applied by hydrologists, they may be unfamiliar to most readers. We therefore lay out in some detail the process used to interpret data from the Otowi member. Readers interested only in the bottom-line results can skip this section without loss of continuity. The analytical tools used in this study are commonly used in data analysis and data mining. They are related to cluster analysis, neural networks, statistical analysis, and image processing. Descriptions of the methods for projecting multi-dimensional data points onto lower dimensional manifolds is given in the User's Manual for Xgobi, a Dynamic Graphics Program for Data Analysis Implemented in the X-Window System (Release 2), Swane et al. (1991). This reference may be found on the internet at:

http://metlab.unc.edu/pub/academic/data_analysis/xgobi

Projecting from six dimensional space onto two dimensions is not a process thoroughly familiar to everyone, and yet everyone has been exposed to it in simple manifestations. The simplest example of such a projection is to select any two of the six variables and plot the points against them. The result depends, of course, on which two variables are selected. Consider the schematic in Figure 2. In three dimensional space, one may think

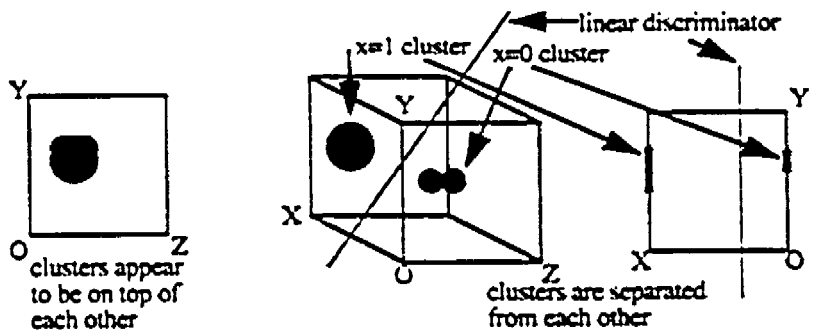

FIGURE 2. Three orthogonal projections present the same three dimensional data.

of a small translucent cube having edges in the directions x, y, and z being observed with one eye. If the cube is far away and rotated just right, only the x and y edges will be visible; all information in the z direction appears piled on top of itself. This is a projection onto x-y space. If that cube is rotated about the y axis by 90 degrees then the z and y edges will be visible and the x information is lost. If the cube is not far away, a similar situation occurs with respect to information piled on top of other information, but what is viewed is a non-orthographic two-dimensional projection. We restrict ourselves to orthographic projections in three and higher dimensions corresponding to distant cubes because they are simpler mathematically and conceptually.

Suppose in three dimensions that there are a number of points in a tight cluster on the x=0 face of the cube and another cluster of points on the x=1 face as shown in Figure 2. These two clusters might appear to overlap each other when looking only at the y and z values as shown on the left. However if the cube bearing these points is rotated so that the x=0 points are separated from the x=1 points as shown on the right, it becomes clear there are two separate clusters. Thus, we see that in three dimensions, two dimensional views can give us information as to the existence of separate sets of points, especially if all possible rotations of the set of points is allowed. It should not come as a surprise, that if we can see the distinct unobstructed points in all specified two dimensional orthographic views (in fact we need only two such views if we use a lot of mathematics), we have the same information as seeing the information in three dimensions. We are particularly attuned to this condition because each of our two eyes see a two dimensional projection of a three dimensional world. Thus our two eyes can distinguish the sets of points in the two clusters as being distinct, and this result is aided and achievable by only one eye if the cube is properly rotated.

Sets of points that are confused in a two dimensional projection might be separable in a higher dimension. If by rotations of the set of points in the higher dimensional space, we find a projection in two dimensions that shows a separation, clearly we know that those points are separated in the higher dimensional space. If the points are separable by a line in two dimensions as in the center or right most projection of Figure 2, we say there is a linear discriminator, i.e. a means by a line to tell which points are in each of two distinct sets. The method of describing this linear discrimination in the higher dimensional space is quite straight forward. In three dimensions, what appears to be a line in the two dimensional orthographic projection, when embedded in the three dimensional space, is a plane. If the plane, like a sheet of paper, is so orientated that only its edge is visible, a line segment is produced in the projection. In the right-most projection of Figure 2, the plane is the y-z plane, x=0.3; in the center projection, the plane edge is shown and the plane is less symmetric. Because the projection piles all information in the projected direction on top of itself, certain parallel lines in the plane all pile on top of themselves. Thus, if in three dimensions two sets of points are separable by a plane, and if we choose any line of that plane as a projection direction, we can make that line appear as a point by looking down the bore of the line. Then the two dimensional projection will project the plane as a line and a linear discrimination is achieved. The same situation holds in higher dimension: if we can see a separation by a line in a two dimensional orthographic projection, a hyperplane separates the data in the higher dimensional space (see Figure 3).

Given a set of points in three dimensions, we can ask the question of whether any specified point is inside the given set or outside. If we have four non-planar points, we can

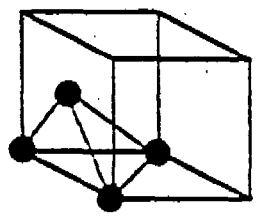

FIGURE 3. Four points in three dimensional space and the tetrahedral convex hull. The concept of inside and outside with respect to the hull of the four points is defined.

make our question have meaning by defining inside as being inside or on the tetrahedron whose vertices are the four points; outside is not being inside. If we have more than four points, we can extend the concept of inside and outside by extending the definition of what is called the convex hull of the points. If the fifth point is inside the other four, the convex hull is defined by the original four and the fifth point's location within the hull is irrelevant in the definition of the hull. If the fifth point is outside the hull, then there is a nearest face of the original hull, and this face contains three points. The hull is thereby extended as the union of two four point regions. In two dimensions, the convex hull of a set of points is that polygon, the one with minimum area, that contains all of the points of the hull. In three dimensions, it is the polyhedron of least volume that contains all of the points. In higher dimensions, it is the polytope of least hyper volume that contains all of the points. Such a hull in three dimensions has planes as faces. If one such face is moved away form the center of the hull, it is no longer of minimum volume. One can conceptualize a convex hull of a 3D set of points having N faces as having N planes that can be moved towards the data set and positioned and restrained by the outer most points, as the inverse of an exploding view.

The concept of a convex hull is closely related to the well-known concept of interpolation. The outermost points of the convex hull have positions whose weighted average produces all the points of the interior of the hull. The weights are taken in the usual sense as being positive real numbers the sum of which is unity. If one chooses two points on the outside vertices of a 3D hull, one produces an edge of the polyhedron by interpolation. If one chooses all pairs of points from two adjacent edges, by interpolation a face of the polyhedron is mapped out. Likewise choosing points on a pair of faces of the polyhedron results in mapping out the interior of the polyhedron. Mathematically, what we have said relies on the fact that the weighted average of a derived set of points, each of which is a weighted average, is a different weighted average of the original points. Here the derived set of points can be separate weighted averages of any subset or proper subset of the outermost points of the hull. Taking a specific numerical example, if we have four points, (0,0,0), (1,0,0), (0,1,0), and (0.5,0.5,0.3), and wish to map out the xy face, the x axis is: $w1(0,0,0) + (1-w1)(1,0,0)$; the y axis is: $w2(0,0,0) + (1-w2)(0,1,0)$; and the x-y face takes any point on the x-axis and any on the y-axis and interpolates:

w[w1(0,0,0) + (1-w1)(1,0,0)] +[1-w][w2(0,0,0) + (1-w2)(0,1,0)] = (w(1-w1), (1-w)(1-w2),0), and this maps out the region on the x-y unit square for various choices of w, w1, and w2. The three weights for the three points (0,0,0), (1,0,0), and (0,1,0) are w*w1+(1-w)w2, w*(1-w1), and (1-w)*(1-w2), and sum to unity. In fact, choosing w1=0, w=x, and w2 = (1-x-y)/(1-x) maps onto (x,y,0), where x and y each lie on the [0,1] closed interval.

An orthographic projection has a particular property that makes it useful with respect to those points derived by a weighted average of the outermost points. The projection of a derived point can be constructed in two ways: 1) it can be computed first as a derived point in the full space, as if a new point there, and then projected to the embedded space (the two-dimensional plane); or 2) the projection of involved outermost points of the hull can each be projected to the embedded space, and then the derived point in the embedded space can be computed in the projection using the same weights as those used in finding the derived point in the full space. The mathematical properties follow from the associative law for multiplication, that order of multiplication makes no difference in computing a product. Simply put, if a point is half way between two points in the full space, it remains half way between in the orthographic projection.

From this it follows that if points lie within a convex hull in a two dimensional projection whose boundary is a given polygon, they will lie within a polytope some of whose faces or edges are related to the edges of the polygon, as in Figure 4. Each edge of the

Projection of polyhedral points onto a plane with hull in presence of a foreign point

Upper surfaces of a polyhedron

FIGURE 4. The convex hull in a plane forming a polygon whose edges are related to the fringe of some of the faces of the polyhedron.

polygon involve two points of the hull. Those two points will be part of the outermost points of the full higher dimensional hull. With all rotations in the higher dimensional space followed by projection onto two dimensions, all possible pairs of adjacent points of the outermost points of the full hull will appear as an edge of a polygon. In particular, the interior point of the polygon in Figure 4, will appear outside the other points and will be part of a new polygon if the polyhedron is properly rotated and projected. With sufficient two dimensional projections of distinct rotations, the full geometry of the higher dimensional convex hull can thus be determined and the concept of inside and

outside can be established by projection. In particular if a foreign point is outside a higher dimensional hull, a projection can be chosen that maps the face nearest to the foreign point into a line of the orthographic projection. In Figure 4, the face is not quite mapped onto a straight line, but by a small change in observation direction the three points of the face will fall onto a straight line. That foreign point then must appear outside the polygon of the projected convex hull.

2.1.2 Application to the Otowi hydrologic data

We now apply the methods discussed in the previous subsection to the hydrologic data for the Otowi member. The well algorithm is as follows. In the six dimensional space described previously, construct 2D convex hulls in the space for LADP-3 as in Figure 5

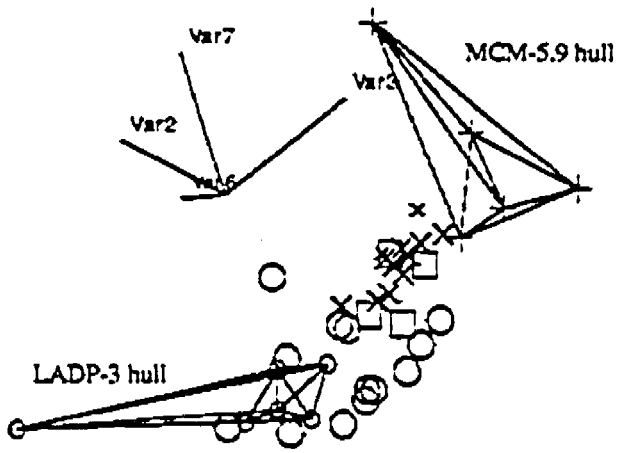

FIGURE 5. Projection of four space onto two showing separability of convex hulls of LADP-3 (o) and MCM-5.9 (+) from rest of space. Other views show other aspects of data.

and MCM-5.9 data. No points of any other well lies inside either of these polygons. Thus, in the full space, no points of the other wells are inside the higher dimensional convex hulls of LADP-3 and MCM-5.9. As noted, the convex hulls include all of the points that can be reached by interpolation, the so-called inside points, i.e. a weighted sum of the reported values with positive weights that sum to unity, but not by extrapolation. By use of these hulls, we remove these two portions of space because they are assigned to the two wells. If we are given any point from one of the two specified wells, we can clearly identify it by whether or not it is inside one of the two convex hulls.

In the remainder of the space we use a linear discriminator to separate the LADP-3-LADP-4 complex, from everything else as shown in Figure 6, and also verify MCM-5.9 is separated from everything else. Since LADP-3 has already been removed from consideration, the first discriminator uniquely identifies the LADP-4 well core samples. The

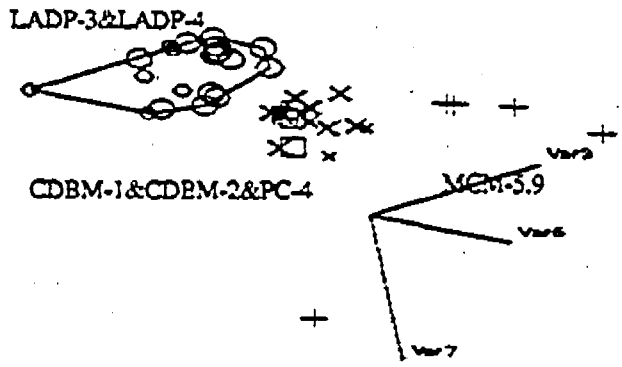

FIGURE 6. Projection showing three separate groups: LADP-3&LADP-4, CDBM-1&CDBM-2&PC-4, and MCM-5.9

second discriminator uniquely identifies MCM-5.9 showing that we didn't have to use a hull; a linear discriminator suffices. What are left are CDBM-1 and the CDBM-2-PC-4 complex. Figure 7 shows that CDBM-2 can be separated from the rest, leaving only

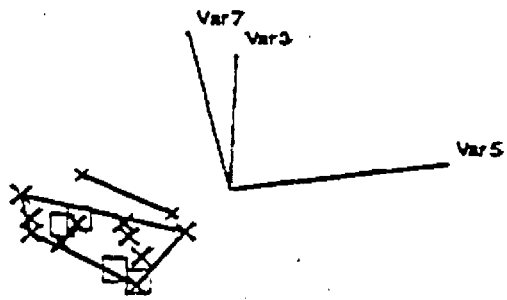

FIGURE 7. Projection of CDBM-1, CDBM-2 and PC-4 (□) showing linear separation of CDBM-2 (x) and the CDBM-1(X)-PC-4 complex. Other wells not plotted.

CDBM-1 and PC-4. Figure 8 shows that PC-4 lies outside the convex hull of CDBM-1. Removing the points in the convex hulls of LADP-3 and CDBM-1, thus, allows the rest of the data to be separated by linear discriminators in various projections.

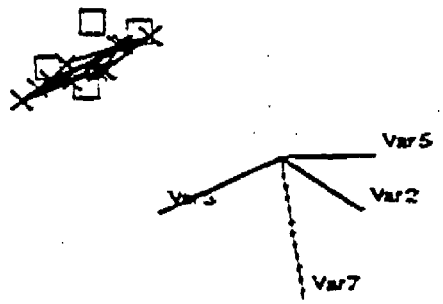

FIGURE 8. Projection showing all PC-4 (□) points lie outside convex hull of CDBM-1 (X). Although it does not appear so in this projection, it is suspected that the convex hulls of PC-4 and CDBM-1 are mutually exclusive. Other wells are not plotted.

2.1.3 Implications of the analysis

We have shown that the wells can be determined uniquely mathematically, in the six dimensional parameter space, implying that there are significant differences in the hydrologic properties of the Otowi member across the Pajarito Plateau. This results begs a geological explanation. Does this mean that the Otowi Member should be further subdivided in order to group expected values of hydro-geological parameters? Note that porosity and petrographical parameters have not been included in this study (nor have moisture or matric suction). They might make the algorithm even simpler. If geomorphological simulations of the pyroclastic flow and subsequent weathering were to be made, these variations of hydrological parameters would be data to which to fit with the simulation parameters. Perhaps these are not needed and geological insights are currently sufficient to provide an explanation of the observed site variations.

Caution needs to be used in interpreting these results to avoid unwarranted conclusions. First, there is no guarantee that with more Otowi Member samples from the same wells or different wells the same relationships hold. The sparsity of core samples may have produced convex hull regions that are too small compared to that for many samples. The optimum location of boundaries between regions also could change with more samples. Furthermore, the uniqueness of the identification could be lost, we then being able only to give a probability of identification. This is especially true of distinctions of sites like LADP-3 and LADP-4 (Fig. 5) or PC-4 and CDBM-1 (Fig. 8) where boundaries are very tightly positioned and points closely straddle the removed hulls, possibly on opposite sides. Finally, Rogers (personal communication, 1999) points out that after revisiting the geologic picks made in these wells, some of the samples originally identified as being in certain geologic units actually belong in other units. Therefore, the present analysis should be updated when the new geologic picks for these samples becomes available.

These results also cast uncertainty on how one should develop estimates of unknown parameters. One model is that each of the forty well samples are equally likely to be

found at each sample from any future Otowi Member well sample. Also at issue is how to model the entire Pajarito Plateau as a single entity of a much larger region. Averaging over the well samples is one possible method. On the other hand, separability of well parameters can continue as it has for the six wells only as long as there is room in the six-dimensional parameter space. Eventually, with many more sites, there will be overlap of parameters in neighboring sites. In a thought experiment, if well parameters were easily obtained in a non-destructive fashion, the Pajarito Plateau ultimately could be described by a six-dimensional density or likelihood function. Because the hydrological parameters are not a complete description of the water transport, a more plausible ultimate geomorphological model might be to have the parameters as a function of longitude, attitude and depth. In this context, depth could be the absolute depth, or a non-dimensional depth with a hydrogeologic unit like the Otowi member. These might be probability distributions, averages over the ensemble of pyroclastic simulations that match the known data. These would couple to a position-based fault data base that also might be modeled digitally, measured, or guessed. The basis for such a picture already exists in Fig. 11 p. 103 in an existing report (Broxton et al. 1995). There the role of the Pajarito, Rendija Canyon and Guaje faults are shown to contribute to vertical flow in parallel with the porous flow through tuff with which we are concerned.

Another method of extrapolation of new data would be to determine which of the three regions in Figure 6 the new well lies, based on the measured quantities such as gravimetric moisture and matric suction. Measurement of the porosity and welding (lapilli aspect ratio) or other parameters described in Elliott (1999) could also help this process enormously. Then, rather than averaging over all the wells, the averaging could be over those in the determined region. Other versions of this type of approach include using radial basis functions in a neural network to obtain mean properties. The radial-basis-function concept of neural networks could be extended to include expected statistical variation information. Such a framework is not known to exist; it could be tied to probabilistic neural networks generalized to continuous variables.

2.2 Unsaturated Conductivity

Rogers et al. (1995) developed an interpretive technique for estimating local recharge rate based on measured hydrologic properties and water content values in samples collected from the vadose-zone tuffs of the Pajarito Plateau. In its simplest form, the method makes use of the fact that under certain limiting conditions, the water content is directly related to the local percolation flux at that location. Consider the simple case of one-dimensional, gravity-driven flow under unsaturated conditions. Assuming homogeneous properties, the one-dimensional flow equation

$$q = k\frac{dH}{dz} \qquad \text{(EQ 1)}$$

Is further simplified by realizing that under these conditions, $\frac{dH}{dz} = 1$, that is, there is a unit-gradient driving force for fluid percolation. Therefore,

$$q = k \qquad \text{(EQ 2)}$$

In the equations above, q is the flux, k is the unsaturated hydraulic conductivity, H is the head, and z is the vertical direction. The unsaturated hydraulic conductivity is related to the water content through relationships such as those developed by van Genuchten (1980). One way to look at this simple relationship between q and k is that under steady state conditions, and for a given recharge rate, the rock attains the water content needed to transmit the water through it under unsaturated conditions. Figure 9 shows the

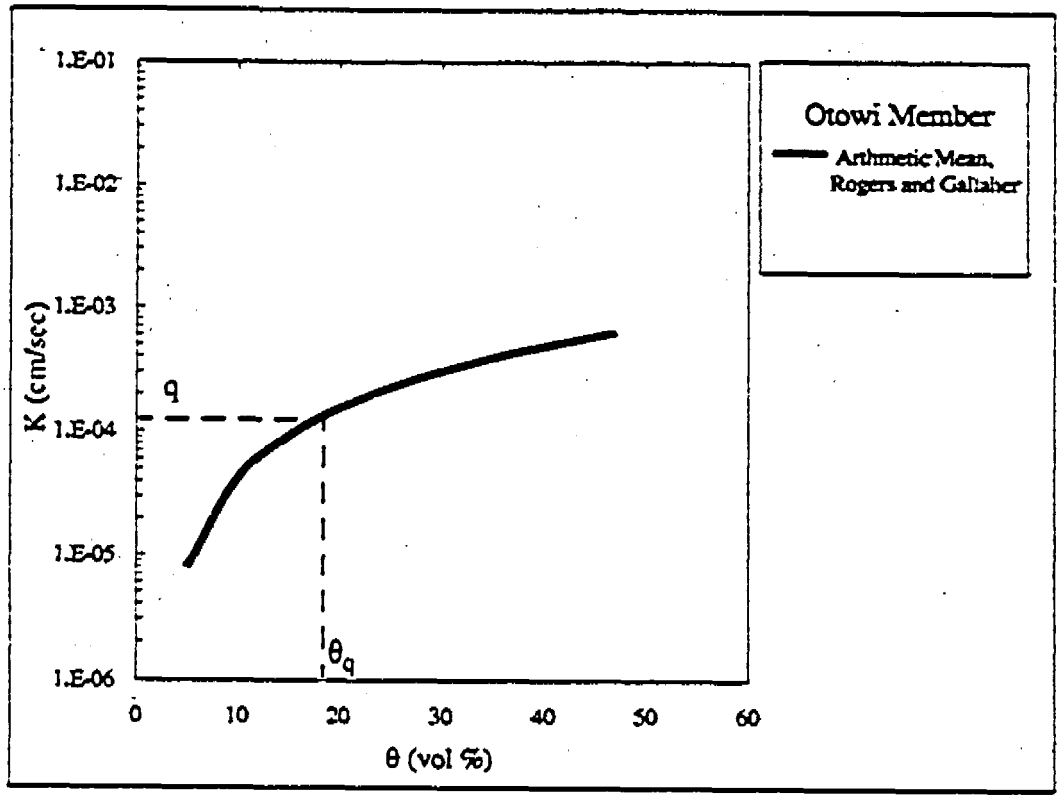

FIGURE 9.

Base-case hydraulic conductivity versus water content for the Otowi member. A given value of q in a one-dimensional, gravity-driven flow scenario yields a particular value of θ_q from this curve.

base-case hydraulic conductivity versus water content curve for the Otowi member. To a first approximation, a given recharge rate q on the figure gives rise to a water content θ_q from the curve. Alternatively, measurements of θ in a given sample, combined with the measured characteristic curve for the same sample, yields an estimate of q. Of course, subtleties in the analysis of actual data sets complicates the interpretation, but the basic concept is embodied in this simple description. Complications for the samples

in the Otowi member that are treated in Rogers et al. (1995) and the present study include:

- incomplete measurements on some samples;
- different analytical techniques for obtaining the measurements;
- different data reduction assumptions in fitting the van Genuchten model to the data;
- the possibility of local conditions that violate the assumptions in the model.

These caveats are treated in the interpretation of the new results in this section.

Compiling percolation flux estimates from a variety of hydrologic settings on the Pajarito Plateau is a crucial activity in support of validation of one of the key conceptual models of the site, namely the importance of topographic location (canyon versus mesa) in controlling the local recharge rate. The present study contributes to that important goal by extending the Rogers et al. (1995) report through the addition of data published since the writing of that article.

The data used were collected from individuals, reports, and publications. Springer et al. (1999): from Springer, Langhorst and Hamilton, "Hydrogeologic Properties of the Bandelier Tuff and Groundwater Occurrence at DP Mesa TA-21", Los Alamos National Laboratory, Los Alamos, NM", preprinted July, 1999. Although the current standard operating procedure used for R-12 and R-25 is to collect in situ gravimetric moisture, H2O activity, and temperature, such data are not available for the less recent wells LADP-3 and LADP-4. For those wells gravimetric moisture has been measured but it has not been converted to volumetric moisture through the bulk density. Measurement of the particle density (average density of solid material) would permit computation of the porosity. Well LAOI-1.1 is described in a D. B. Stephens & Associates report. Here moisture retention curves are presented and saturated hydraulic conductivities given.

There are five new borehole data sets we are interpreting: Wells R-25, R-12, LADP-3, LADP-4, and LAOI-1.1. Their locations are shown in the attached map (Figure 10). In addition other borehole sites previously used in the Otowi member are shown. These are SIMO-1, CDBM-1, CDBM-2, PC-4, MCM-5.9A, and AB-7. However, AB-7 and

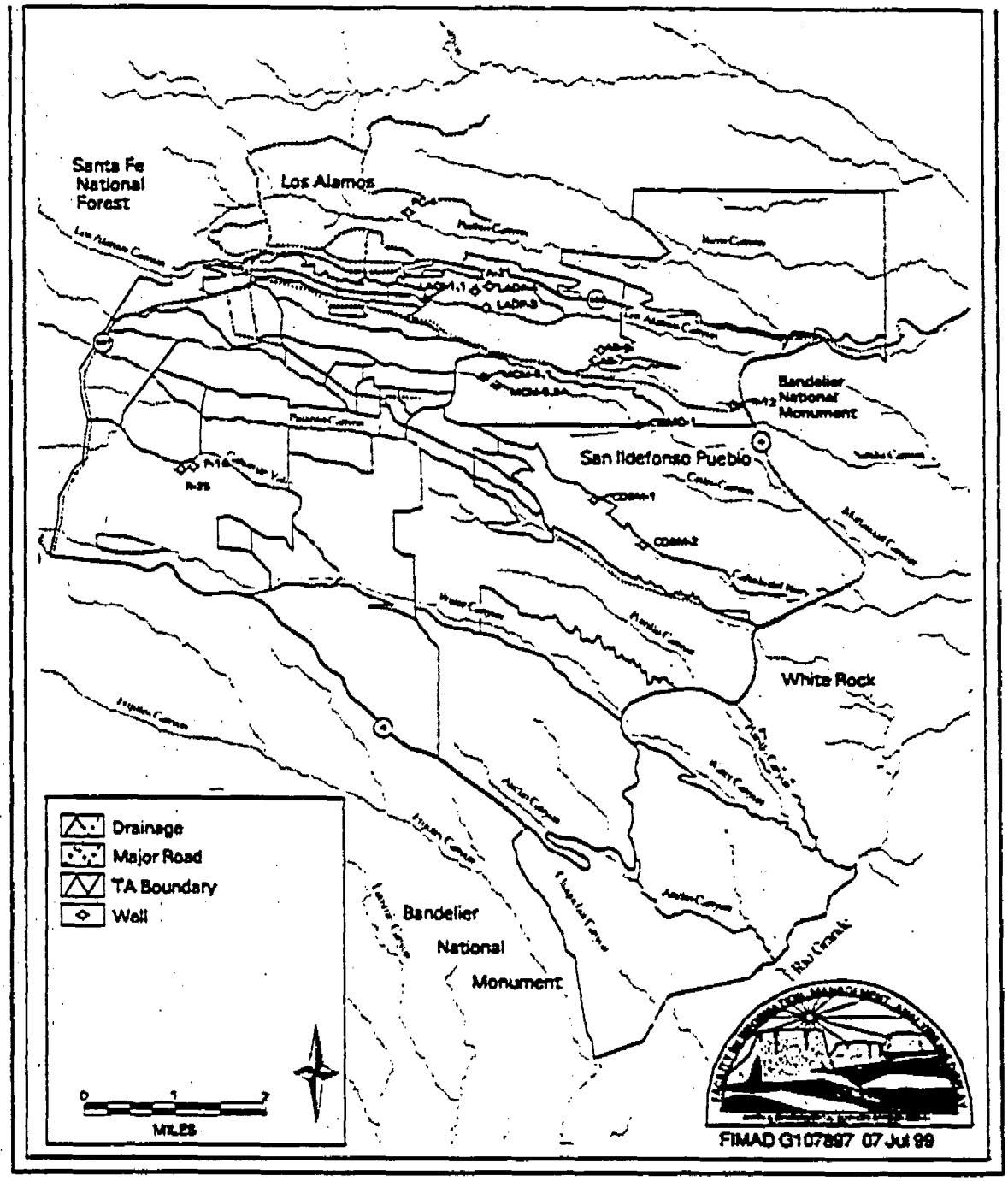

FIGURE 10. Locations of wells used in the recharge analysis

SIMO-1 have incomplete hydrological parameters. Table 3 shows the types of data and

TABLE 3. Summary of available data for the Otowi member

well design ation	R-25	R-12	LADP-3	LADP-4	LAOI-1.1	SIMO-1	CDBM-1	CDBM-2	PC-4	MCM-5.9A	AB-7
ψ(z)	Y	Y			N						
Reten			YT	YT	YR	Y	Y	Y	Y	Y	-2
Dmin	509'	31.3'	57'	293'	72'	71'	104'	67'	109'	120'	70'
Dmax	(747'sat) 853'	102'/ 112' pumice	308'	573'	294'	90'	189'	68'	168.5'	165'	80'
Table		C-1									
page		35-39	97	99		68	A-9.....	.....	B-9	70	
ψ(z)	Y	Y			N						
Reten			YT	YT	YR	Y	Y	Y	Y	Y	-2
Dmin	509'	31.3'	57'	293'	72'	71'	104'	67'	109'	120'	70'
Dmax	(747'sat) 853'	102'/ 112' pumice	308'	573'	294'	90'	189'	68'	168.5'	165'	80'
Table		C-1									
page		35-39	97	99		68	A-9.....	.....	B-9	70	

their depth range. In this table, G indicates gravimetric water content by% weight. Y is yes. YT indicates tentative data from Springer et al. YR indicates recently obtained data. GG indicates gravimetric data in graphical form only. LAOI-1.1 data apparently has not been fit to van Genuchten parameters, and R-12 samples are scheduled for testing at the end of FY-99 for porosity, particle density, bulk density, saturated hydraulic conductivity, water retention curves and possibly additional tests.

Most of the Otowi units are consistent with gravity driven flow within a small factor. This means that in a one-dimensional model, the unsaturated hydraulic conductivity is nearly the percolation flux. For this condition to accrue, the magnitude of the suction gradient needs to be of order unity or less. The precision of head measurement is 10-12m H_2O. The accuracy is quoted equivalent to 40 m, but repeated measurements on distilled H_20 shows that systematic error is much less. Equilibrium time for unchanging sample is 3 +- 1.5 minutes. Manufacturer of equipment recommends replacement of CX-2T at high potentials (near 1.5MPa to 0 suction) by SC10A.

LAOI-1.1. Calculated suction is not measurable by mirror psychrometry because of the nearness to saturation. The average computed suction gradient is 0.025 to 0.01. Note that parts of LAOI-1.1 Otowi Member are nearly saturated and some samples had to be repacked. We use the in situ measured moistures carrying the designation of "estimated" to get ψ. The result is plotted in Figure 11.

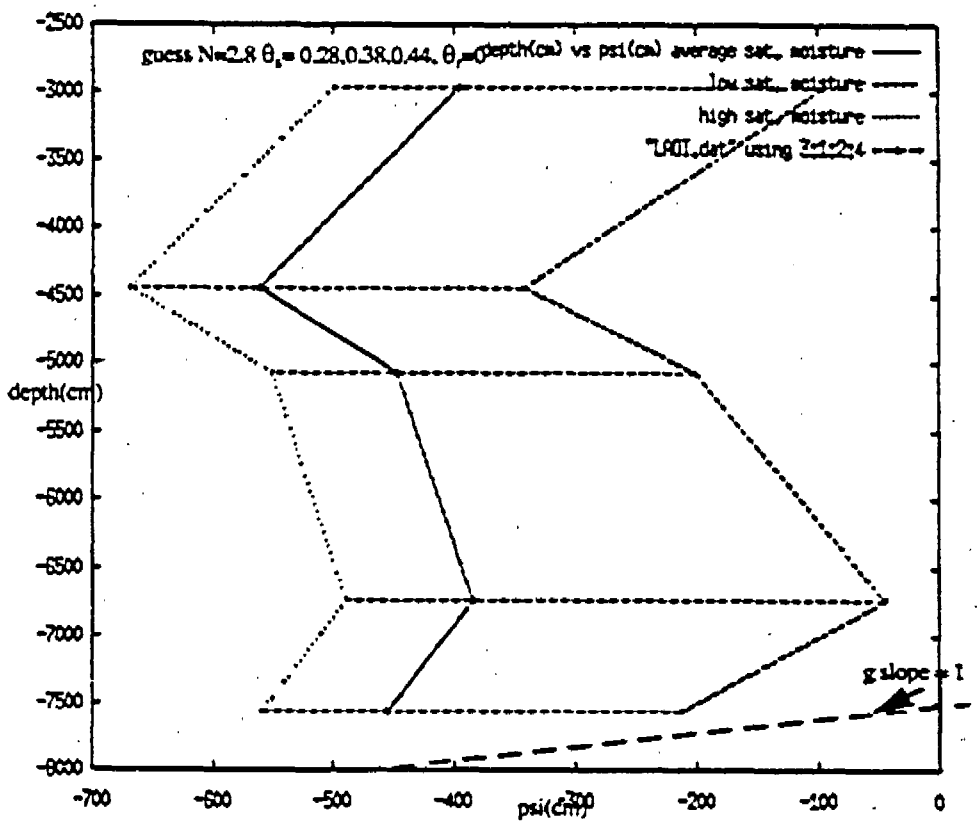

FIGURE 11. Depth profile of computed matric suction for well LAOI-1.1 under assumptions of low average, and high saturated moisture parameter. Mirror psychrometry gives a standard error in psi of nearly 1000 cm. Suction forces are small compared to gravity.

LADP-4. Mirror psychrometry measurements of suction is consistent with zero suction throughout the Otowi Member within measurement error. It has average suction gradient of 0.23.

LADP-3. Mirror psychrometry measurements of suction is consistent with zero suction throughout Otowi Member within measurement error. It has average suction gradient of +0.10 (top) to -0.20 (bottom). The negative suction gradient is too weak for upwelling.

R-25. Mirror psychrometry measurements of suction is consistent with zero suction throughout Otowi Member within measurement error. The average suction gradient, should it exist, is < 1. Standard mirror psychrometry matric suction error of R-25 is 12.0 m H2O.

R-12 with gravity sometimes negligible. The lower part of the Otowi Member from 75' to 90' has apparently a significant suction gradient of -8g (opposing gravity). Towards the surface the suction gradient is as large as -400 g (Table 4). This condition

TABLE 4. R-12 Matric Suction Values (+g indicates in the direction of gravity, -g, opposed)

depth	suction (cm)	|dPsi/dz|	direction
20. ft (600 cm)	-21841--1200		
not Otowi		400	g
25. ft (750 cm)	-77961--1200		
		400	-g
30. ft (900 cm)	-22889--1200		
		14	-g
75. ft (2250cm)	-3976--1200		
		8	-g
90. ft (2700 cm)	0.0		

suggests substantial upwelling. Standard matric suction error of R-12 measurements is 10.6 m H_2O. (If one were to use the AquaLab CX-2T claimed error equivalent to 40 m, the suctions in the quoted range would be zero within measurement error).

However, the gravimetric moisture is only 2% at 25' depth, a region above the Otowi. At this depth, the suction has very large magnitude. Its value was measured twice. This condition is similar to conditions reported (Rogers et al., 1995) for the Tshirege unit 2a at the TA-54 MDA G borehole G-5, and MDA G and MGA L moisture profiles [Kearl et al 1986]. Moisture flows to this low-potential region from above and below and may act as a barrier to infiltration at this lateral location. Such conditions may be enhanced by fractures and may be related to airflow (Rogers et al., 1995). This region may also be associated with pyroclastic surge deposits. This type of structure is sometimes called a vapor phase notch. In well MCM-5.1, such a notch occurs at 54' depth, but there the interpretation is clouded by poorly defined moisture retention curves in the dry region with a high value of moisture retention parameter (15%). Furthermore in MCM-5.1, another smaller vacuum region is measured at 82.5', but the significance is not as large compared to expected measurement errors, and the moisture is >20% without a correspondingly large moisture retention parameter. Because the hydrological parameter measurements have not yet been completed, we do not know how well the moisture

retention curves will be characterized. This region has been characterized as highly porous; it makes infiltration from the surface improbable.

R-12(Raw) Otowi STANDARD ERROR = 1694/1.414=1200 cm.

K for R-12 in Otowi. At the time of writing, we are still awaiting hydrological parameters for R-12, and we have very uncertain predictions based on either of two methods. We use log mean values for the unsaturated conductivity, and the factors in parentheses are uncertainties in the log expressed as multipliers or divisors. K is not appropriate as an estimate of recharge for this well because of vapor gap.

Note that as psi -> 0, K -> 8 E-5 cm/s

BY GRAVIMETRIC MOISTURE (2 to 16%) 1.1 E-9 (*/1)-> 3 E-7 (*/6)

BY MATRIC SUCTION (-780 m at 25° to -0 m at 110°) 1E-9 (cutoff)->8 E-5 (*/6)

K for R-25. We are still missing hydrological parameters for R-25 and these have very uncertain predictions based on either of two methods. We use log mean values for the unsaturated conductivity over all wells. The two methods assume R-25 is an average well, but the conclusions given below based on gravimetric moisture and those based upon matric suction show that the average low moisture result does not overlap with average matric suction result; the highest moisture result does overlap, and only if we go beyond the mean value and allow variations within the standard error bands to get overlap the lowest moisture has slight overlap. The outlier well core MCM5.9A-130' seems to have a similar problem.

The factors in parentheses are uncertainties in the log expressed as multipliers or divisors. The variations in K with depth via the moisture interpretation challenge the 1-D model; all other wells vary in K by 1.5 orders of magnitude for that variation in gravimetric moisture.

Note that as psi -> 0, K -> 8 E-5 cm/s

By gravimetric moisture: K (cm/s) = E-8(*/4)@8% to E-6(*/5) @19%

By matric suction (0+-10m@514' to 0+-10m@667')

K (cm/s) = 1.E-4(*/6) @ psi = 0 to 1E-7(*/6)@ psi = 10m.

K for LADP-4 (based on gravimetric moisture and Springer parameters). K = 4 E-8 to 1 E-9 cm/s average depending on depth. More variations due to deviations from expected parameters exist.

Log average over depth = 6 E-9 cm/sec.

K for LADP-3 (based on gravimetric moisture and Springer parameters). Note at upper end of LADP-3 Springer et al. (1999) gives no hydrological parameters. We use LADP-well averages for these samples. Saturation varies from 56% to 76%. More variations due to deviations from expected parameters exist.

K = 1 E-6 cm/s (@17 m) to 4 E-7 cm/s (@56 m) to 1 E-6 (@92m).

Log average over depth = 7 E-7 cm/sec.

K for LAOI-1.1. The determination of a guess for K can be based on a number of approaches. We describe two approaches which turn out to be equivalent. Before we proceed, however, we need to establish a relationship between θ_s and porosity, n. Clearly θ_s is less than or equal to n, the difference being associated with air pockets or unconnected voids. Even so, we can use the relative invariance of the underlying rock density to remove some variance associated with θ_s. Removal of the dependence on bulk density is shown in the upper set of points labeled + in Figure 12. Although the upper set of

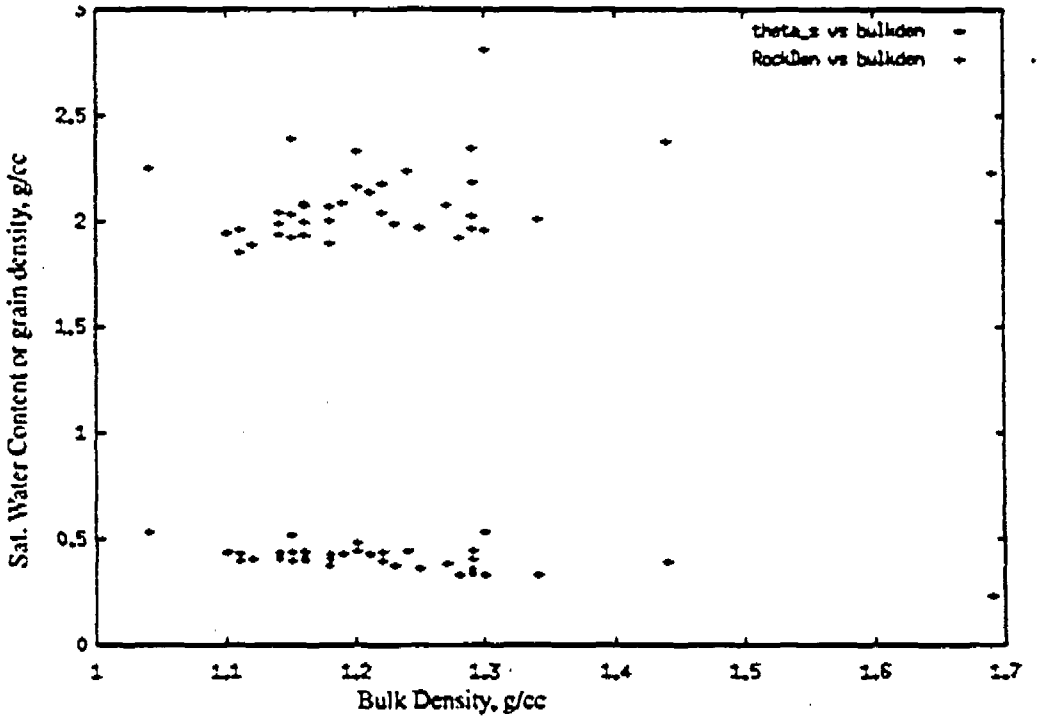

FIGURE 12. Saturated water content and grain density versus bulk density, well LAOI-1.1

points appear to have more variance, when plotted on a log scale in Figure 13, this is not so.

The three trial values we will use for θ_s are then taken as a fixed fractions of the porosity, dividing the latter by unity, 1.2 and 1.4; the value 1.2 being taken as the most likely to account for the difference between constant value and 2.65. The values computed using the porosity information are substantially larger than when ignoring it because the porosity at LAOI-1.1 is substantially larger than estimates of porosity at other Otowi wells.

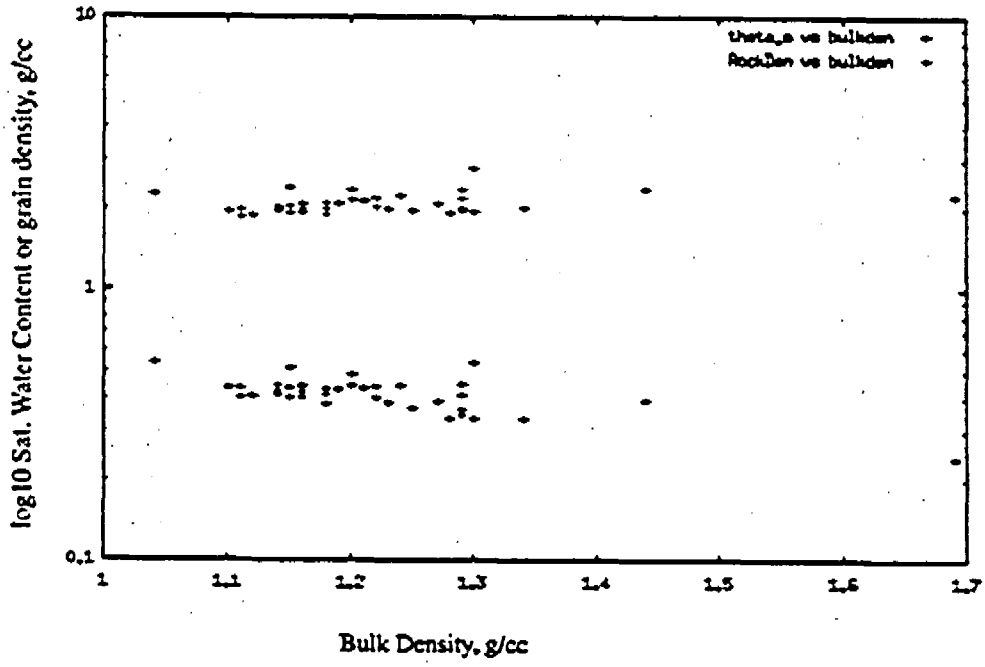

FIGURE 13. Saturated water content and grain density versus bulk density, well LAOI-1.1, log scale. for y axis

Next we show that direct calculation of the log K average is the same as doing a least square procedure in which we find the value of K that reduces a particular variance to a minimum. The method we will formulate is a comparison of a calculation of K_s from moisture versus the measured experimental values, $K_{s,ex}$ of same. The overall hydrogeologic effect is that with K constant, as $\tilde{\theta}$ increases, K_s compensates by a decrease. The other hydrogeologic parameters are considered less volatile. The method is based on a fit of the Mualem (1976) form used by van Genuchten, described in Section 6.1. Suppose we fix M and choose that value of K (or log K) that minimizes

$$\Lambda = \sum_z \left\{ \log[K_{s,ex}(z)] - \log\left[\frac{K}{F[\theta(z), M]}\right] \right\}^2 \qquad \text{(EQ 3)}$$

where $K_{s,ex}(z)$ is the experimentally measured K_s at depth z, and $\theta(z)$ is the experimentally measured value of the volumetric moisture at depth z that determines $\tilde{\theta}$. By algebra an equivalent formulation is minimization of

$$\Lambda = \sum_z \left\{ \log F[\bar{\theta}(z), M] - \log\left[\frac{K}{K_{s,ex}(z)}\right] \right\}^2 \qquad \text{(EQ 4)}$$

and in Figure 14 we show various fits of K = E-4, E-5, and E-6 using three choices for

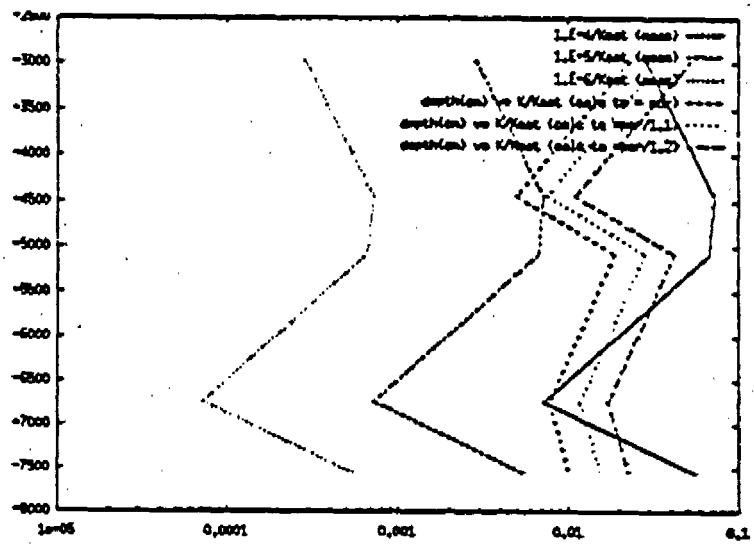

FIGURE 14. Fits of depth versus relative permeability data, Well LAOI-1.1

θ_s.

The above choice of K is also equivalent mathematically to minimizing:

$$\Lambda = \sum_z \{\log[K_{s,ex}(z) F[\bar{\theta}(z), M]] - \log K\}^2 \qquad \text{(EQ 5)}$$

The quantity in the brackets is now the computed value of K given the experimental saturated conductivity and the experimental moisture. Here the best value of K is given by:

$$\log K = \frac{\sum_z \log[K_{s,ex}(z) F[\bar{\theta}(z), M]]}{\sum_z 1} \qquad \text{(EQ 6)}$$

This is the log average of the computed K from data gives the appropriate values. Formally this result follows from differentiating Λ with respect to logK and setting the

result to zero. Log average over depth at expected saturated moisture = 7 E-5 cm/s (See

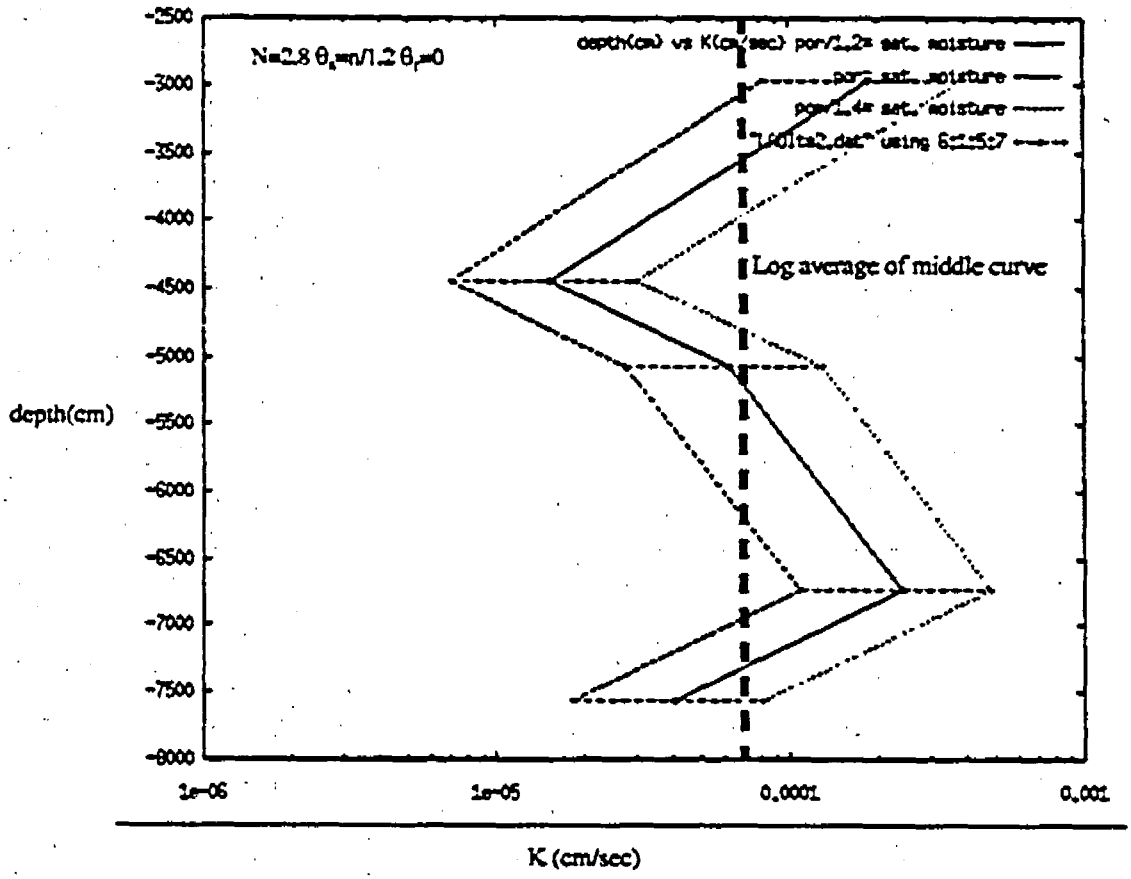

FIGURE 15. Depth profile for hydraulic conductivity K (cm/s) for LAOI-1.1 with various saturated moisture assumptions. Log average at N=2.8 and porosity/1.2 gives K = 7E-5 cm/sec.

Figure 15). The variations of K are at most a factor of 4 on the expected curve, whereas the variations in $K_{s,ex}$ is about a factor of 10. The standard error of $K_{s,ex}$ is said to be about a factor of two [Mark N. Ankey D.B. Stephens & Associates], and that accounts for part of the deviations from average.

Fortunately, we were recently able to obtain the complete LAOI-1.1 report and there drainage curves were reported. The pressure head went from 0 m to over 130 m for each sample examined. The following calculation uses the maximum observed moisture for the saturated value and the minimum moisture for the residual moisture. A fit of the retention curve to the Genuchten form would be a more reliable way to analyze these data, but such a technique is beyond the present scope of this paper, it being reserved for

future work. Here the log average is 4.5E-5 cm/sec. Using average properties for all the moisture parameters except K_s we had obtained a log average of 2.E-4 cm/sec. Using calculated porosity as an estimate basis for the saturated moisture we obtained 7E-5 cm/sec.; and using the data from the report without parametric fits we obtained 4.5E-5 cm/s As Figure 16 shows, the fit to the retention data is critical with respect to the choice of

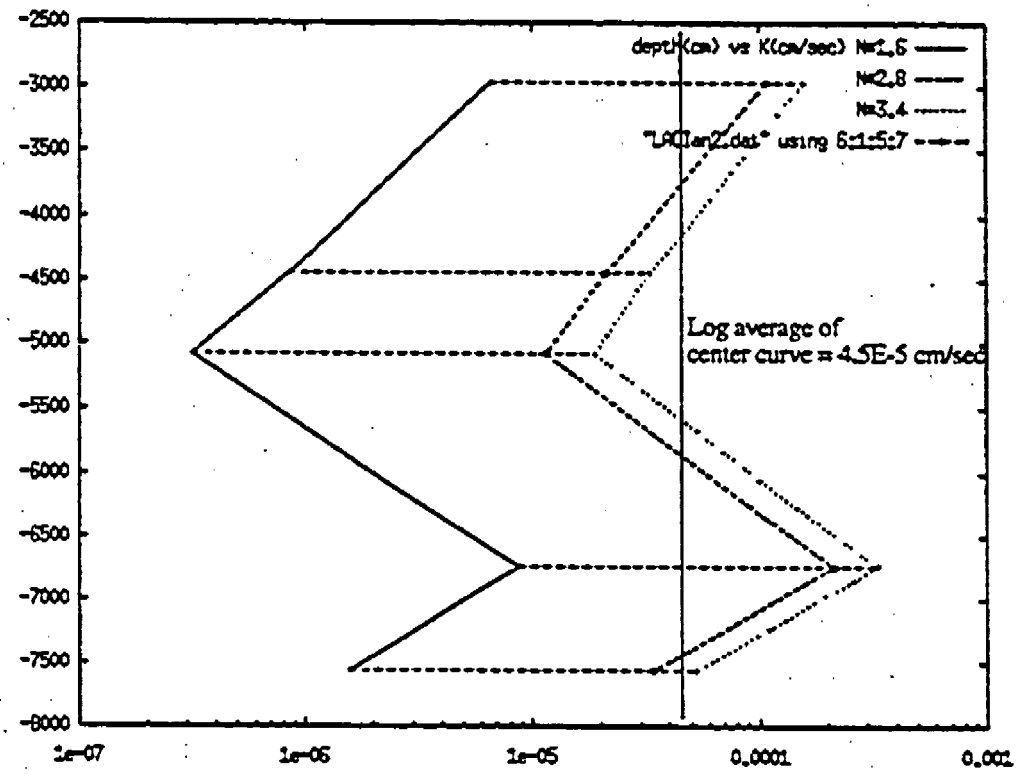

FIGURE 16. Fits with various N values and $\theta_s=\theta_s+0.01$, $\theta_r=\theta_r-0.01$, Well LAOI-1.1

the exponent, N. Conceivably, the value could be an order of magnitude further lower. However, fitting the retention data parametrically will resolve this uncertainty.

The value of N in the fit above appears to be quite important. It can be determined by a best fit to the moisture retention data. Although such a determination is beyond the scope of this paper, we have made one fit to data at 96.7 to 97.7 feet using the estimated data. This is shown in Figure 17.

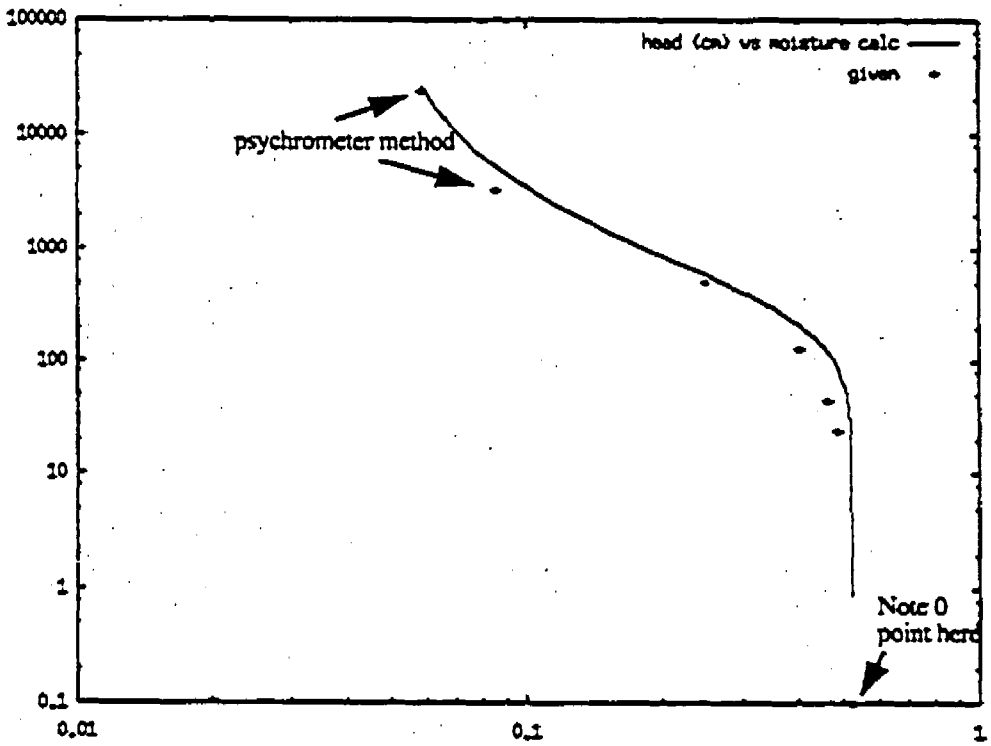

FIGURE 17. Showing fit to van Genuchten form of retention data of D.B.Stephens & Associates with values of α = 4.45E-3 cm, N=1.8, θ_s = 0.52001 θ_r = 0.048 (not optimized) for LAOI-1.1 96.7'-97.7'

This fit suggests that a value of N= 1.8 is appropriate for one depth in the Otowi member and is a likely guess for values elsewhere. In conjunction with the previous curve, this suggests that a value of K = 5.E-6 cm/s is more appropriate. More work needs to be done to establish these conditions at other depths.

2.2.1 Relevance of the 1D Model

A number of the caveats of 1D flow are discussed in Elliott (1999). As discussed earlier, assuming one-dimensional flow does occur and that gravitation directed flow dominates, the flux, q, is given by q=K, where K is the unsaturated hydraulic conductivity (Freeze and Cherry, 1979). In a number of cases we have computed K and find variations as a function of depth. This means that in 1D there is a continual source (sink) of H_2O where ever dq/dz is positive (negative). Either a perched-like (over-dry) condition exists throughout or the 1D model fails.

2.2.2 Comparison of results to previous studies

Interpretations of data from this type of model has been subjected to cross checks by comparison with the Rogers et al. (1995) report. Table 5 summarizes the recharge rate

TABLE 5. Summary of recharge rate results

Well	Our log avg K (cm/s)	Estimated Recharge Rate (mm/y)
LADP-3	7E-7	220
LADP-4	6E-9	1.9
R-12	E-9 to 8E-5 dry porous barrier above moist Guaje Pumice bed below	0.3 to 2.5e4
R-25	2E-8 to E-4 inconsistent assuming average values	6.3 to 3.2e4
LAOI-1.1 using θ and K_s data	[2E-4 N=2.8 θ_s= 0.38, θ_r=0] [7E-5 N=2.8 θ_s=n/1.2 θ_r=0] [4.5E-5 N=2.8 θ_s=θ_s+0.01, θ_r=θ_r-0.01] 5 E-6 (one LAOI fit N=1.8, see Fig. 15)	1600 (using the Figure -- result)

results. In Rogers et al. (1995) they found significantly lower fluxes (0.1 to 1 mm/y) in drier canyons such as Canada del Buey and Potrillo. At Area G, they determined extremely small flux values (of the order of 0.06 mm/y), attributing these to evaporative drying within the mesa. The highest values they obtained were 90 mm/y on a relatively wet mesa at TA-16 and 230 mm/y near a surface impoundment at TA-53 (LANSCE). The flux values estimated in Los Alamos canyon wells LADP-3 and LAOI(A)-1.1 are in this range or higher, in keeping with our designation of this canyon as a wet canyon. Well LADP-4 has an estimated recharge rate similar to that of the dry canyons of Rogers et al. (1995) mentioned above. Finally, it is probably too early to compare the results of R-12 and R-25 to other sites, because of the lack of data needed to complete the analysis. In summary, the Los Alamos canyon wells span the range from drier conditions to wet canyon conditions in a manner that is consistent with our current conceptual model for recharge on the Pajarito Plateau.

2.3 Conclusions

We have found considerable variation within analyzed core samples from wells designated as part of the Otowi strata. The variations are sufficiently systematic that individual wells can be identified by their parameters by an algorithm we have described this Section. This result casts doubt on the approach that prediction of an unknown well's properties, selected at random from the plateau, can proceed by assuming unknown properties are mean properties without consideration of the possible deviations. On the other hand, when averaging properties over the plateau for use in a model, deviations

tend to average out. In particular, we have shown that for well R-25 the choice of type of mean measured properties (moisture or suction) leads to two nearly incompatible conclusions as to the value of the hydraulic conductivity. This result simply says that the Otowi member at R-25 cannot be characterized using mean properties and a simple one-dimensional flow conceptual model. Other methods of prediction of properties of an unknown well, not totally relying on mean properties, could be more successful in prediction by matching moisture content versus matric suction within the member well to such curves for other wells.

Better access to existing data would also be helpful. The current effort to catalog and warehouse hydrologic data in a central database will correct this problem in the future.

Finally, we have shown that the observed moisture flux for well LADP-3 is consistent with our log average of properties over depth. We have also discussed the existence of a possible porous barrier in a well R-12 core above the Otowi member. The highest hydraulic conductivity we found is for well LAOI-1.1, which is 0.8 to 4 orders of magnitude higher than other values in the table. This value appears to be correlated to high recharge rate in the vicinity of the Guaje Mountain fault. The four methods used to compute this conductivity resulted in values that differed by a factor of forty. The largest value used averaged quantities for the hydrodynamic parameters. The reported value used recently discovered data which permitted more accurate determination of the effective saturation and an assumed value of N=1.8 based on one fit. Of the newly analyzed wells, LAOI-1.1, LADP-3, and R-12 are located in or near canyons; LADP-4 is located away from Los Alamos canyon, and exhibits lower estimated recharge rates than the canyon wells. Therefore, this compilation supports the basic conceptual model of recharge on the Pajarito Plateau.

3.0 Stratigraphic model and grid generation

To ensure an accurate reflection of our current state of understanding of the hydrogeologic system, the geologic framework model is the basis for defining the geologic material geometries that the computational grids are required to honor. A two and three-dimensional grid, representing portions of Los Alamos Canyon, are created for the two groundwater flow and transport models described in this report. The process for creating each of the computational grids is described below.

3.1 Stratigraphy of the Los Alamos canyon model

Accurate modeling of groundwater flow and transport in Los Alamos Canyon requires the integration of geologic model information with computational grids. EES-1 geologists used Stratamodel to create a three-dimensional geologic framework model for Los Alamos Canyon. The geologic framework model consists of 20 distinct geologic units. This model, developed by geologists in the geology group (EES-1) of LANL's Earth and Environmental Sciences Division is the product of a continuous process of model development and improvement in support of hydrogeologic workplan activities, including the development of numerical flow and transport models such as the present study. The current list of defined stratigraphic units and their accepted designators is listed in Table 6.

TABLE 6. Stratigraphy of the Los Alamos canyon model

Group/Formation	Unit Name	Symbol
Tshirege member of the Bandelier Tuff	Unit 5	Qbt5
	Unit 4	Qbt4
	Unit 3	Qbt3
	Unit 2	Qbt2
	Vapor-phase altered member of unit 1	Qbt1v
	Glassy member of unit 1	Qbt1g
	Tsankawi Pumice	Qbtt
Cerro Toledo Interval of the Bandelier Tuff	Cerro Toledo	Qct
Otowi member of the Bandelier Tuff	Otowi member ash flow	Qbof
	Guaje Pumice bed	Qbog

TABLE 6. Stratigraphy of the Los Alamos canyon model

Group/Formation	Unit Name	Symbol
Puye Formation	Puye fanglomerate	Tpf
	Totavi lentil	Tpt
Cerros del Rio Basalts	Basalt 4	Tb4
	Basalt 3	Tb3
	Basalt 2	Tb2
	Basalt 1	Tb1
Tschicoma Formation	Tschicoma Latite	Tt2
	Tschicoma Dacite	Tt1
Santa Fe Group	Chaquehui (volcaniclastic) aquifer unit)	Tsfuv
	Santa Fe Group undifferentiated	Tsfu

Figure 18 shows a two-dimensional cross section of the model, illustrating the complexity of the current conceptualization of the subsurface. Figure 19 depicts the full three-dimensional model stratigraphy.

3.2 Two-dimensional grid generation process

For the two-dimensional computational grid, the first step in the process is to identify and define the domain of the computational grid. The western boundary of the two-dimensional grid is located at New Mexico (NM) state plane coordinates (492916.5, 541257.7), just west of the Omega Bridge. Note that all State Plane coordinates are specified in meters. The eastern boundary extends in a one-dimensional fashion from the western boundary to a coordinate location of (502959.6, 539688), just west of the intersection of State Route (SR) 4 and New Mexico State Highway (NMSH) 502.

In the two-dimensional model, the extent of Los Alamos Canyon is represented by drawing a one-dimensional line as closely as possible down the center of the canyon. To do this, the length of the canyon was traced from the western to the eastern boundary using a digital topographic map as a reference in Stratamodel (See Figure 19). To account for the bends in Los Alamos Canyon, the one-dimensional line consists of eight

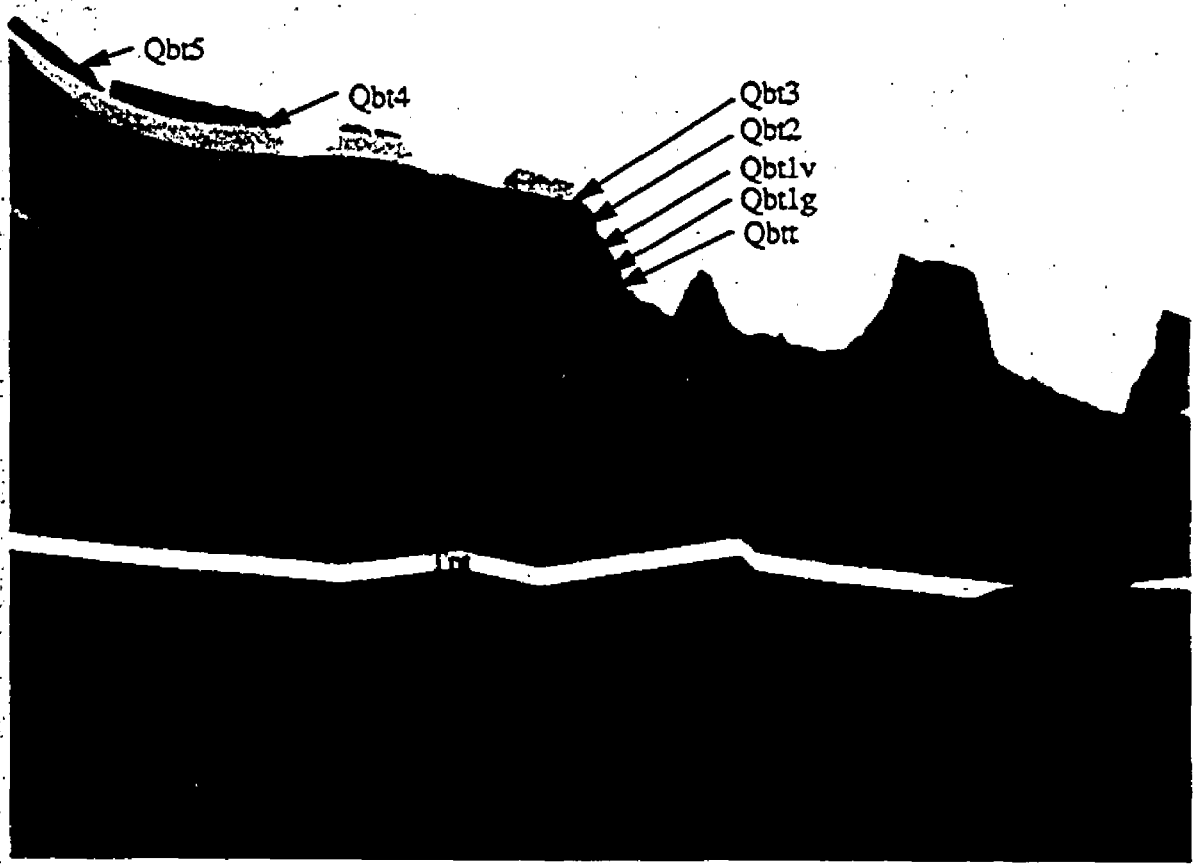

FIGURE 18. Two-dimensional cross section through the stratigraphic framework model for Los Alamos canyon

FIGURE 19. Geologic framework model for the Los Alamos canyon model study area

segments and nine vertices (See Table 7 and Figure 19). Since three points are needed to

TABLE 7. Starting and ending points of line segments comprising cross-sections extracted from the geologic model in State Plane Coordinates (Meters).

Segment Number	Start (x, y)	End (x, y)
1	492916.5, 541257.7	494470.9, 541090.1
2	494470.9, 541090.1	495065.3, 540861.5
3	495065.3, 540861.5	496497.9, 540754.8
4	496497.9, 540754.8	496924.6, 540617.7
5	496924.6, 540617.7	497518.9, 540587.2
6	497518.9, 540587.2	498722.9, 540267.1
7	498722.9, 540267.1	499439.2, 540419.5
8	499439.2, 540419.5	502959.6, 539688

define a plane, an additional point is added to the line segments, on the z axis, below one of the known points to create a plane that is aligned to the x,z axis (See Figure 20). Planes are created for each of the eight line segments, representing the eight regions of Los Alamos Canyon (See Figure 21).

The next step is to translate the geologic model, using a utility program called strat2avs, converting the element-based Stratamodel into an element-based Advanced Visualization System (AVS) formatted grid file. The eight planar regions of Los Alamos Canyon

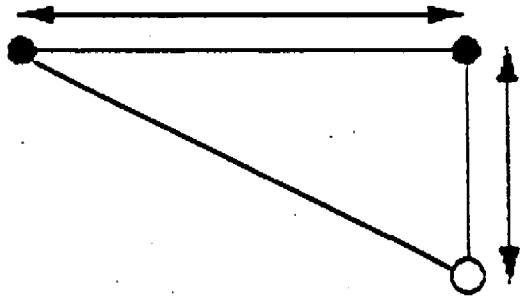

FIGURE 20. Schematic of three points in space to define planes of the two-dimensional model

are extracted from the three-dimensional geologic model individually, using strat2avs. The strat2avs code preserves the original Stratamodel geometries and layer truncations so that each planar region defines a two-dimensional cross section of the Canyon bottom. The adjacent two-dimensional cross-sections (x,z plane) are merged edge-to-edge to form one continuous two-dimensional non-planar surface for use in the grid generation code LaGrit, similar to a geologic fence diagram running the length of the Canyon bottom (Figure 21).

For flow and transport modeling using the Finite-Element Heat- and Mass- Transfer Code (FEHM), the two-dimensional non-planar grid must be converted into a planar grid (Figure 21). The adjustment of the non-planar two-dimensional grid to a planar grid is achieved by translating the original coordinates to a relative coordinate system, so that the non-planar surface can be aligned along a line with a y value equal to zero. This process is akin to straightening the original fence so that all segments fall on a single plane, and the resulting x coordinate becomes the distance along the canyon. The original x, y, and z coordinates are copied into three new attributes that will be used later in the grid generation process to help correlate translated coordinates to the original NM state plane coordinate system of the grid. The original x and y coordinates are translated from a NM state plane coordinate origin point at (492916.5,541257.7), the location of the first point in segment 1, to a relative coordinate system with a new origin at (0,0).

With the new origin at (0,0), the two-dimensional grid is rotated eight times by calculating the angle between the line defined as having a y value equal to zero and each point where the segments comprising the non-planar grid were joined together (See Figure 4). When the last rotation is finished, the y coordinate values are reviewed and their proximity relative to zero is evaluated. The y-coordinate values were found to be within 10^{-8}

FIGURE 21. Two-dimensional model geologic framework before and after placing along a constant x axis

of zero, an acceptable tolerance level, indicating that all of the y-coordinates are set equal to or very close to zero. Once the translation is complete the x, y, and z coordinate values are converted from feet to meters.

An important part of the grid generation process is to insure the quality of the two-dimensional planar grid. Numerous activities are performed to insure grid quality and usability in flow and transport calculations. The first is to identify and remove zero-volume elements, those that contains no volume or thickness. Zero-volume elements occur when nodes that are vertically adjacent to each other in the element are coincident or have the same z elevations. Zero volume elements were introduced into the two-dimen-

sional grid when the planes defining the grid were extracted from the stratigraphic framework model. The planes cut an edge of the hexahedral (cube) elements comprising the three-dimensional geologic framework at a grazing angle producing zero volume elements in the extracted two-dimensional grid. The LaGrit code is used to query the grid to identify and list element numbers of the zero-volume elements. Four zero-volume elements were found in the Los Alamos Canyon grid. Generalized Mesh Viewer (GMV), visualization software, is then used to identify the locations of the zero-volume elements. They are then removed manually if they are located in a position that has no impact on the overall geometries of the grid. The zero-volume elements for Los Alamos Canyon are located on the top exterior edge of the grid, and it was determined that removing them from the grid would not adversely affect the representation of the geology.

Another activity performed to insure grid quality is to eliminate unwanted artifacts and sharp pinch-outs. Unwanted artifacts primarily consist of sliver elements that were introduced during the geologic model building process when geologic surfaces become truncated instead of continuously extending across the grid. By viewing the grid in GMV, the sliver elements are identified and examined, and are manually reassigned material numbers to make them part of a larger adjacent unit (see Figure 22). Sharp angular pinch-outs are eliminated because they significantly increase the number of nodes produced during subsequent stages of the grid generation process. Elements representing sharp angular pinch-outs are identified and reassigned to a larger adjacent unit, resulting in blunt vertical pinch-outs in the unit of interest. Unwanted artifacts and sharp pinch-outs must be eliminated from the grid in order to compile an accurate list of materials that comprise the grid (See Figure 23). Materials with thickness measurements that are substantially smaller than other materials are reassigned to adjacent materials that have larger thickness measurements. This will insure grid quality and decrease the size of the grid by preventing the addition of unnecessary nodes when parts of the grid are refined.

At this stage of the grid generation process, we identify and then consolidate and/or remove materials in the grid that are not important for computational flow and transport calculations. Construction of the geologic framework model introduced numerous geologic material layers that were labeled as different materials but were in fact the same or "equivalent" materials. Equivalent geologic materials in the computational grid are consolidated and reassigned a unique material number. Materials that are part of the topographic surface and not part of the canyon bottom are manually identified and removed from the two-dimensional grid. These materials occurred in the grid because line segments that comprised the two-dimensional grid only approximated the actual canyon bottom and in some cases they cut across portions of the sloped topographic surface. Materials that are located below the water table are also removed from the two-dimensional grid. The final list of materials for the grid is complete when consolidation and removal of unnecessary materials is accomplished.

Once the final list of materials is compiled, the overall distribution of the nodes within the grid is enhanced to improve computational efficiency. A node-position smoothing algorithm in the LaGrit grid generation software is used to reposition nodes, which in the process decreases the total number of nodes that define the geometries of the materials. Repositioning and decreasing the number of nodes produces a better distribution of those nodes that do not make up surfaces sharing common boundaries (non-interface

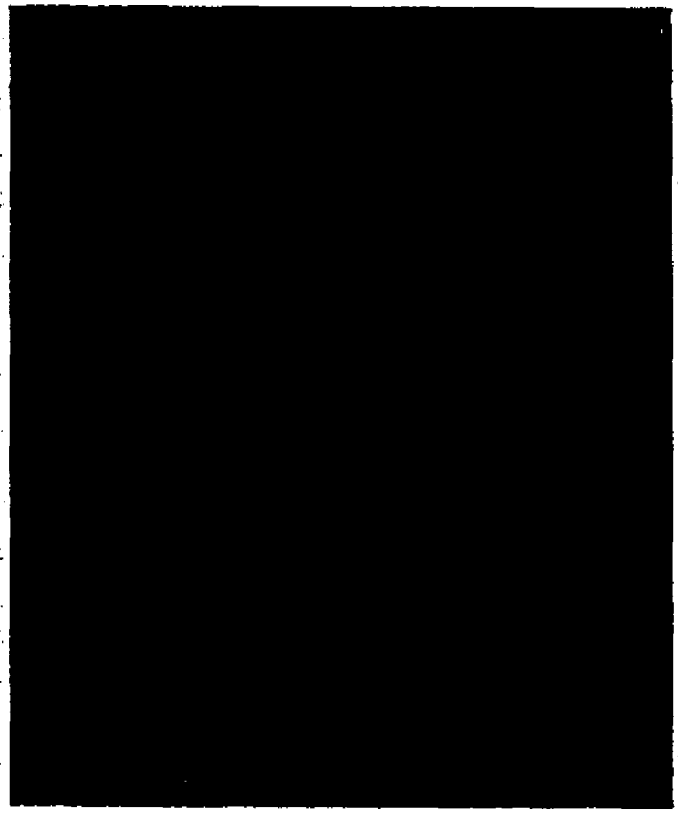

FIGURE 22. Representation of sliver elements during the grid generation process

nodes). The improved distribution decreases the ratio of width to height (aspect ratio) of elements within the materials comprising the grid. The computational efficiency of the grid is increased significantly after using the LaGrit smoothing algorithm (see Figures 24 and 25 for an illustration of node distributions before and after smoothing).

When the enhancement of node distribution is complete, appropriate grid resolution is determined and the grid is globally de-refined and refined. To do this, we methodically review and adjust the resolution of each material in the grid through a step by step process. Part of this process involves tailoring the grid for the study at hand. For example, because of the importance of the Guaje Pumice bed and its interface with the Puye Formation, high resolution was required there. With modeling requirements established, the entire grid is de-refined based on the measure of an element's edge length. The parameters for each material in the grid are determined by manually measuring each material using GMV. The grid is globally refined to obtain the resolution needed to model flow and transport for materials that require significant refinement. A value of 20 meters is used for the global refinement of all of the materials in the grid (see Figure 26).

FIGURE 23. Representation of thin hydrogeologic units during the grid generation process

The next step in the de-refinement and refinement process is to refine all the materials in the grid. The materials that require the highest level of refinement or resolution are refined, followed by refinement of materials that need a lower level of resolution. Refinement steps are carried out until all of the units are refined to the appropriate level. To insure that extra nodes are not created during this process, materials with elements requiring lower resolution that are adjacent to materials with elements requiring higher resolution are de-refined using the value of 20 meters to retain the initial level of refinement performed on the grid (See Figure 27).

The finite volume computational formulation of the FEHM code requires that all angles that are greater than 90 degrees (obtuse angles) be removed. The final step in the grid generation process is to identify and remove elements that have obtuse angles. Obtuse angles are eliminated by an automated algorithm in LaGrit.

When all grid generation processes are complete, overall grid quality is checked by performing a review of the grid elements to verify that grid element volumes, aspect ratios, and node attributes are accurate, based on the actions performed throughout the grid generation process. When the grid verification is complete, the applicable data files are written in a format compatible for use as input to FEHM. The final version of the two-dimensional grid for Los Alamos canyon consists of 57,004 nodes,111,256 tetrahedral elements, and contains 11 materials (See Figure 28).

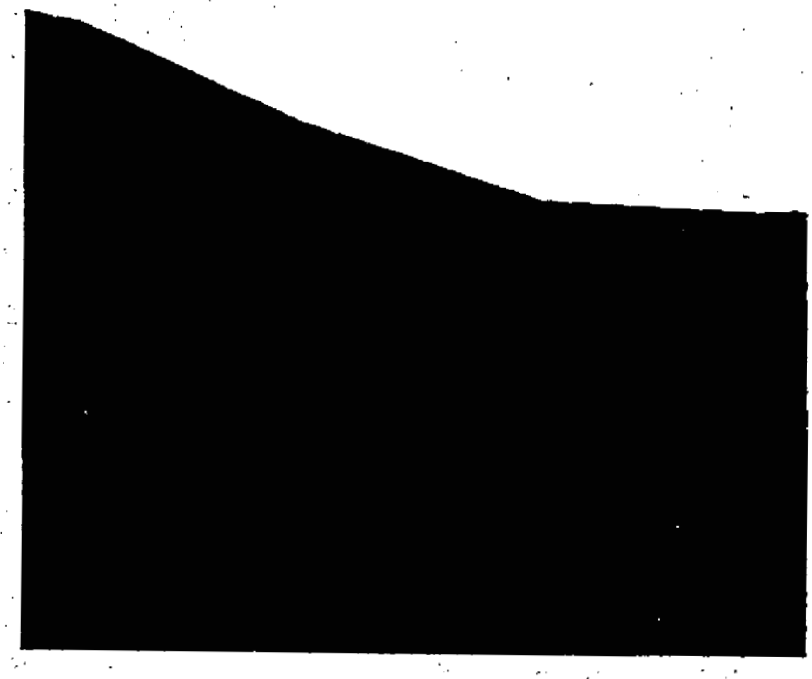

FIGURE 24. Node positions before smoothing in the two-dimensional grid generation process

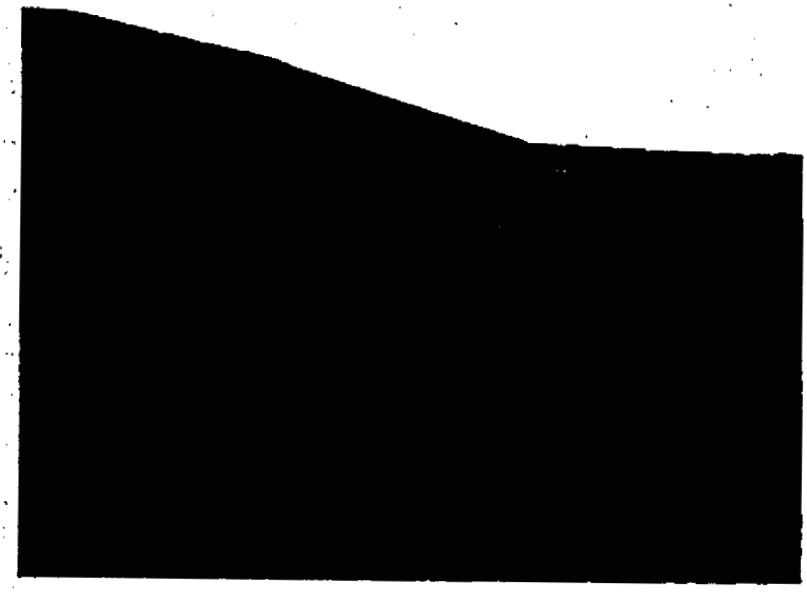

FIGURE 25. Node positions after smoothing in the two-dimensional grid generation process

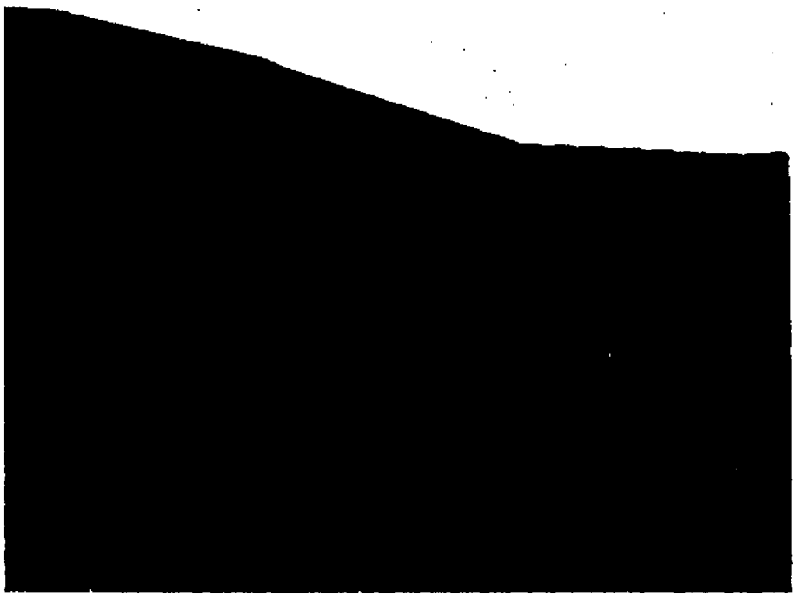

FIGURE 26. Node positions after global refinement to a level of 20 m.

3.3 Three-dimensional grid generation process

As with any numerical model development, the process to create a three-dimensional computational grid for Los Alamos Canyon begins with the selection of the model domain. For the three-dimensional Los Alamos Canyon grid the model domain was selected by understanding historical information about contaminant releases and important sites along the canyon that may be relevant to contaminant transport issues in the canyon. It is deemed necessary that areas such as TA-21, TA-2 (the Omega West reactor), DP canyon, and well R-9 be within the domain of the three-dimensional grid. The Los Alamos canyon model domain is rectangular in shape and encompasses most of Los Alamos canyon, DP canyon, and some of the adjacent mesas to the north and south of Los Alamos canyon. The model domain extends from the topographic surface to a depth

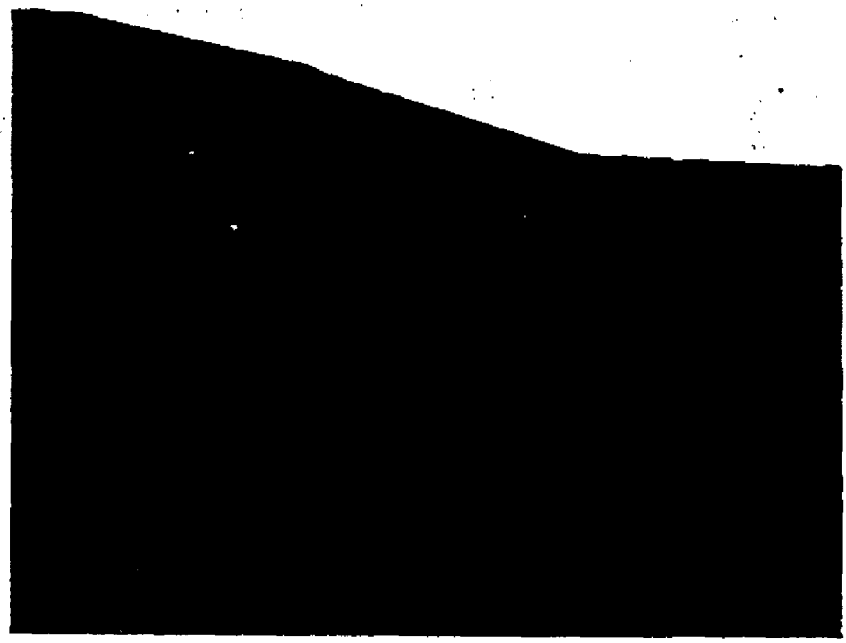

FIGURE 27. Section of the two-dimensional grid after refinement to capture the Guaje Pumice bed.

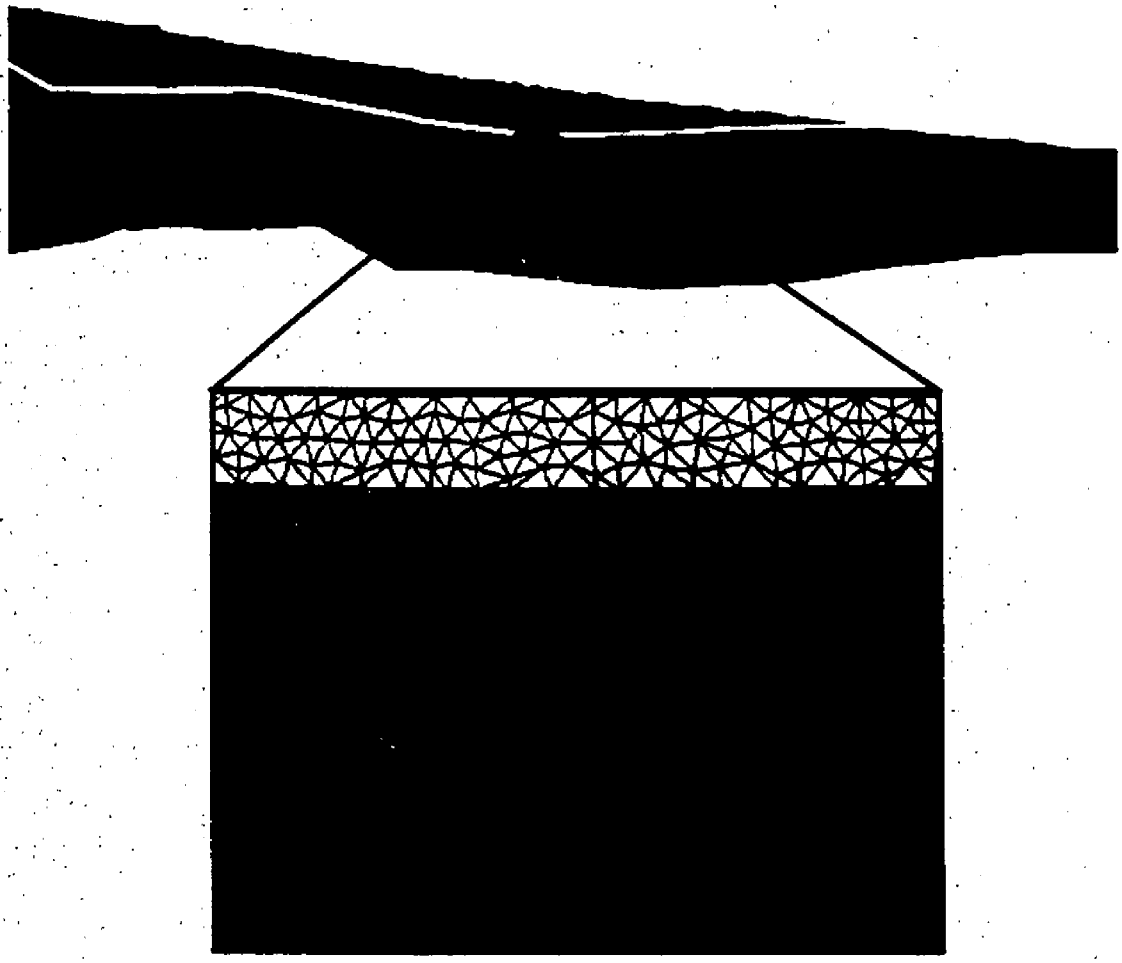

FIGURE 28. Final two-dimensional grid for Los Alamos canyon

of 1650 meters (See Table 8). Within this grid, we capture both the mesas and the can-

TABLE 8. Model Domain for Three-dimensional grid in State Plane Coordinates (Meters)

Grid Dimension	Minimum Extent	Maximum Extent	Difference
X	West: 494,450.0	East: 503,650.0	9200.0
Y	South: 539,550.0	North: 541,550.0	2000.0
Z	Bottom: 1650.0	Top: 2250.0	600.0

yon in the same grid, so that recharge boundary conditions and contaminant releases can be applied correctly. One of the major constraints on the grid building process is to keep the total number of nodes as low as possible but, at the same time ensure that there is adequate resolution in the areas of interest (See Figure 29).

The next step is to select the initial point distribution/resolution for the nodes of the underlying base computational grid. Further refinement, described below, is made from this initial point distribution. The initial point distribution is dependent on the resolution required to capture the various sections of the model and adequate, after refinement, to capture geologic features. For the purposes of this numerical model, the horizontal resolution on the mesas and upstream of contaminant release sites was chosen to be coarse, whereas greater node resolution was applied in the canyon bottoms. An initial grid resolution of 100 meters is used for the horizontal and 40 meters for the vertical (see Figure 30 for a schematic of the base grid before refinement).

Once an initial point distribution for the grid is established, increased resolution is applied along the canyons. A polygon is defined that encompasses areas in the canyon that require more resolution (Figure 29). A technique called Octree Mesh Refinement (OMR) is used to refine elements with at least one node that falls within the polygon. These elements are given four times the initial resolution in all dimensions. OMR allows for the refinement of the node resolution within the canyon bottoms while leaving the initial node distribution in other areas. After applying the OMR technique the X and Y cell resolution is 25 meters and the Z cell resolution is 10 meters (see Figure 31 for a schematic picture of the grid at this stage).

Once the OMR method is used and a desirable point distribution is achieved for the grid, the next step in the process is to read in all of the geologic surface information from the geologic framework model using strat2avs. The geologic surfaces read into LaGriT to identify which elements and nodes belong to the various geologic units using a series of logic commands. The elements are hexahedral when the geologic materials are assigned. When the hexahedral elements are divided into tetrahedral elements and some geologic materials are removed, all of the tetrahedral elements composing the original hexahedral element are removed as well. This method was developed because if only one or two tetrahedral elements were to be removed, then holes would appear in the grid that would cause numerical problems with flow and transport calculations. Therefore, once hexahedral elements and nodes are identified, the AMR grid is converted into a tetrahedral grid. Although this tetrahedral grid does not satisfy all criteria for grid quality, it can be used to set the correct geologic materials. Since equivalent materials in the

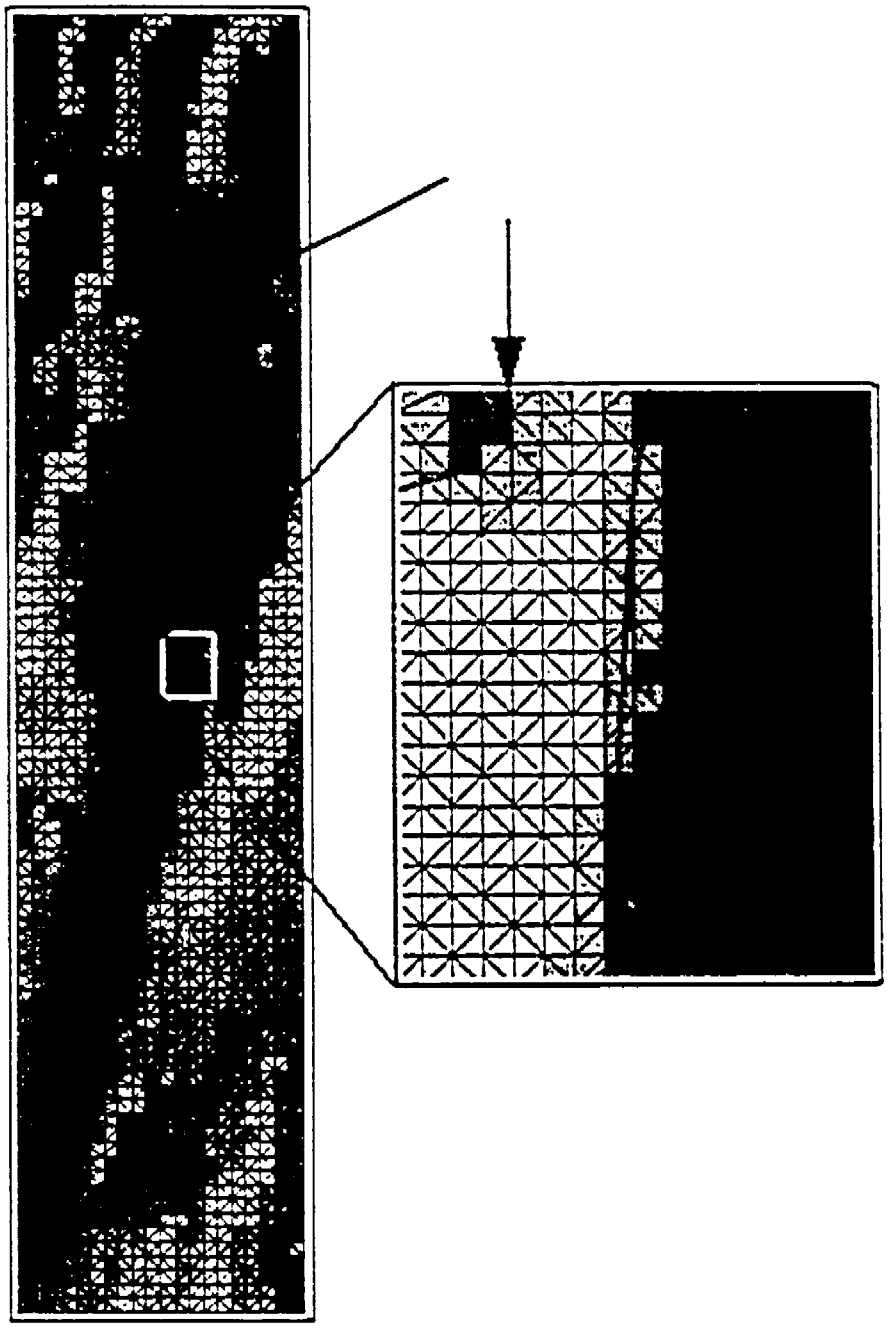

FIGURE 29. Plan view of three-dimensional grid showing the areas of enhanced grid resolution along Los Alamos and DP canyons.

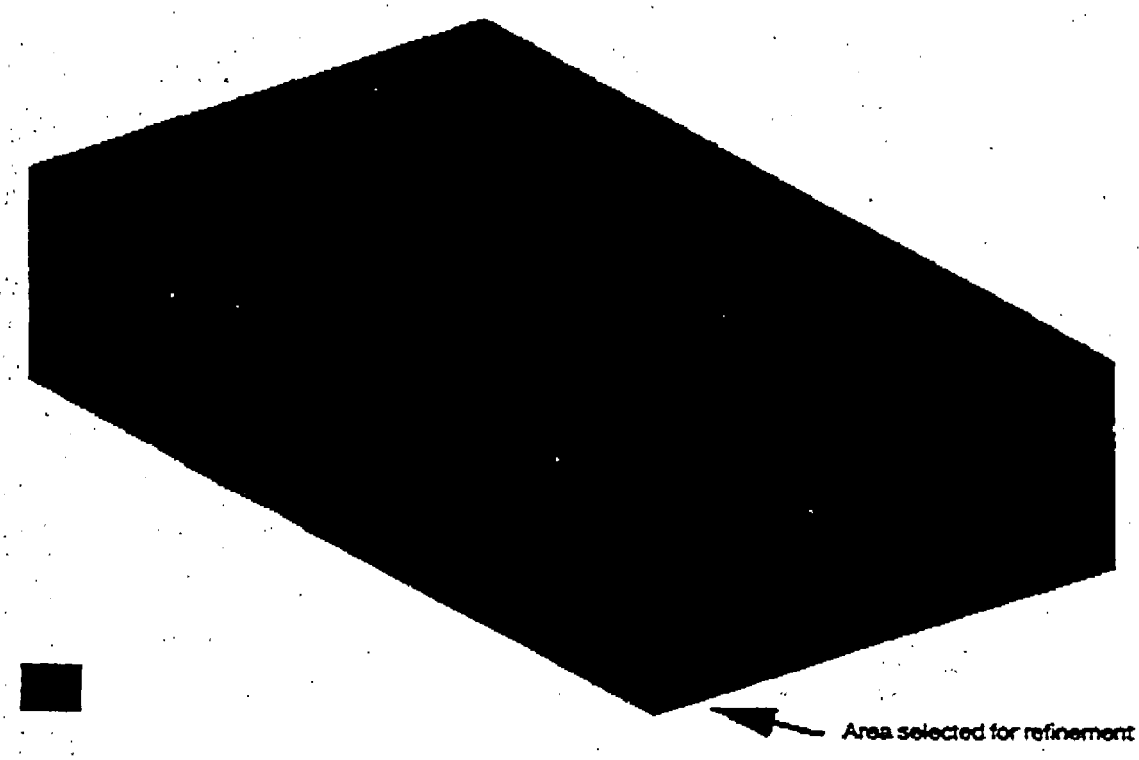

FIGURE 30. Schematic of the base grid in the OMR grid refinement process.

geologic model building process are artificially broken out into separate materials they are recombined at this point in the grid generation process.

A parallel process to the one listed above starts with the OMR grid produced after running the OMR commands on the initial point distribution. The nodes are copied and are reconnected to establish an element connectivity using a command in LaGriT to ensure a Delaunay grid. At this point in the grid generation process there are two different grids, one which has the elements identified with the correct geologic materials, and another that is a Delaunay grid but without geologic materials established. Because the former grid has the correct element materials set, it is used as a source to interpolate the element materials and set elements correctly on the Delaunay grid. The algorithm in LaGriT loops through each of the elements in the sink grid, computes the centroid of the sink element, finds the element of the source grid this point is inside, and assigns the sink element the material value from the source grid element. After the interpolation procedure occurs the non-Delaunay grid is no longer used in the grid generation process.

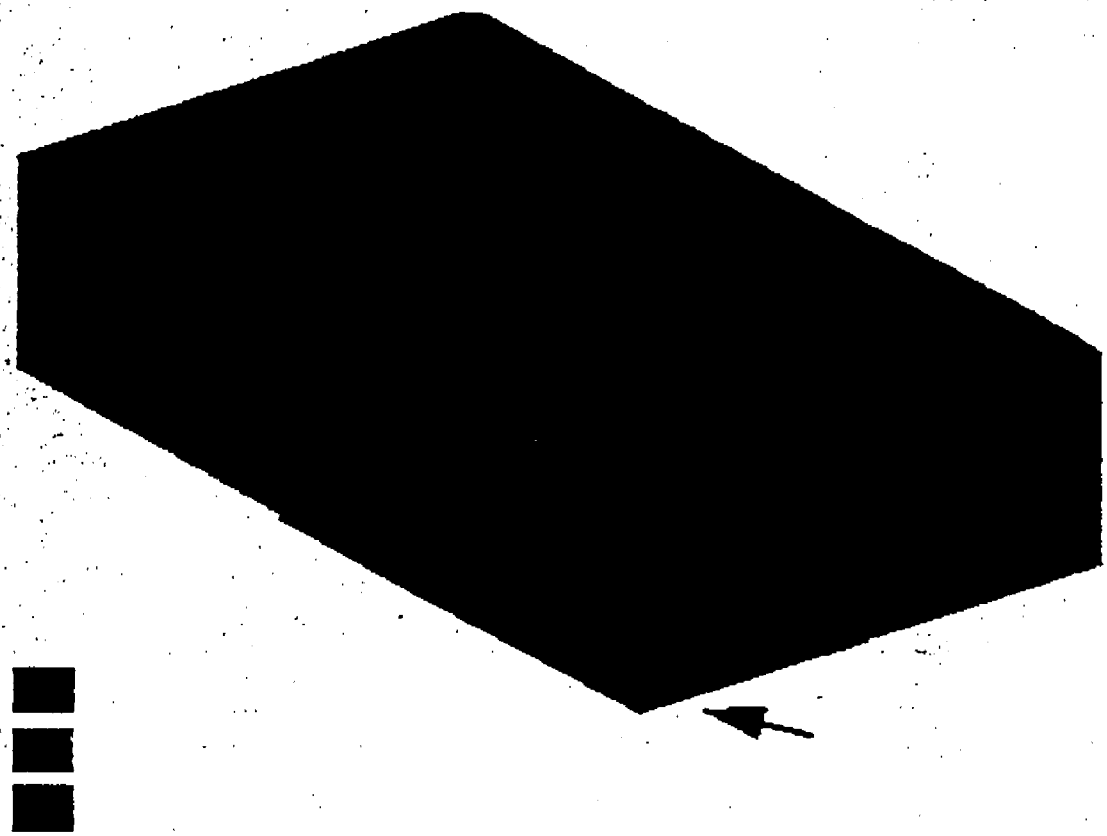

FIGURE 31. Schematic of the grid after refinement using the OMR grid refinement process.

At this point it is possible to remove all of the elements that are identified as being above the topographic surface. Then, the geologic surfaces must be re-read into LaGrit to establish the correct node materials for the grid. Once the nodes are correctly identified, LaGriT is used to create all of the files required by FEHM for flow and transport computations. The final grid, shown in Figure 32, is a three-dimensional grid that is composed of 301,436 nodes, 1,688,457 elements, and 14 unique materials.

3.4 Relative merits of the two- and three-dimensional grids

The purpose of developing both two- and three-dimensional grids is to take advantage of the properties of each to perform various flow and transport model analyses. A major advantage of two-dimensional grids is the smaller number of nodes and elements. Calculations run very quickly, making the grid appropriate for scoping calculations and sensitivity studies. When very high spatial resolution is required, two-dimensional grids are also necessary. However, since the grid is two-dimensional, there are limitations as to what spatial variability of flow properties can be captured in the model. In tow-

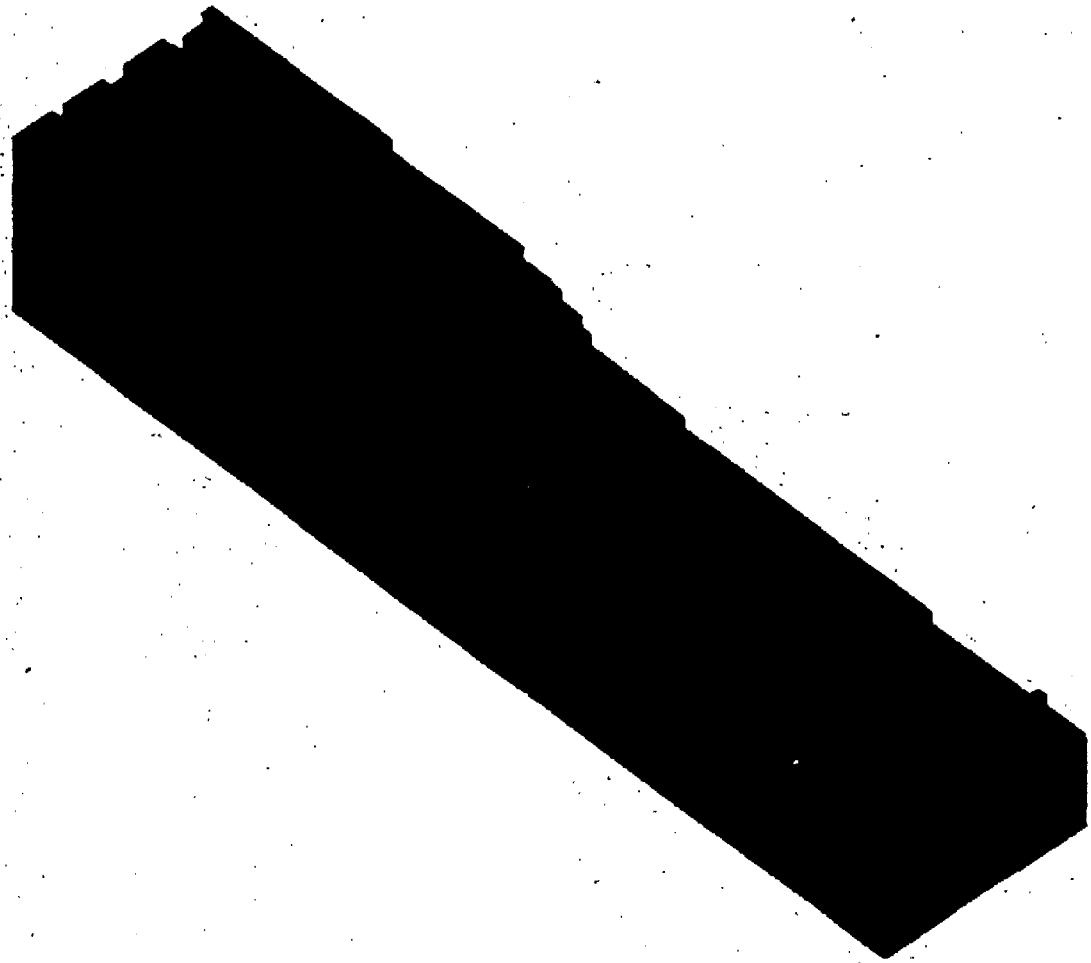

FIGURE 32. Final three-dimensional computational grid for Los Alamos canyon

dimensional simulations, the model domain implicitly assumes that flow is negligible in the direction normal to the grid.

This problem is relaxed in the three-dimensional grid, at the cost of greater computational times and a somewhat reduced grid resolution. With respect to grid resolution, an advantage of the OMR technique is the control over node distribution. In a typical orthogonal finite difference grid, an entire row, column or layer is refined. With the OMR refinement algorithm, there is a smooth transition from coarse elements and refined elements, resulting in a grid with excellent computational properties using a minimum number of nodes.

With respect to the grid generation code itself, another advantage of the OMR algorithm is that it is readily parallelizable, allowing grids to be generated on multi-processor computers. This decreases the time required to create the grids.

4.0 Summary of Water Budget Study for Los Alamos Canyon

This section summarizes the water budget study of Gray (1997), who provides estimates of the fluid recharge into the subsurface rocks under Los Alamos canyon, below the alluvium/bedrock interface. This study, with experimental data collected over a three-year period from 1995 to 1997, allows for a detailed estimate of the ultimate disposition of water entering Los Alamos canyon. We summarize the measurements and model results of this study because it forms the foundation for arguably the most important model input, namely the recharge rate. The water flux entering the deep vadose zone controls the water contents and percolation fluxes in the model, and hence will exert a strong control on the flow and transport modeling. For more detailed discussions of this work, see Gray (1997).

4.1 Conceptual Model for water budget

Gray's work focuses on the water budget and fluid flow in the surface water stream and shallow alluvial aquifer in Los Alamos canyon. The fundamental model equation used to evaluate the water budget is:

$$I = P - R - ET - \Delta S \qquad \text{(EQ 7)}$$

where I is infiltration, P is precipitation, R is runoff, ET is the evapotranspiration term, and ΔS is the change in fluid storage. Since there was no experimental basis for estimating ΔS, Gray assumes it to be zero, listing it as an uncertainty in his analysis. Given this assumption,

$$I - P - R - ET \qquad \text{(EQ 8)}$$

The water budget calculations employed data from a several sources, briefly summarized below. Details can be found in Gray (1997).

Meteorological data. LANL Meteorology Group (ESH-17) and the U. S. Department of Agriculture Bureau of Natural Resources Conservation. Five precipitation measurement stations were used to collect the precipitation and snowpack data. Then, at one of these stations, data on latent heat energy flux were also collected. This method measures wind velocities and humidity in an attempt to estimate the potential for evaporative loss of water (a portion of the ET term).

Streamflow data. LANL Environmental Surveillance Group ESH-18. Three streamflow gages were instrumented to provide estimates of surface water flow rates. These data were used by Gray in both an overall water budget for the canyon and a detailed water budget calculations.

4.2 Annual Water Budget Results

Figure 15 of Gray (1997) shows the results from the overall water budget performed for Los Alamos canyon. The key result from this aspect of Gray's work is the estimation of the relative amounts of ET, runoff, and recharge to the deeper vadose zone. Over the three-year period of that study, Gray found that 71% to 83% of the water introduced into Los Alamos canyon was lost to evapotranspiration. Gray points out the many limitations and uncertainties in this estimate. Given the direct influence of this term in the water budget indirectly on recharge rate, a more comprehensive study of the *ET* processes is warranted. Most of the rest of the water not undergoing evapotranspiration is estimated to be recharging the deeper vadose zone, whereas runoff was found to be relatively small. Average recharge rates applicable to the Los Alamos canyon watershed were found to range from roughly 100 to 200 mm/y for the period of study. These values are average values for the watershed, and might be expected to be higher locally directly beneath the stream channel.

4.3 Detailed Water Budget Study

In addition to the overall water budget, Gray (1997) conducted a detailed study using measured data and a numerical model to further break down the components of the water balance. A calibrated numerical flow model of the alluvial aquifer was developed to analyze the spatial and temporal distributions of recharge in the canyon. Gray divided the canyon alluvial aquifer model into nine zones that corresponded to locations of the monitoring wells used in the model calibration. The model calibration procedure involved adjusting the drain conductance term that controlled the water flux leaving the alluvial aquifer (and entering the underlying bedrock) to match the water level data. The other terms in the water budget (excepting the storage term) were also included in the model, so that the calibration procedure provides a direct estimate of the spatially dependent recharge rate along the canyon. Table 9 (adapted from Gray, 1997, Table 8)

TABLE 9. Summary of detailed water budget (adapted from Table 8 of Gray, 1997)

Zone	Location	Recharge, mm/y	ET, mm/y	Downgradient loss, mm/y
1	LA Reservoir to 1100 ft east of bridge	714	464	56
2	end of Zone 1 to LAO-C	213	167	223
3	LAO-C to LAO-0.6	566	158	547
4	LAO-0.6 to LAO-0.8	1076	0	148
5	LAO-0.8 to LAO-1	222	195	93
6	LAO-1 to LAO-2	408	28	111

TABLE 9. Summary of detailed water budget (adapted from Table 8 of Gray, 1997)

Zone	Location	Recharge, mm/y	ET, mm/y	Downgradient loss, mm/y
7	LAO-2 to LAO-6	399	93	46
8	State Rd. 4 to Lab Boundary	362	139	19
9	East of Lab Boundary	325	121	0

shows the results of this analysis. The highest recharge rate of 1076 mm/y occurs in Gray's zone 4, corresponding to well LAO-0.8. This well falls in the Guaje Mountain fault zone, and was determined to have a strikingly low water level. This observation, and the numerical model calibrated to it, suggest high recharge in this zone, perhaps due to an enhanced permeability due to fracturing. Zones 1 and 3 also exhibit higher than average recharge. Gray postulates that Zone 3 may be higher because of its proximity to the Guaje Mountain fault, and Zone 1 recharge may be high due to a greater saturated thickness in this portion of the canyon. The rest of the Los Alamos canyon study area exhibited lower recharge rates.

4.4 Application of the Water Budget Study to the Present Model

The recharge values obtained from Gray (1997) in Los Alamos canyon were applied directly to the two- and three-dimensional models. Figure 33 shows the recharge map superimposed above the two-dimensional model domain. Regions of high recharge are captured in the model, most importantly the Guaje Mountain fault zone. The recharge rates so applied in two dimensions are expected to be maximum values, for reasons explained further in Section 6.2. Nevertheless, the spatial dependence along the canyon bottom is defined in each simulation of the present study by scaling the values each by a single constant factor, thereby retaining this spatial dependence in each model run. In three dimensions, the recharge map is applied over the two-dimensional top surface of the model as follows. The model developed here assumes that the recharge occurs along the entire bottom of the alluvial aquifer. Conceptually, even if water travels in a thin ribbon in a stream channel on the surface, the alluvium/bedrock interface should act as a small "basin" where water percolates under the influence of a positive head in the alluvial aquifer. Therefore, we obtained, through digitized renderings of the extent of alluvium in Los Alamos canyon, the areal extent of alluvium along the canyon. We then overlaid this region on the top surface of the three-dimensional model and identified every top node of the grid falling within the region. The appropriate recharge was then applied to each of these nodes.

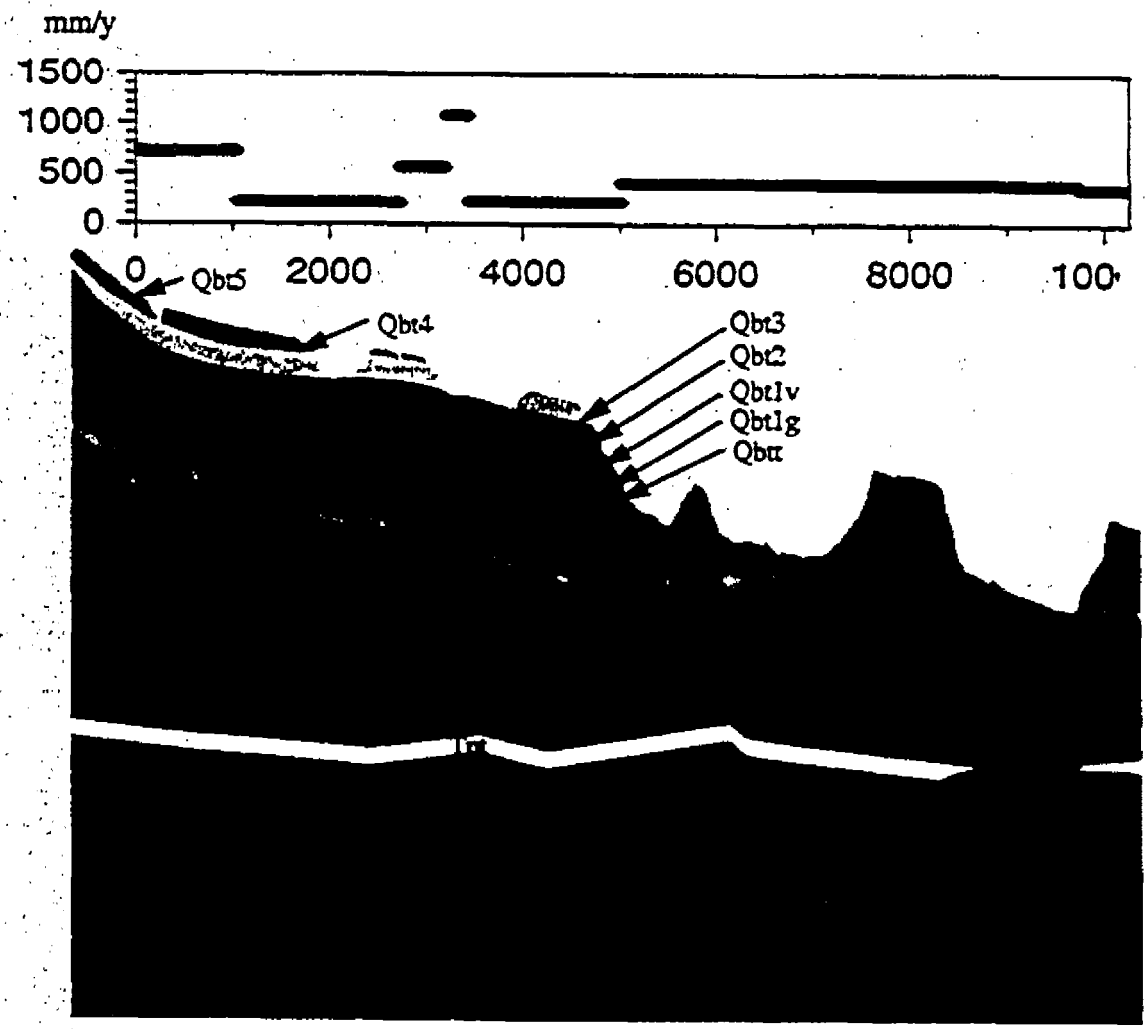

FIGURE 33. Recharge map along Los Alamos canyon in relation to the model stratigraphy. Derived from the water budget study of Gray (1997).

5.0 Contaminant Source Term

Dale and Koch (1999) have compiled a comprehensive history of the major release sites that have led to contaminant releases into Los Alamos and DP canyons. Their report, reproduced in Appendix 1 of the present study, provides the basis for the summary information provided in this section. Since this report focuses mostly on fluid flow and tritium transport, much of the information in the Dale and Koch compilation is not directly used. It's importance will be in the next stage of model development in which the simulation of contaminant transport will be undertaken. We summarize the report here, and refer the reader to the report for further details. Information on tritium concentrations in the alluvial groundwater is used in this study. These data are presented below and used in Section 8.0.

5.1 Contaminant Release Sites

There are a host of possible contaminant source sites for Los Alamos and DP canyons resulting from past and present Laboratory operations. The most important of these for our purposes are:

TA-1 (Townsite). A variety of septic systems, storm drains, and outfalls have introduced contaminants into Los Alamos canyon at the old TA-1 site. Quantities of effluents and concentrations of contaminants are generally unknown. Many of these sites have undergone remediation and cleanup. Suspected contaminants include actinides, fission products, metals, and solvents.

TA-41 (Weapons Development Facility). This site was used, starting in the early 1940's, for nuclear weapons development and long-term studies on weapon subsystems. Storm drainages, a sump pit, an abandoned septic tank, and a sewage treatment plant were operational and possibly introduced contaminants such as actinides and tritium into Los Alamos canyon.

TA-2 (Omega West Reactor Site). This site, located in Los Alamos canyon, was used since 1943 to house and operate a series of research reactors. Early reactors were fueled by aqueous uranyl solutions, whereas other reactors were fueled by solid fuel elements. A variety of contaminants (mostly radionuclides) are suspected to have been released into the canyon. Most relevant to the present study is tritium, which resulted from a leak in the primary cooling water system at the reactor. The leak occurred from a break in a weld seam in a section of the delay line running from building TA-2-1 to the surge tank. This leak was discovered in 1993, and tritium was detected within the Guaje Mountain fault zone. Typical concentrations in the cooling water ranged from 15.7×10^6 to 20.2×10^6 pCi/L. The duration of the leak is not documented, but measurements measurements of tritium concentrations in alluvial aquifer well LAO-1 (located at the eastern boundary of TA-2) suggest that the leak may have begun between November 1969 and January 1970. This reactor was permanently shut down in 1994.

TA-21 (DP Site). A variety of outfalls from treatment facilities and releases from absorption beds have released contaminants from this nuclear materials research and processing facility since the early 1940's. Major release sources include:

- The 21-011(k) outfall, a discharge line that carried treated waste water from industrial waste treatment plants to a discharge point on the south slope of DP canyon from approximately 1952 to 1985. A significant input of tritium is introduced to the Los Alamos/DP canyon system from this source.
- MDA T, four absorption beds that served as seepage pits for the disposal of liquid wastes from plutonium processing operations. Contaminants include, among others, plutonium and ammonium citrate.
- MDA V, an area that comprises three absorption beds used for liquid waste disposal from a laundry operation. These pits were in continuous operation from 1945 to 1961.

TA-53 (LANSCE). Operations from LANSCE have introduced contaminants such as tritium, metals, and variety of radionuclides including plutonium. The primary release sources are identified as PRS 53-002(a and b), a series of three surface impoundments. Two of these, the northern impoundments, were operated from the early 1970's to 1993. Both were designed as clay-lined retention ponds, but they frequently filled to capacity and had to be discharged.

5.2 Tritium release information for Los Alamos Canyon

For the purposes of this study, tritium is the contaminant of greatest interest. Clearly, because of the complexity of the multiple release sites, and the uncertainty of some of the releases, such as the Omega West Reactor leak, quantification of the tritium input to the subsurface cannot be accurately estimated through recorded discharges and processing documentation. Fortunately, the tritium concentration measurements for alluvial aquifer wells in Los Alamos canyon form a detailed picture of the concentration-time history in this aquifer. Since the conceptual model consists of fluid from the aquifer recharging the deeper vadose zone, these measurements can be used directly to define the tritium mass input to the model. Figures 34, 35, 36, and 37 show the tritium concentration in pCi/L versus time in wells LAO-C, LAO-1, LAO-3, and LAO-4.5, respectively. Each plot has a time 0 of January 1, 1967, and continues to the present time. For comparison purposes, all plots are on the same concentration scale, a log scale from 100 to 10^6 pCi/L. Well LAO-C is located to the west of any major release sites, and is considered to be indicative of background tritium concentrations. As mentioned earlier, well LAO-1 is located due east of the Omega West Reactor, and shows the influence of the reactor leak in its rise to high concentrations in the late 1960's. Downstream monitoring wells LAO-3 and LAO-4.5 undoubtedly see the influence of the reactor leak, but also have their own input sources from TA-21 and possibly LANSCE. In Section 8.1, we show how these data are used in combination with the recharge estimates along the canyon, to set the mass loading of tritium for the transport model.

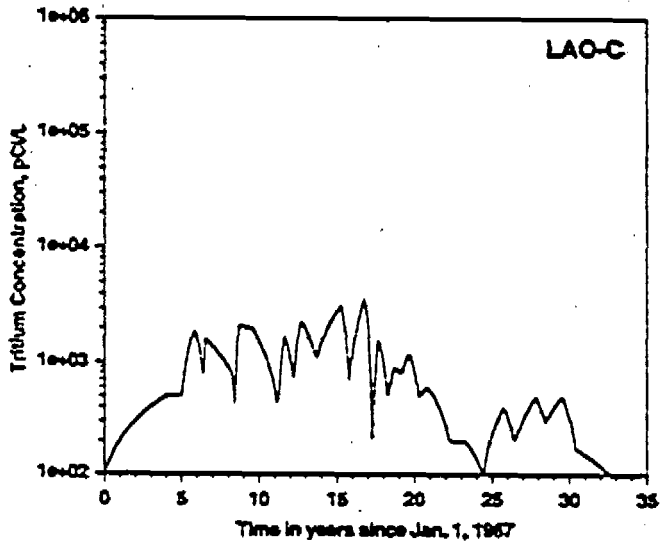

FIGURE 34. Concentration-time history for tritium in alluvial well LAO-C in Los Alamos Canyon.

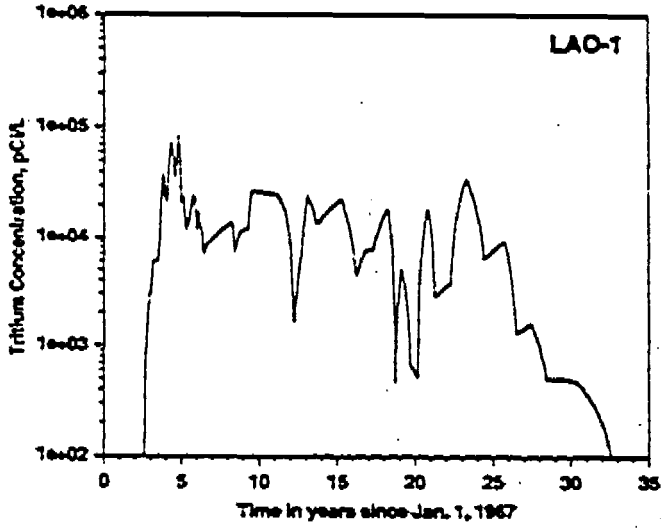

FIGURE 35. Concentration-time history for tritium in alluvial well LAO-1 in Los Alamos Canyon.

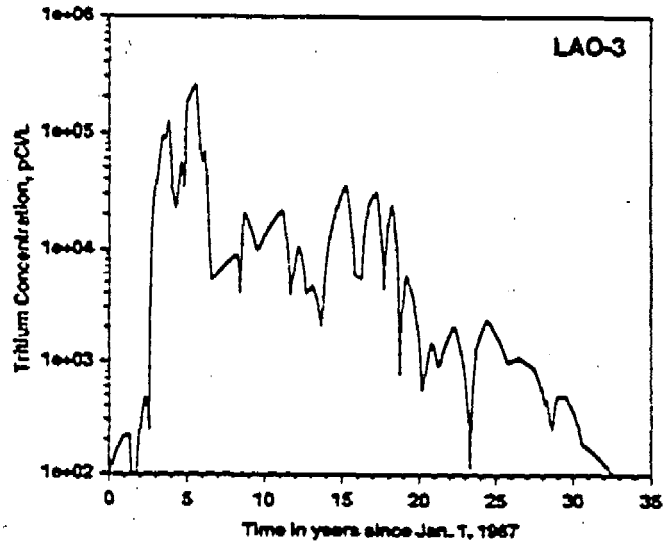

FIGURE 36. Concentration-time history for tritium in alluvial well LAO-3 in Los Alamos Canyon.

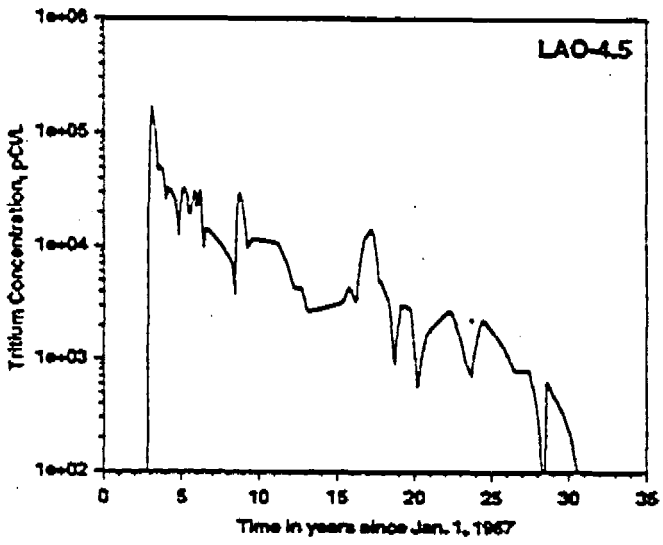

FIGURE 37. Concentration-time history for tritium in alluvial well LAO-4.5 in Los Alamos Canyon.

6.0 Two-dimensional flow model results

In this section we present the results of two-dimensional flow simulations that explore the range of behavior possible given the uncertainties in the hydrologic properties and boundary conditions. Two-dimensional modeling, using the 2D canyon-bottom grid (Figure 28) is used in this section to facilitate the execution of a large number of computations in a reasonable time. Three-dimensional runs performed in the next section examine those issues for which a complete characterization of the three-dimensional system is necessary. For example, an additional observation well (LADP-4) is include in those comparisons that is not present in the two-dimensional model. Nevertheless, sensitivity to many different aspects of system behavior can reasonably be performed in two dimensions.

This section is organized as follows. First, a brief description of the numerical simulator FEHM is provided. Next, specific implementation issues associated with the two-dimensional model are discussed. Then, base case runs are presented, along with comparisons to available well observation data in Los Alamos canyon. These simulations use the base case hydrologic properties given in Section 6.3 and the estimated steady state recharge results abstracted from Gray (1997). Variations in the assumed values of recharge are included to illustrate the sensitivity of the model to recharge. Then, transient simulations are reported that establish the critical time scales over which the model predicts the flow system to change. Transients due to episodic pulses of large quantities of water (run-off or storm events), as well as longer-term transients are examined. This analysis is followed by a study of the sensitivity of the model to variations in hydrologic properties of key hydrologic units. Finally, a new numerical approach for incorporating the influence of thin, low-permeability zones at stratigraphic interfaces is presented, followed by numerical simulation results of fluid flow and potential contaminant pathways. The concept of lateral diversion of water is incorporated into these models. The results of these two-dimensional simulations establish the key sensitivities of the model, and act as a lead-in to the three-dimensional flow and transport model results.

6.1 Finite Element Heat and Mass (FEHM) Model

The Finite Element Heat and Mass (FEHM) code simulates heat conduction, heat and mass transfer for multiphase flow within porous and permeable media, and noncondensible gas flow within porous and permeable media. The code handles model geometries in two or three dimensions, and has a variety of solute transport model options available for use. For details of the fundamental model equations solved by the code, see Zyvoloski et al. (1997).

In the present study we use the flow model option that assumes isothermal conditions. This reduces the computational burden and, for this application, introduces little or no error to the calculated result. In unsaturated media, the relative permeabilities and capillary pressures can be specified using a variety of characteristic curve models. In the present study, we use the van Genuchten (1980) functions due to the fact that the available data have been reduced using this model. The van Genuchten relative permeability functions are described by the following formulae:

$$R_l = \begin{cases} \left[1.0-\left(1.0-\hat{S}^{\frac{1}{\lambda}}\right)^{\lambda}\right]^2\sqrt{\hat{S}}, & \hat{S} < S_{lmax} \\ 1.0, & \hat{S} \geq S_{lmax} \end{cases} \qquad \text{(EQ 9)}$$

$$R_v = 1.0 - R_l \qquad \text{(EQ 10)}$$

where $\hat{S} = \frac{S_l - S_{lr}}{S_{lmax} - S_{lr}}$ and $\lambda = 1 - \frac{1}{n}$, where n is an experimentally determined exponent.

The relative permeabilities R_l and R_v are restricted by the requirement that $0.0 \leq R_l \leq 1.0$ and $0.0 \leq R_v \leq 1.0$. The relative permeability functions are truncated to the appropriate value if the these conditions are violated. The capillary pressure is described by the following equations

$$P_{cap} = \begin{cases} P_{capmax}, & P_{capl} \geq P_{capmax} \\ P_{capl}, & P_{capl} < P_{capmax} \\ 0.0, & S_l \geq S_{lmax} \end{cases} \qquad \text{(EQ 11)}$$

where $P_{capl} = P_0\left[\hat{S}^{-\frac{1}{\lambda}} - 1.0\right]^{1.0-\lambda}$, $\hat{S} = \frac{S_l - S_{lr}}{S_{lmax} - S_{lr}}$, $P_0 = \frac{1.0}{\alpha_G}$, and $\lambda = 1 - \frac{1}{n}$ (n and α_G are experimentally determined parameters).

The van Genuchten capillary pressure curves approach an infinite value as S_l approaches 0 and 1. This requires the use of extrapolation techniques. At low saturations both linear and cubic fits are available. At high saturations a linear fit is used.

Model equations very similar to these are used in the interpretation of water content data in Section 2.2). One difference is that FEHM formulates the water balance in terms of fluid saturation (volume of fluid/volume of void space) instead of volumetric water content. In the numerical model results description below, we post-process all model output by converting fluid saturations to water content to allow for direct comparison with the data.

6.2 Two-dimensional model implementation

The development and use of the stratigraphic model and generation of the two-dimensional canyon-bottom grid was discussed in Section 3.2. In this section, we describe the specific implementation issues associated with setting the flow boundary conditions and other parameters in the model. Recharge along the canyon bottom is a three-dimensional process. In the three-dimensional model, it is relatively straightforward to apply an estimated recharge rate on all grid nodes identified as representing the interface of the alluvium bottom and the bedrock. In a two dimensional model, we implicitly assume that there are no variations in recharge in the third dimension, in this case the horizontal direction normal to the canyon. Because of this approximation, the appropriate flux to be input to the two-dimensional model is not necessarily the value along the canyon bottom. In reality, concentrated recharge beneath the canyon is likely to spread laterally away from the canyon into area above which the recharge is much lower. Therefore, the appropriate recharge to apply to the two-dimensional model is probably less than the value directly beneath the canyon. In this study, we assume that the relative flux entering the subsurface at different location along the canyon remains the same, but the absolute value of recharge is uncertain. To implement the recharge boundary condition, the recharge map of Gray (1997) summarized in Section 4.3 is used to specify the flux versus distance along the canyon as segments of spatially constant recharge rate. These segments were defined based on the location of the alluvial aquifer wells and the numerical modeling studies performed by Gray. In the two-dimensional grid, the grid points along the top of the model are identified within each segment, and the grid generation process determines the area normal to the upper surface of the model (for an assumed 1 m thickness of the two-dimensional model domain) for each node. The required input, the fluid mass flow rate, is then determined for each top node by multiplying the recharge rate by the area.

The bottom boundary condition represents the water table. The water table is estimated from results compiled by Keating (personal communication, 1999). Any node falling below this surface is assigned a value of saturation equal to 0.999 to represent the regional aquifer. Therefore, the vadose zone model domain extends only down to this surface, and the bottom region is simply a boundary condition rather than a calculated result.

Steady state flow model results are obtained by performing a transient flow calculation in which the initial condition is developed based on an educated "guess" of the fluid saturation of the rock, or by using the final state from a previous model run. The details of this process are unimportant because the final state is the only model result used in transport simulations. The model is run to very long times, and a check is performed to ensure that the global mass balance for water is satisfied. In transient flow simulations, the initial state is typically an appropriate steady state model result, and the transient model run is performed at an equation tolerance sufficient to result in small mass balance errors.

6.3 Hydrologic properties

The hydrologic properties of the tuffs and sediments in the numerical model greatly affect the flow and transport behavior predicted in the simulations. In the present study, a variety of variations are made on the base-case properties discussed in this section to

examine the impact of uncertain parameters on the model results. Nevertheless, a base-case set of parameters is required to establish a reference set of hydrologic properties and boundary conditions for use in the model sensitivity studies. Tables 10 and 11 list

TABLE 10. Geologic designators, model unit numbers, permeabilities and porosities for the hydrogeologic units in the Los Alamos canyon model

Hydrogeologic Unit	Geologic Designation	Unit Number in Model - 2D/ 3D	Permeability, m^2	Porosity
Unit 3, Tshirege member	Qbt3	NA/21	1.01e-13	0.469
Unit 2, Tshirege member	Qbt2	NA/20	7.48e-13	0.479
Vitric unit, Tshirege member	Qbt1v	NA/19	1.96e-13	0.528
Glassy unit, Tshirege member	Qbt1g	25/18	3.68e-13	0.509
Basal Pumice unit, Tshirege member	Qbtt	24/NA	1.01e-12	0.473
Cerro Toledo Interval	Qct	23/17	8.82e-13	0.473
Otowi Member	Qbof	22/16	7.25e-13	0.469
Guaje Pumice Bed	Qbog	21/15	1.53e-13	0.667
Cerros del Rio Basalt, Puye	Tb4	19/13	2.47e-12	0.3
Tschicoma basalt	Tt2	17/11	2.96e-13	0.3
Cerros del Rio Basalt, Santa Fe Group	Tb3	15/9	2.96e-13	0.3
Puye Formation	Tpf	14/8	4.73e-12	0.25
Totavi Lentil	Tpt	13/7	4.73e-12	0.25
Santa Fe Group	Tsfuv	12/6	2.65e-13	0.25

TABLE 11. Parameters in the van Genuchten model for unsaturated characteristic curve for each unit

Hydrogeologic Unit	Geologic Designation	Unit Number in Model - 2D/ 3D	van Genuchten α parameter, m^{-1}	Residual moisture content	van Genuchten n parameter, unitless
Unit 3, Tshirege member	Qbt3	NA/21	0.29	0.045	1.884

TABLE 11. Parameters in the van Genuchten model for unsaturated characteristic curve for each unit

Hydrogeologic Unit	Geologic Designation	Unit Number in Model - 2D/ 3D	van Genuchten α parameter, m^{-1}	Residual moisture content	van Genuchten n parameter, unitless
Unit 2, Tshirege member	Qbt2	NA/20	0.66	0.032	2.09
Vitric unit, Tshirege member	Qbt1v	NA/19	0.44	0.009	1.66
Glassy unit, Tshirege member	Qbt1g	25/18	2.22	0.018	1.592
Basal Pumice unit, Tshirege member	Qbtt	24/NA	1.52	0.01	1.506
Cerro Toledo Interval	Qct	23/17	1.52	0.01	1.506
Otowi Member	Qbof	22/16	0.66	0.026	1.711
Guaje Pumice Bed	Qbog	21/15	0.081	0.01	4.026
Cerros del Rio Basalt, Puye	Tb4	19/13	0.1	0.066	2.
Tschicoma basalt	Tt2	17/11	0.1	0.066	2.
Cerros del Rio Basalt, Santa Fe Group	Tb3	15/9	0.1	0.066	2.
Puye Formation	Tpf	14/8	5.	0.01	2.68
Totavi Lentil	Tpt	13/7	5.	0.01	2.68
Santa Fe Group	Tsfuv	12/6	5.	0.01	2.68

the hydrologic properties used in the two- and three-dimensional models developed for Los Alamos canyon. The first table contains permeability and porosity values used for each unit, and the second table lists the unsaturated hydrologic parameters for the van Genuchten (1980) formulation used in the present study for the characteristic curves.

The process for setting or estimating the hydrologic parameters in these tables followed a series of steps, as listed below:

- If measured values are available from core samples, use the mean values for all samples in that unit. The main data source for these parameters is Rogers and Gallaher (1995). All units of the Bandelier tuff are covered in this category, although data are scarce for some units.
- If measurements are not available but a porous continuum representation is appropriate, assume values typical for the type of medium that the unit consists of. Sedimen-

tary units (the Puye formation, Totavi Lentil, and the Santa Fe Group sediments) fall into this category.

- If a porous continuum model is of questionable validity, use an effective continuum approach to capture the role of fractures in an approximate way. In the present study, we have classified the units Tb3, Tb4, and Tt2 in this way. For these units, we assume that the medium can be characterized assuming a low-permeability matrix (assumed to be 1.e-18 m^2) and fractures in capillary-pressure equilibrium with the matrix. For fracture permeabilities (listed in Table 10, as opposed to the rest of the units, for which matrix permeability is listed) preliminary air-permeability measurements in Well R-12 are used to estimate the permeability values. Details of the effective continuum model formulation can be found in Zyvoloski et al. (1997). In essence, the low matrix permeability results in complete saturation of the matrix, with the majority of the water flux traveling through the fractures.

The approach for assigning the hydrologic properties for these units is similar to that of Dander (1997) in his model of Mortendad canyon, and the MDA G model of Birdsell et al. (1999). Parameter values assumed in the present study are in most cases exactly the same as or very close to parameters listed in those reports.

The validity of the continuum model for flow and transport through the Bandelier tuff units is a major assumption that influences the results of this modeling effort. The assumption implies that even when fractures are present, they are either insufficiently connected, or of insufficient capillary suction to keep water in them over long flow distances. The matric potential of the porous tuffs are probably considerably stronger than the fractures, and hence there should always be a driving force for water present in fractures to imbibe into the matrix. The key technical issue, which must be considered to be an open question in the field of unsaturated zone hydrology, is whether the driving force is sufficient to result in a flow process that is dominated by matrix percolation. Field tests being performed at the Nevada Test Site in tuffs similar to those of the Bandelier tuff suggest that fracture flow is difficult to sustain over long distances under unsaturated conditions (Gilles Bussod, personal communication, 1999). Therefore, we tentatively conclude that the model assumption is valid, but await further confirmation from field test results at the Nevada Test Site and elsewhere.

6.4 Two-dimensional base-case flow simulations

In this section, the base-case hydrologic parameters determined from the analysis of available data from all wells on the Pajarito Plateau (Section 2.0) are used to determine the two-dimensional base case flow field. Recharge is mapped from the equivalent steady state recharge map along the canyon bottom developed from Gray (1997) and summarized in Section 4.3. Recall that Figure 33 shows the base-case recharge rate along the canyon bottom alongside the hydrostratigraphic section of the two-dimensional model. As previously discussed, this map is thought to represent a maximum recharge rate that should be applied in a two-dimensional model. Therefore, the sensitivity to recharge rate is examined by scaling each recharge rate by a constant factor less than one. This approach implicitly assumes that the relative quantity of water entering the subsurface at different locations is the same, but the total amount is unknown due to uncertainties in the various terms in the water budget. Total recharge maps varying over an order of magnitude are used in this sensitivity analysis.

Volumetric water contents predicted in the model are compared to measured values in three wells located in Los Alamos canyon: LADP-3 (Broxton et al., 1995), LAOI(A)-1.1 (Longmire, unpublished data, 1999), and R-9 (LANL, 1999). Table 12 shows the

TABLE 12. Coordinate along the canyon for each of the observation wells

Well	State Plane X Coordinate (m)	State Plane Y Coordinate (m)	Coordinate Along Canyon (m)
LADP-3	497735	540553	5673
LADP-4	497792	540934	not in LA canyon
LAOI(A)-1.1	496650	540694	3798
R-9	502384	539754	9665

State Plane coordinates and the "along-canyon" coordinate of each observation well. The water contents predicted by the model are obtained by defining a 15 m wide region centered at its coordinate location and querying the model for the water content of any node falling in the thin region. An additional borehole, LADP-4 (Broxton et al., 1995), is located in DP canyon, and thus can only be used in calibrating the three-dimensional model (Section 7.0). Volumetric water content is chosen as the primary measurement used to evaluate the model results for two reasons. First, adequate data on water content is available from virtually all vadose zone characterization wells, and when combined with hydrologic information, yields important insights on fluid flux through unsaturated rocks (see, for example, Rogers et al., 1995, and Section 2.0 of the present study). Second, although matric suction values could also theoretically be used, data sets are often less than complete, and the accuracy of the field measurements normally used degrades significantly at low values of suction. Therefore, we restrict our attention to the water content measurements. Future updates of this model may incorporate more refined matric suction data from the newer characterization wells.

We begin by displaying graphically the predicted results of the fluid saturation versus position in the two-dimensional model domain. The most obvious affect present in the model result of Figure 38 shows the overriding importance of stratigraphy on the computed fluid saturation. Rocks are differentiated based on hydrostratigraphic characterization and given different sets of hydrologic properties. Therefore, this result is not surprising. The inset in the figure shows the level of detail present in the model. Contrasting fluid saturation with depth over a few meters is present in this model. A characteristic of this two-dimensional model that is different than other models developed for sites on the Pajarito Plateau such as MDA G (Birdsell et al., 1999) and Mortendad canyon (Dander, 1997) is the absence of significant thickness of the Tshirege member of the Bandelier tuff. Los Alamos canyon cuts deeply into the Bandelier tuff such that the Otowi member is the first unit encountered beneath the alluvium in the canyon bottom over much of the model domain. In the eastern portion of the model, the Otowi is not present, and instead the Cerros del Rio (Tb4) is the first unit encountered. This is the case at R-9, where the stratigraphic section consists only of basalts and the Puye Forma-

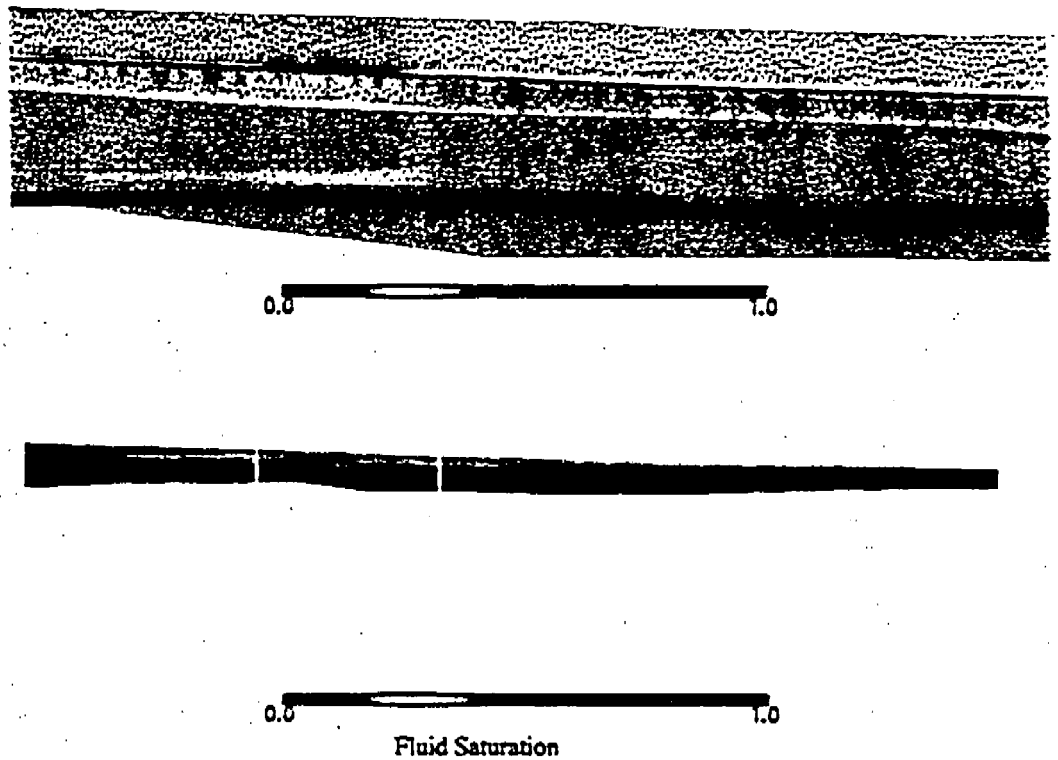

FIGURE 38. Fluid saturation versus position in the two-dimensional, base-case model

tion. Of course, the Tshirege member is present in the three-dimensional model, which captures Los Alamos and DP canyons, and mesas in the model domain.

Quantitative comparisons of model and observations are presented in Figures 39 (LADP-3), 40 (LAOI(A)-1.1), and 41 (R-9). In the figures, the variable *I* represents the base-case recharge map, and the other curves are results for the base map divided by 2, 5, and 10. The LADP-3 results over an order of magnitude in recharge rate generally captures the moisture-content profile of the well, which consists of data points in the Otowi member, including the Guaje Pumice Bed. Both the profile within the majority of the Otowi member and the rise in water content values in the Guaje Pumice Bed are well matched by the simulations. Distinguishing among these recharge rates is beyond the ability of our current data and understanding of key uncertainties, as will be demonstrated in the sensitivity analyses presented in subsequent sections. The right hand plot in Figure 39 shows the predicted and measured water content profile of the entire depth

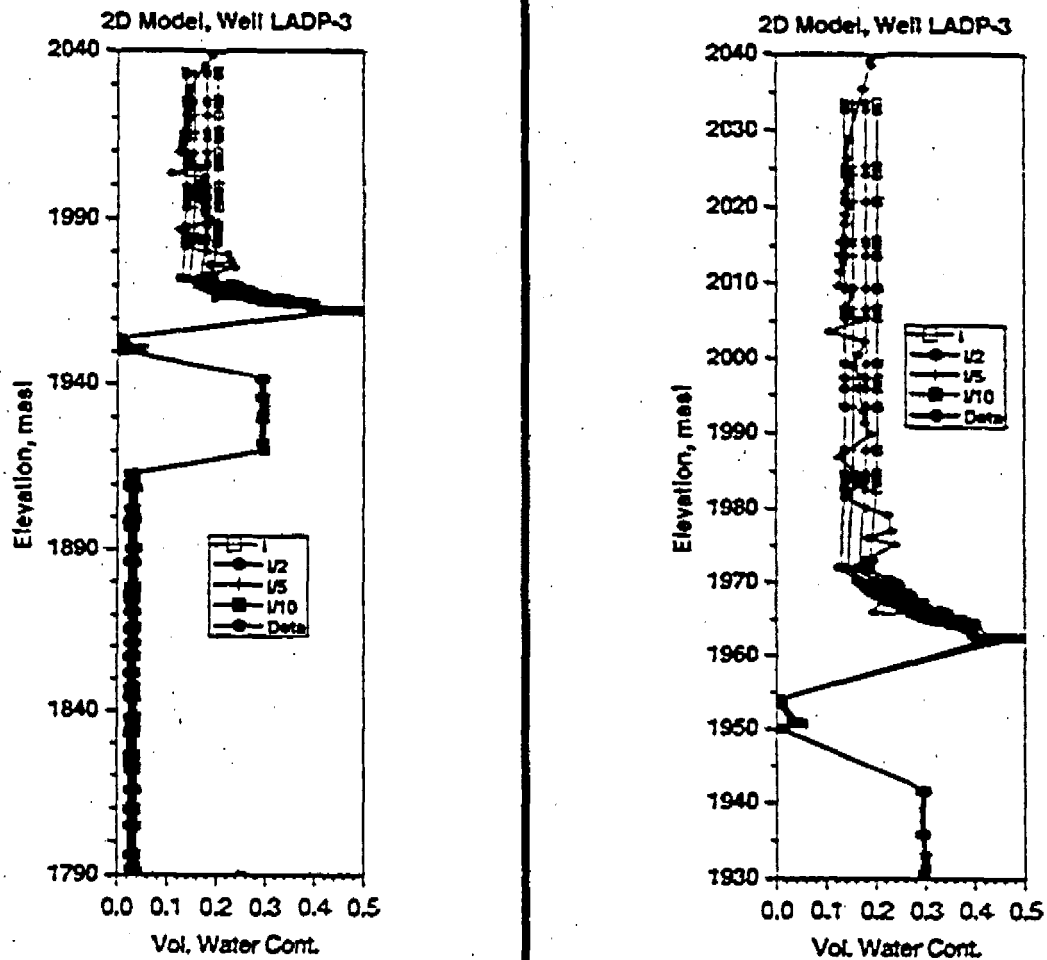

FIGURE 39. Comparison of volumetric water content predicted by the two-dimensional model to the data from well LADP-3

of the vadose zone, illustrating that only the upper third of vadose zone is actually covered by LADP-3.

Well LAOI(A)-1.1 shows generally wetter core samples than predicted by the model (Figure 40), even for the base recharge map, which is the largest recharge rate studied. There are several possible reasons for this discrepancy. The hydrologic properties of the tuffs in the vicinity of this well could be different than the mean values used in these

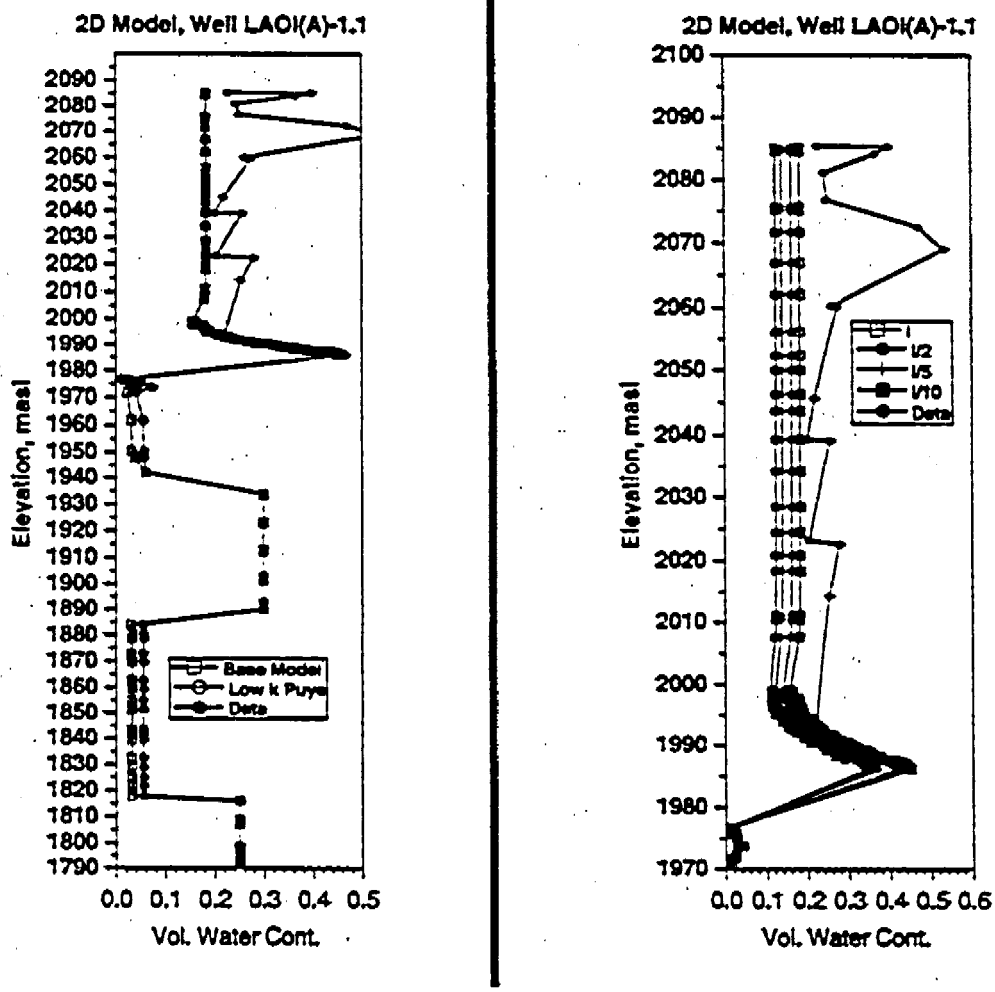

FIGURE 40. Comparison of volumetric water content predicted by the two-dimensional model to the data from well LAOI(A)-1.1

simulations. Although the van Genuchten parameters are not available for core from this well, the K_{sat} values are actually larger on average than the mean value of K_{sat} reported by Rogers and Gallaher (1995) that was used for the base case. Alternatively, the recharge map of Gray (1997) may underestimate the recharge rate in the vicinity of this well. A related source of error relates to the location of this well with respect to the surface water stream channel. If well LAOI(A)-1.1 is located directly in the channel, and local recharge rates are actually much higher than the average value used in the two-

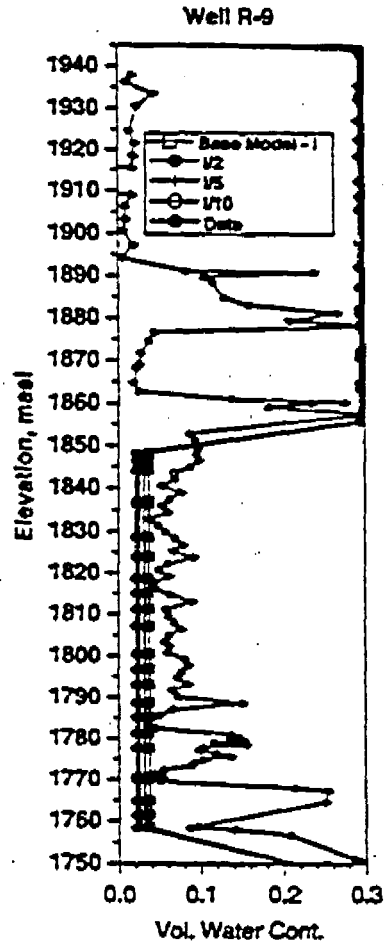

FIGURE 41. Comparison of volumetric water content predicted by the two-dimensional model to the data from well R-9

dimensional model, then the model would underestimate water contents, especially near the surface, before the concentrated region of high recharge is able to diffuse laterally as it percolates downward. Whatever the reason, the discrepancy is such that the model underpredicts water contents in LAOI(A)-1.1, while overpredicting water contents slightly in LADP-3. Therefore, in the absence of additional parameters or a different recharge map, we regard the fit to the data represented by the base-case properties and

recharge to be an adequate reference case on which further sensitivity analyses can be performed in two dimensions.

Well R-9 is somewhat less interesting as an observation well for matching fluid saturations at the present time due to the lack of an acceptable conceptual model and numerical representation for the basalt units and the Puye Formation. In Figure 41, the data clearly show a level of detail in the hydrologic state of the rock that is not captured by the model. The lack of a good fit is not surprising given the apparent heterogeneities in these rocks compared to the homogeneous assumption of the model within each unit. The model currently assumes that these units behave as equivalent porous continua with the matrix controlling the permeability until it becomes nearly saturated, at which time fractures transmit the fluid. For unit Tb4 (the uppermost unit in R-9) the matrix porosity was arbitrarily chosen to be 0.3 and the permeability is very low, yielding a predicted water content of about 0.3 throughout the horizon. If that porosity had been chosen to be only a few percent, the low water contents would have been matched, but without any real improvement in the flow conceptualization and corresponding flow model. Therefore, we chose to leave the porosity at 0.3 to highlight the inadequacy of the model for these units, rather than to conceal it by choosing a parameter so as to "make the answer come out right." Similarly, the conceptual model of the Puye Formation needs to be improved, although we arguably can change the hydrologic parameters of this unit to obtain a better fit to the data. Qualitatively, lower K_{sat} values would improve the model fit in the Puye Formation by raising the volumetric water contents. We chose to leave the base case properties at their current values, highlighting the need to improve the conceptualization of this unit's flow characteristics, perhaps through the introduction of heterogeneous property distributions. A sensitivity analysis demonstrating this point is performed in Section 6.6.

6.5 Transient flow simulations

Having obtained acceptable matches to the water content data using the base-case hydrologic properties and recharge map, several transient flow simulations were performed to examine the key time scales over which changes in the forcing function (recharge rate) changes the water content distribution in the vadose zone. This sensitivity analysis is performed to study the validity and limitations of the steady state flow assumption in calibrating water content data to understand the time frame over which changes in recharge affect the model results.

Although an annual average recharge rate is assumed in the steady state models presented in the previous section, recharge is likely to be a more transient phenomenon. Gray (1997) shows that in Los Alamos canyon, water levels in alluvial aquifer wells fluctuate with season in response to summer storm events and spring runoff from snowmelt. It is not clear to what extent these transients are damped by the surface and alluvial aquifer flow processes. To test the potential influence on vadose zone water contents, we take a "worst-case" approach to bound the problem. In the first simulation, we test the sensitivity of the model to a very sharp impulse of water corresponding to the entire predicted recharge of one-half year concentrated in a one-week time period. This bounding case is intended to model the case of all recharge occurring in a single spring runoff event and a single summer storm event. Figure 42 shows the predicted water content profiles in LADP-3 and LAOI(A)-1.1 in response to such an event. The influence is only felt in the uppermost ten meters or so of the vadose zone. The quantity of water input

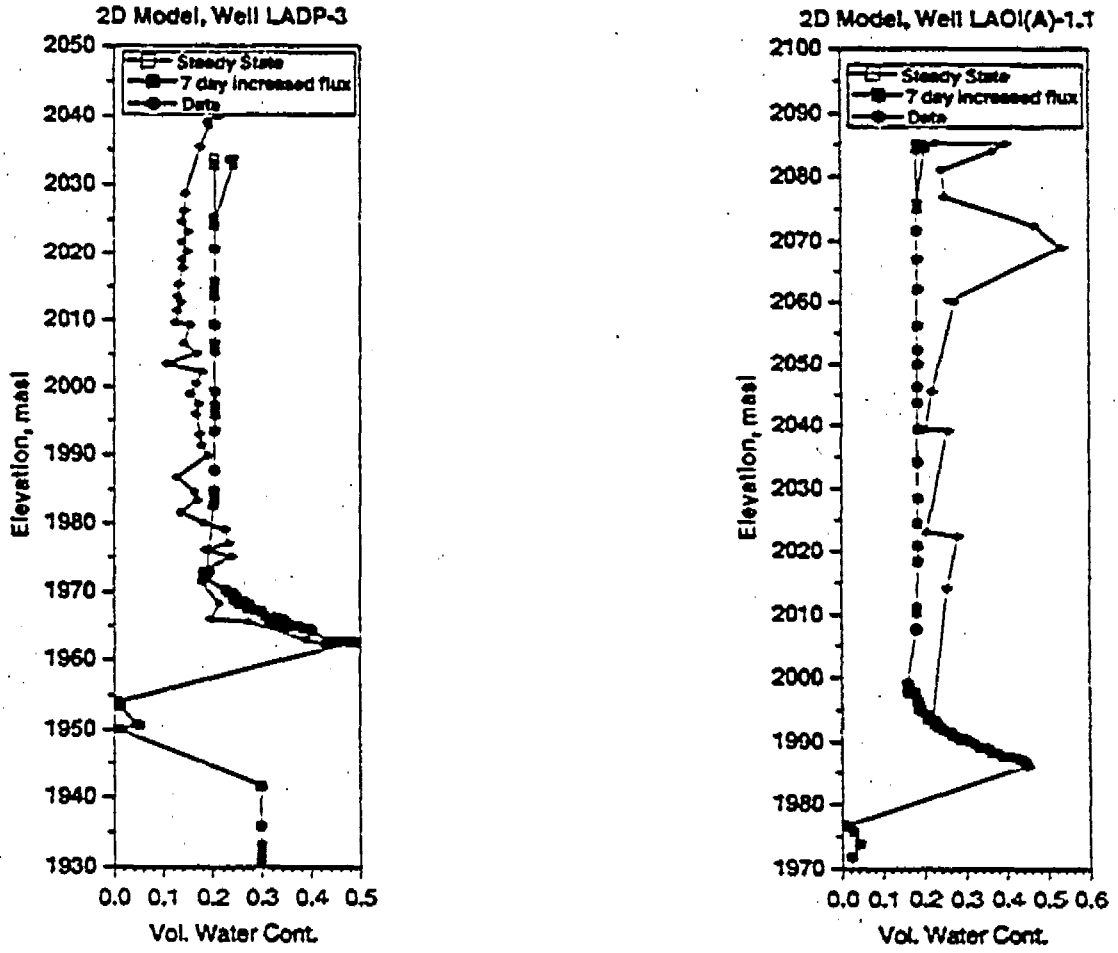

FIGURE 42. Predicted volumetric water content profiles in wells LADP-3 and LAOI(A)-1.1 in response to a single one-week storm event.

during the event, though intense, is insufficient to have a significant influence on the water content profile. These events would then be followed by a half-year of no recharge, which would cause the profile to bounce back to nearly its original state. Therefore, the assumption of steady state conditions over time scales of years should have no influence on the interpretation of the water content profiles in the observation wells, except possibly very close to the surface (alluvium-bedrock interface).

Longer-term variability in the recharge rate over years or decades could also complicate the interpretation of water content measurements, and thus need to be examined. Changes in climate, either due to global effects or random sequences of several consecutive wet or dry years could impart a change to the water content profile that would not be captured in a steady state model. Alternatively, if outfalls from treatment facilities result in a significant increase in recharge rate, a transient over the time scale of years or decades could result. Figure 43 shows the results of a simulation in which the *1/5*

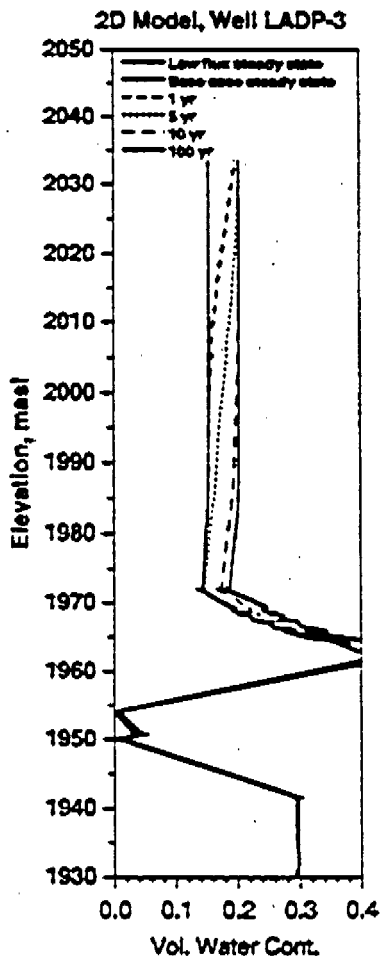

FIGURE 43. Predicted volumetric water content profile in wells LADP-3 in response to a change from the 1/5 recharge map to the 1 recharge map.

recharge steady state is used as an initial condition, and the rate is increased to the base-case recharge map at time zero. The plot shows that over a time period of a few years, the water contents increase to significant depths. Within about a decade, the profile throughout the entire section of the Otowi member reflects the new, higher recharge rate. At times of one or a few years, the transient water content profile shows curvature similar to that seen in several of the observation wells, including LADP-3 and LAOI(A)-1.1. This does not necessarily mean that the curvature is caused by such a transient, but simply that reasonable variability in recharge rates over years to decades complicates the interpretation of the water content profiles. This simulation is meant to provide a caution against over-interpretation of the details of the water content profiles. Furthermore, it is recognized from this analysis that the match of a steady state model to the data in Los Alamos canyon represents the fluid flow characteristics of the system within the previous ten to 100 years leading up to the collection of the water content data. In general, this result is dependent on the hydrologic conditions of the particular model area. Wet canyon systems with high recharge rates have transient time periods of this order of magnitude, while dry mesas may take upward of thousands of years to attain a new steady state water content profile when recharge rate changes.

6.6 Sensitivity to hydrologic property uncertainty

As was discussed in Section 6.3, there is significant uncertainty in the hydrologic property values that are appropriate to use in a large-scale model such as the Los Alamos Canyon model. Some of the uncertainty is due to true variability in the hydrologic properties in space, and is reflected in the ranges of parameters obtained from multiple samples in the same stratigraphic unit. Related to this variability is the possibility that properties such as permeability may vary systematically with location on the Plateau, perhaps a result of proximity to the source Some uncertainty is also due to measurement error. Finally, in some units, very little core data are available, a problem that is compounded by the difficulty of obtaining representative samples for measurement. The end result is a series of parameter determinations that exhibit a range of property values, raising the issue of which parameter values to use in each hydrogeologic unit.

To examine the issue of hydrologic property uncertainty, we have performed several additional two-dimensional model runs in which one or more parameters are varied from the base-case values. We compare these model results to the water content data and to the base-case predictions of water content in an effort to quantify the extent to which these uncertainties cast doubt on the validity of the base-case model. The main focus of these sensitivity has been in the Otowi member, in keeping with our approach of examining this unit first in our overall scheme of attempting to understand vadose zone flow and recharge processes by studying this ubiquitous unit. We also perform a simple sensitivity of k_{sat} of the Puye formation in an additional simulation.

The base case parameter set used the mean values of the hydrologic parameters for all units, including. This practice has been used in other modeling studies on the Plateau, including Dander (1997) and Birdsell et al. (1999). However, it is unclear whether a different approach might be more representative for capturing the hydrologic behavior in an average sense. To examine this point, Figure 44 plots the unsaturated permeability versus water content predicted using the individual van Genuchten parameters and k_{sat} measured for individual cores from the Otowi member (the light gray curves in the fig-

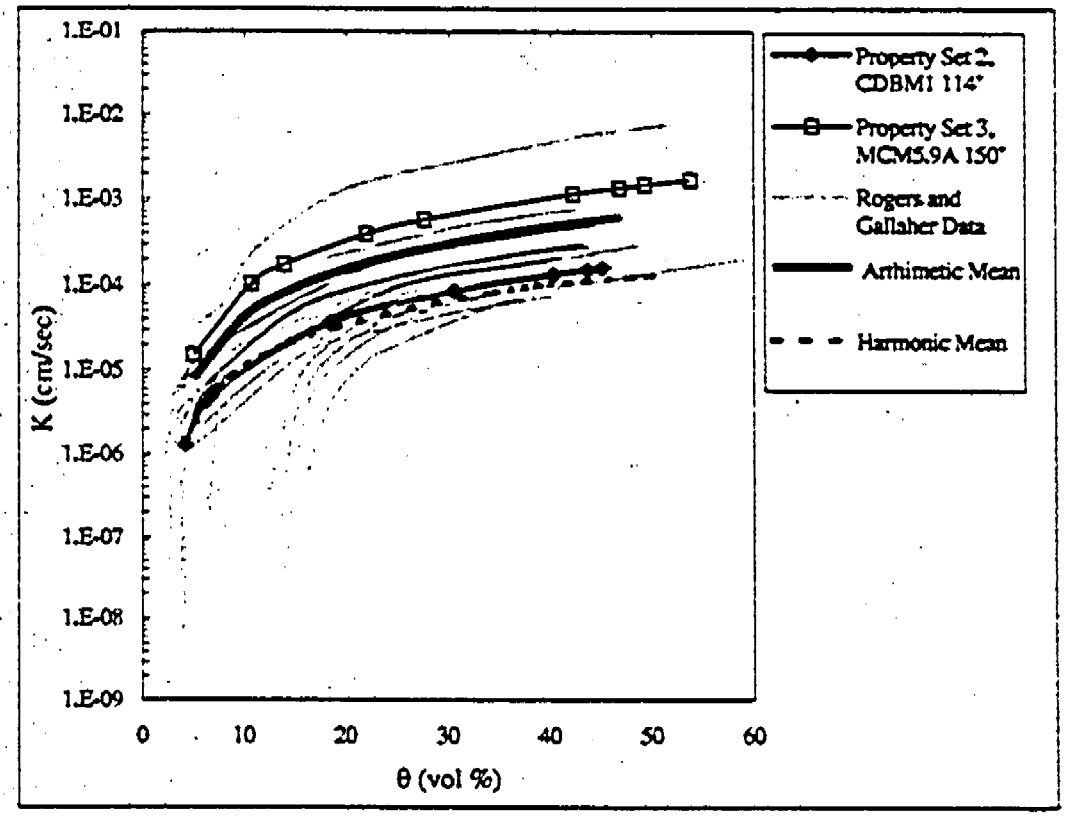

FIGURE 44.

Unsaturated permeability versus water content for the Otowi member. Light gray curves - core samples from Rogers and Gallaher; Heavy curve - base-case parameters; Property Sets 2 and 3 - property sets chosen to bracket the behavior in the sensitivity analysis.

ure). The data were obtained from the Rogers and Gallaher (1995) compilation of parameter values. The heavy curve is the composite curve (i.e. the base case) computed using the arithmetic mean of all parameters. It is significant that the curve derived from the arithmetic mean falls on the high end of the family of curves from the individual core samples, suggesting that perhaps this method is not the best way to obtain a representative parameter set. A better approach would appear to be to use the harmonic mean of k_{sat}, which would result in the dashed curve in Figure 44. To examine the influence of this effect on the model results, two additional model runs were performed. Instead of using a different averaging approach, we selected individual samples whose permeability versus water content curves fall on either side of the base-case curve, and identify these two cases as Property Sets 2 and 3. Figure 45 shows the impact of changing the properties of the Otowi member in this way on the predictions at LADP-3 and LAOI(A)-1.1. The curve labelled "Property Set 2" predicts somewhat higher saturations in the Otowi member, whereas the "Property Set 3" curve predicts lower values. Since in LAOI(A)-1.1 the base case underpredicts the saturation, Property Set 2 results in a

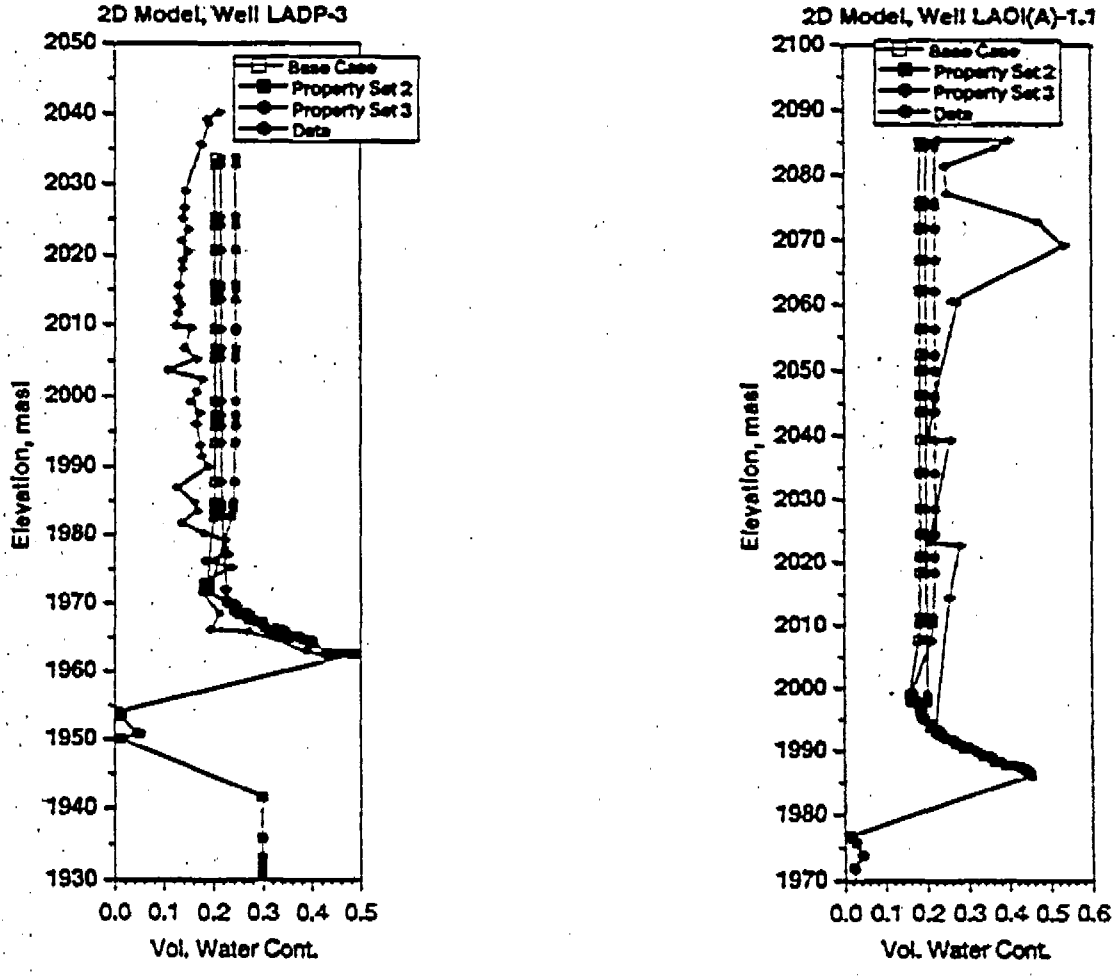

FIGURE 45. Predicted volumetric water content profiles in wells LADP-3 and LAOI(A)-1.1 for different property sets.

closer match than the base case. Of course, the opposite is true in LADP-3, where the base case overpredicts the water contents. The selection of a particular averaging method warrants further investigation. However, from this analysis we conclude that this uncertainty could give rise to a difference in predicted water contents that is roughly equivalent to a factor of three to five difference in the recharge rate.

One additional sensitivity analysis performed on properties of the Otowi member relates to the issue of possible systematic differences in hydrologic properties in the model area relative to the Plateau as a whole. Recall that the Rogers and Gallaher (1995) data for the Otowi member did not include more recently collected data from Wells LADP-3 and LADP-4, which are in the area of study. Springer et al. (1999, unpublished data) report hydrologic parameter data for samples obtained from these and other wells to supplement the information in Rogers and Gallaher (1995) in the vicinity of Los Alamos canyon. Figure 46 plots the Springer et al. permeability versus water content data for the

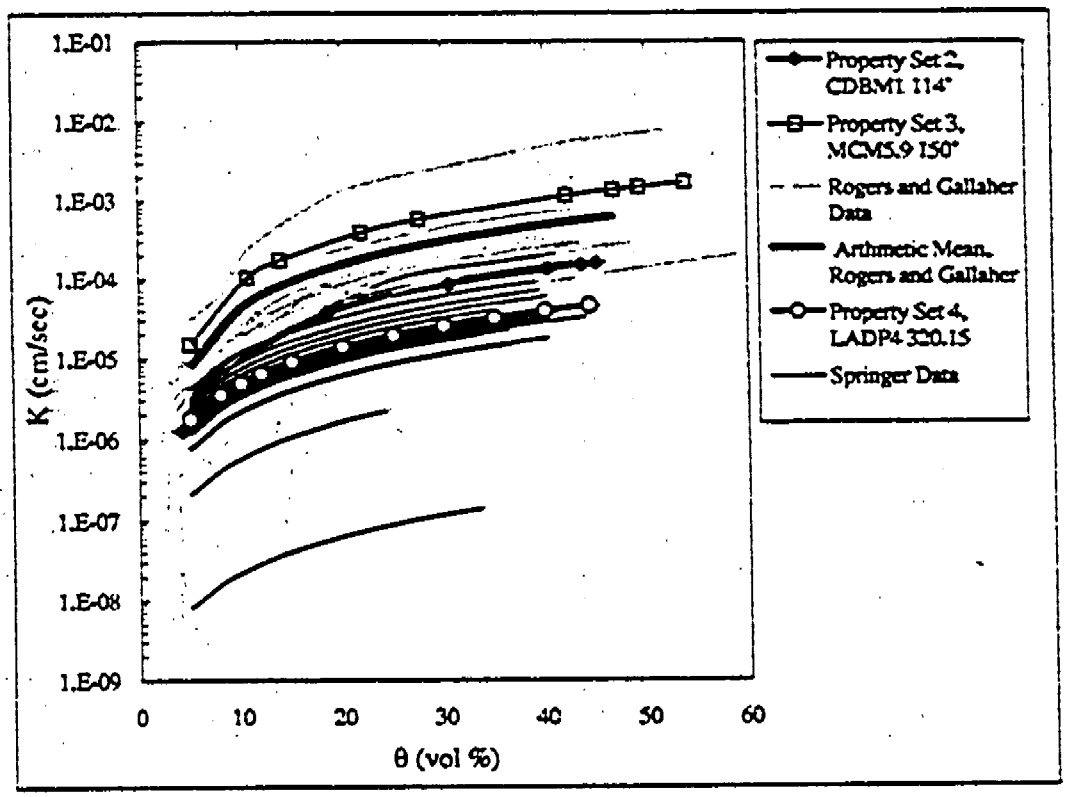

FIGURE 46. Unsaturated permeability versus water content for the Otowi member, including newly collected data from Springer et al. (1999, unpublished data). Other curves are the same as in Figure 44.

new samples dark, solid curves with no symbols, comparing them to the Rogers and Gallaher data. The new data from LADP-3 and LADP-4 on average fall below the majority of the previously reported curves for the Otowi member. It should be stressed that the Springer et al. (1999) data are unpublished and hence subject to revision. One avenue to pursue to investigate the differences is to determine if Springer et al.'s approach to curve fitting is comparable to that of Rogers and Gallaher (1995). Springer notes that in contrast to Rogers and Gallaher (1995), the new data were fit by allowing the saturated water content θ_s to be varied in the regression, whereas Rogers and Gallaher (1995) assumed this value was equal to the porosity. Methodological differences could be the cause of the differences in the data sets, rather than true systematic variability in hydrologic properties. This possibility should be investigated by re-fitting the Rogers and Gallaher (1995) data using the same methodology as used by Springer et al. (1999).

Assuming that these new parameters hold, then the behavior of the Otowi member will also change in numerical models, and specifically the LADP-3 and LADP-4 data should be used directly in the Los Alamos canyon model. To anticipate this, we performed an additional two-dimensional simulation using parameter values for the Otowi member from a representative curve from the Springer et al. (1999) data set, namely sample LADP4 320.15, which we call Property Set 4. Figure 47 shows the changes in the model results at LADP-3 and LAOI(A)-1.1 of this change in Otowi parameters. Higher water contents are predicted in the Otowi member for this new data set, as was the case for Property Set 2 above. In general, an updated model using these new parameters would need somewhat lower recharge rates to fit the data with the same degree of accuracy as the current base case. As before, the magnitude of the differences are equivalent to a change in the recharge rate of roughly a factor of three to five. Therefore, obtaining site-specific hydrologic data, and deciding upon a common method for reducing the data to obtain hydrologic parameters, appears to be an important in future data collection and modeling activities.

The last parameter sensitivity investigated in this section uses a k_{sat} for the Puye Formation that is an order of magnitude lower than the base case value used in the base case. There is one well (R-9) in the Los Alamos canyon model domain that penetrates significant portions of the Otowi member and has a complete data set of water content values. Figure 48 shows the impact of lowering the permeability used for the Puye formation by an order of magnitude from the base case. Clearly, this lower permeability results in a better fit to the data than does the base-case parameters. Nevertheless, we must stress the need to formulate a more complete conceptual model for flow and transport through highly heterogeneous units such as the Puye Formation. Obtaining a better fit to the data is less important in this case than properly accounting for the highly complex and possibly tortuous fluid flow pathways through this formation.

6.7 Lateral diversion at stratigraphic interfaces

One of the primary assumptions implicit in the formulation of a flow and transport model that is based on a stratigraphic framework model is that the stratigraphy exerts an overriding effect on the flow parameters and processes. If this is true, then the hydrologic properties at a numerical grid point can be populated based on the stratigraphic unit that point falls in. In fact, the approach used in this modeling study is that the finite

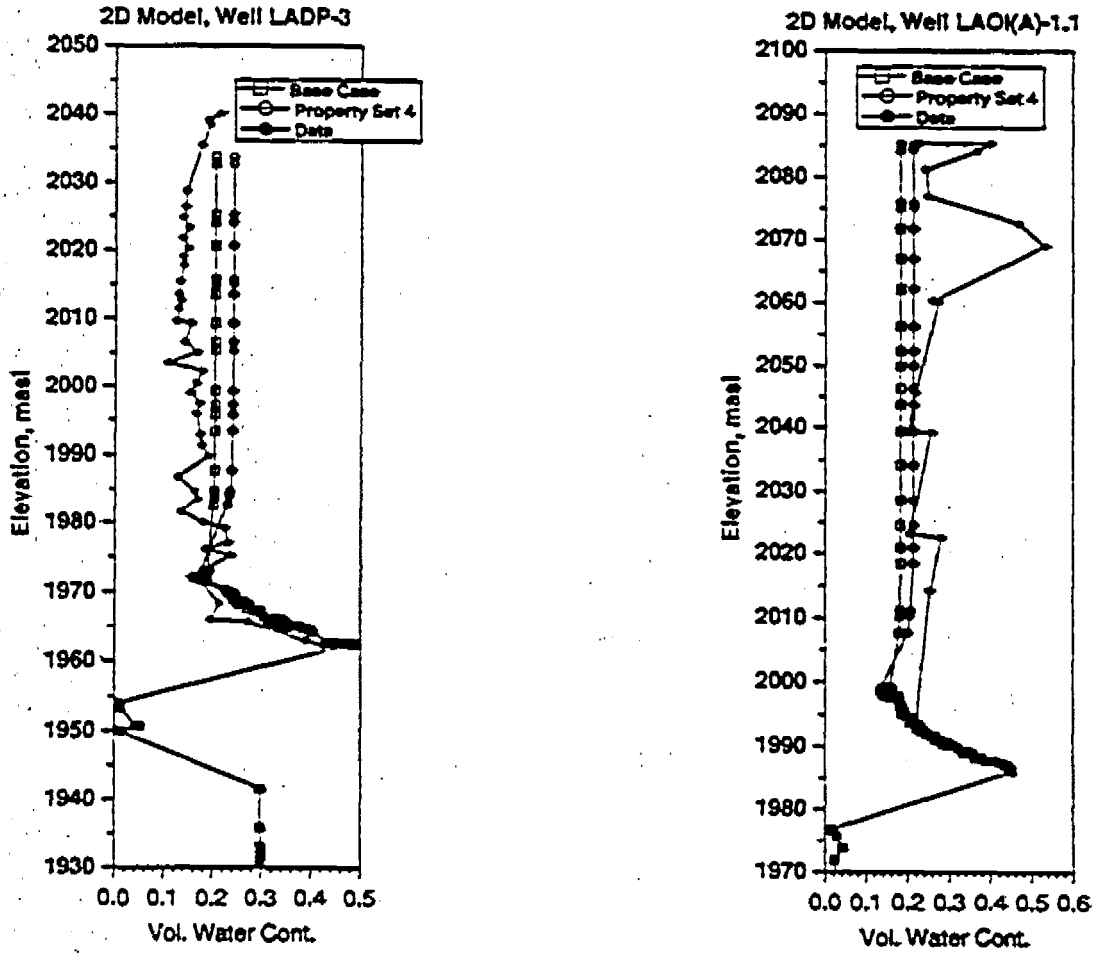

FIGURE 47. Predicted volumetric water content profiles in wells LADP-3 and LAOI(A)-1.1 for a representative set of Otowi properties from LADP-3 and LADP-4 (from new data of Springer et al., 1995).

element grids themselves need to be built based upon the need to replicate the layered stratigraphy present in the subsurface. While this approach is undoubtedly a valid starting point, there may be important features of the hydrologic system that are not captured adequately. For example, the numerous observations of perched water and possibly lateral diversion of downward percolation of fluid are difficult to capture if mineral alteration or heterogeneities within a hydrostratigraphic unit are the cause. Without a means to change the model parameterization locally through the use of low-permeability barri-

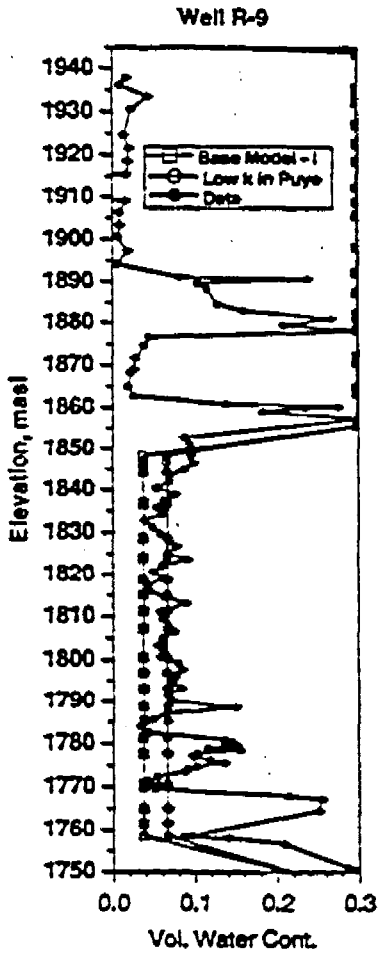

FIGURE 48. Predicted volumetric water content profiles in wells R-9 for a saturated permeability value an order of magnitude lower than the value assumed for the base case.

ers, it is difficult to reconcile the perched water with the currently measured hydrologic properties of the current hydrostratigraphy. Mean hydraulic conductivity values for the Bandelier tuff are several orders of magnitude larger than the highest proposed recharge rates for the plateau. This fact implies that if only mean values are used everywhere in a vadose zone model, the rocks will transmit all fluid under unsaturated conditions, and no perching or lateral diversion will occur.

Nevertheless, in Los Alamos canyon and elsewhere, perched water has been found within and at the base of the Guaje Pumice Bed of the Otowi member, and within the basalt units and the Puye Formation. Careful characterization of the rock in the vicinity of the perched water in wells such as LADP-3 (Broxton et al., 1995) has uncovered fine-scale permeability contrasts that explain the perched water occurrence. In LADP-3, Broxton et al. (1995) report the presence of a several inch thick clay layer at the base of the Guaje Pumice Bed on top of the Puye Formation. They postulate that this clay may be a paleosoil that today acts as a permeability barrier that diverts downward percolating fluid.

A key issue in the development of the numerical model for Los Alamos canyon is how to practically handle such barriers. Although relatively thin layers can be incorporated directly into the finite element grid, there are practical limitations to this approach, including computational inefficiencies and the lack of detailed data at the scale required to construct a model of extreme grid resolution (centimeter scale grid spacing). The current limit of grid resolution is such that we can handle the units presently characterized in the geologic model, but finer-scale heterogeneities cannot be built into the grid directly.

An alternative approach has been taken in this study, namely an approach that considers the *interfaces* between hydrogeologic units to be important transition regions where hydraulic properties such as the saturated permeability may be different than those in either of the units above or below the interface In this formulation, the LADP-3 observation of a clay layer is handled by assuming that a reduction factor can be applied to the permeability for those parts of the model where the Guaje Pumice Bed and the Puye Formation are connected. Assuming this factor to be much less than unity means that the intervening clay layer has a large influence on the permeability field at that interface.

The numerical implementation of this conceptual model was developed and added to the FEHM code for this modeling study. In most finite difference or finite element codes, including FEHM, when any two connected nodes in the model connected to one another have a different permeability, a harmonic average permeability is applied for that connection. The new feature added to the code is to allow the user to specify a constant multiplier called the permeability reduction factor to any connection on an interface between two hydrostratigraphic units where this effect is present. In this way, the permeabilities within each unit are their original values, but the permeability applied for water passing through the interface is reduced. When the reduction factor makes the permeability at the interface small enough, lateral diversion or perching can occur, depending on the dip of the interface and the local recharge rate.

Because the application of a reduction factor may seem like an ad hoc concept, we present a simple example that allows calculation of the reduction factor. Consider the model geometry in Figure 49. On the left-hand figure, two units of somewhat different permeability are adjacent to one another. Considering for the moment the flow to be one-dimensional, steady-state, saturated flow, the pressure drop $P_2 - P_1$ from point 2 to point 1 can be obtained by realizing that the flux within each material is the same, so that:

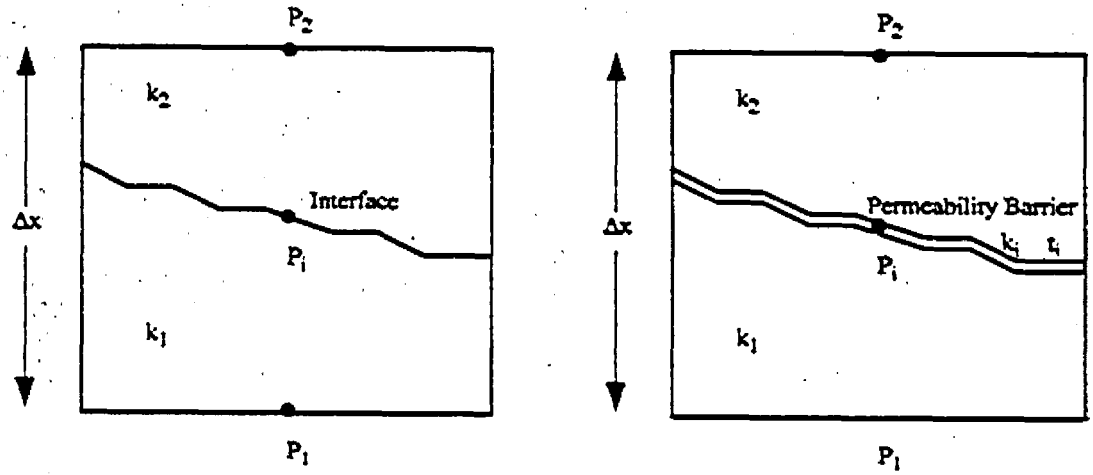

FIGURE 49. Schematic diagram of the conceptual model geometry for the interface between two hydrogeologic units. a) model without low-permeability barrier. b) model with low-permeability barrier.

$$q = \frac{k_2}{\Delta x/2}(P_2 - P_i) \qquad \text{(EQ 12)}$$

$$q = \frac{k_1}{\Delta x/2}(P_i - P_1) \qquad \text{(EQ 13)}$$

Where q is the water flux, k_1 and k_2 are the hydraulic conductivities, and P_i is the pressure at the interface. These equations can be combined to eliminate this intermediate pressure, resulting in:

$$q = \frac{k_{harm}}{\Delta x}(P_2 - P_1) \qquad \text{(EQ 14)}$$

where

$$k_{harm} = \frac{2k_1k_2}{k_1 + k_2} \qquad \text{(EQ 15)}$$

Notice that the composite permeability across this interface is the harmonic average of the two permeabilities. This is the reason that codes such as FEHM apply a harmonic average for connected nodes that have different permeability values. Now consider the right-hand diagram of Figure 49. A similar derivation can be applied for flow in a system containing a thin layer at the interface between the units of thickness t_i and hydraulic conductivity k_i. The result, after algebraic manipulation, is:

$$q = \frac{k_{comp}}{\Delta x}(P_2 - P_1) \qquad \text{(EQ 16)}$$

$$k_{comp} = \frac{1}{\frac{1}{2k_1} + \frac{t_i}{\Delta x k_i} + \frac{1}{2k_2}} \qquad \text{(EQ 17)}$$

The composite permeability k_{comp} across the interface now contains a term that includes the permeability and thickness of the low-permeability layer. When this layer is not present, the permeability reduces to the harmonic average of k_1 and k_2, but in cases in which k_i is low enough, the low-permeability layer effectively controls the composite permeability across the interface.

Returning to the example of the Guaje/Puye interface, some reasonable parameter values illustrate the point. Using the base-case values of permeability for these two units, the harmonic average permeability (the relevant value in the absence of the clay layer) is 3×10^{-13} m^2. When we include the clay layer, we need to apply a characteristic dimension for the term Δx, which in a numerical model is the typical grid spacing at this interface. If we assume a 5 cm clay layer, $\Delta x = 2$ m, and $k_i = 1 \times 10^{-17}$ m^2, we obtain an effective permeability across the interface of 4×10^{-16} m^2. Comparing this value to the harmonic average permeability, we find that the permeability reduction factor for this example is $3 \times 10^{-13}/4 \times 10^{-16} = 0.0013$. Clearly, the possibility exists that thin layers can exert a strong influence on the flow system.

In this study, we restrict our attention to the Guaje/Puye interface, and treat the permeability reduction factor as an uncertain parameter that is varied systematically to examine the impact on flow. Figure 50 shows the predicted water content profiles in Wells LADP-3 and LAOI(A)-1.1 for the base case and three values of the permeability reduction factor. As this factor decreases, saturations increase in the Guaje Pumice Bed as water is restricted from percolating into the underlying Puye Formation. Since a porosity of the Guaje Pumice Bed is set at 0.667, a water content of this value represents perched water. The lower two reduction factors in Figure 50 clearly exhibit perching at these two wells, whereas the base case and the 0.01 case do not, although the 0.01 case has buildup of fluid saturation at the interface, and small amounts of perching in others parts of the model.

A more complete view of the saturation distribution for this set of simulations can be seen in Figure 51. In these plots, the total horizontal distance is approximately 600 m, and the high-recharge zone near the Guaje mountain fault is at the left hand side of each

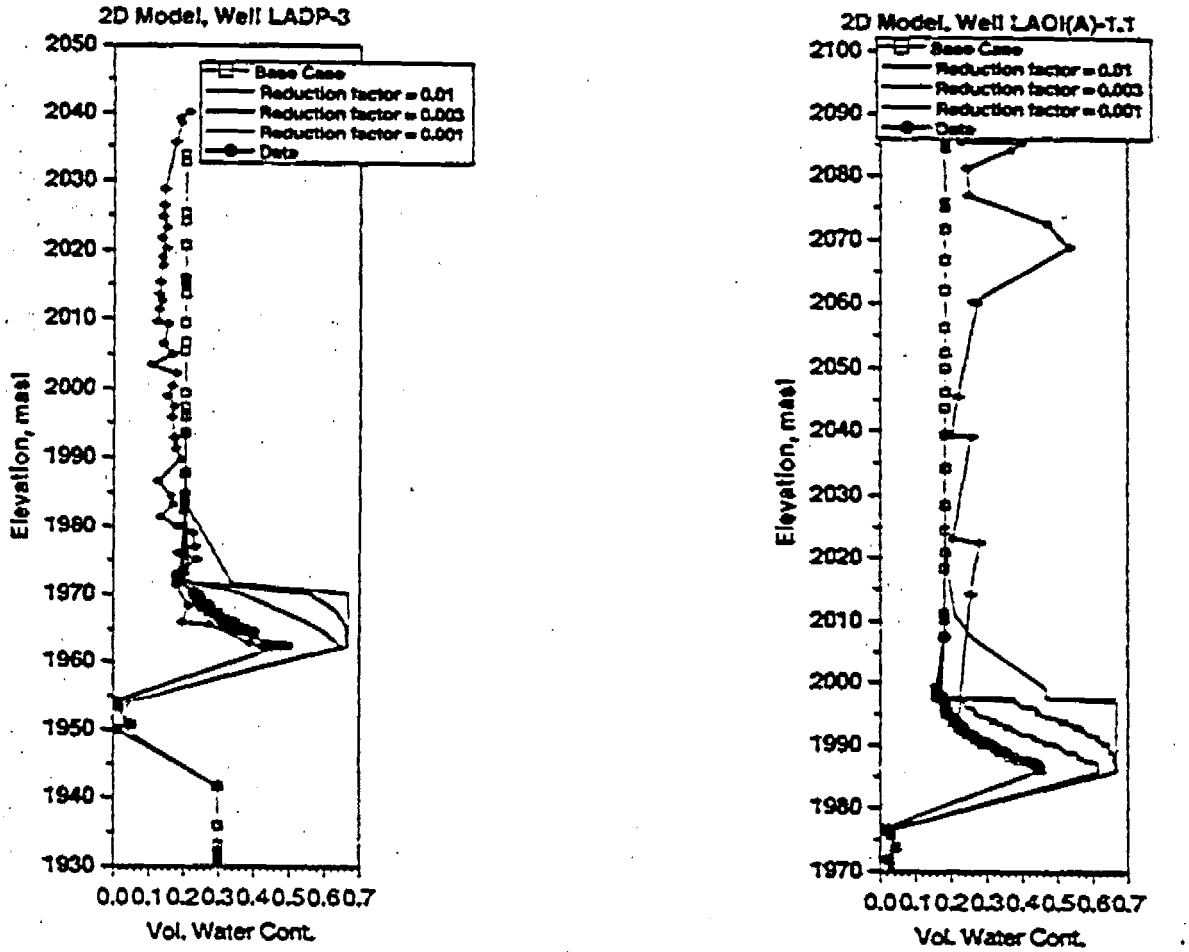

FIGURE 50. Comparison of base-case and lateral diversion cases for predicted water contents of Wells LADP-3 and LAOI(A)-1.1

image, and well LAOI(A)-1.1 is approximately on the right hand edge. The base case saturation distribution shows a very slight buildup of fluid (slightly higher saturations) in the Guaje Pumice bed beneath the high-recharge zone, but no perching. When the reduction factor is 0.01 (Figure 51b), perching is simulated beneath the high-recharge zone, but is limited in horizontal extent. Apparently, this reduction factor is enough to begin to induce perching under regions of highest recharge, but where recharge is lower, wetter but still unsaturated conditions exist in the Guaje Pumice bed. Figures 51 c and d

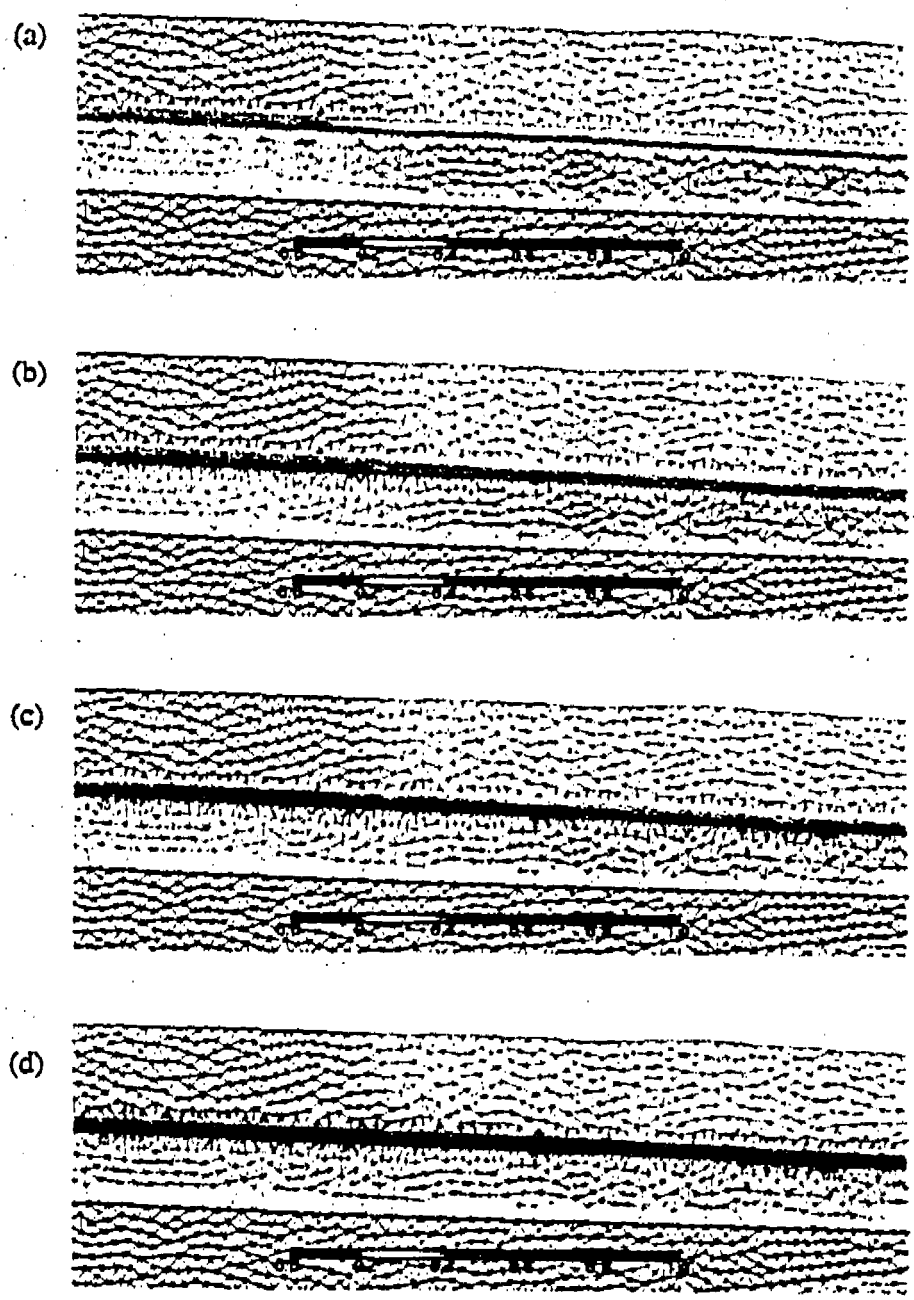

FIGURE 51. Saturation distributions in the vicinity of the Guaje Mountain fault and well LADI(A)-1.1. a) base case. b) reduction factor = 0.01. b) reduction factor = 0.003. b) reduction factor = 0.001.

show progressively more perching within the Guaje Pumice bed as the reduction factor is lowered further.

The implications of this flow behavior for contaminant transport can be examined by performing particle tracking simulations. Figure 52 shows the results of a contaminant release scenario in which mass is released with the recharge fluid in the high-recharge zone. The FEHM particle tracking model is used for these simulations. The plots and the method for reporting the concentrations provide an approximate picture of the concentration for a release of contaminants over a long period of time, and thus are semi-quantitative. Figure 52a illustrates that under the base-case conditions, the hydrologic behavior governed by the property sets used does not yield lateral diversion of fluid. Since there are strong indications of perching and evidence of lateral diversion of water and contaminants, there is a significant deficiency in the model in this aspect. This limitation can clearly be taken care of using the new interface reduction factor concept developed in the present study. Perching (Figures 51b, c, and d) and lateral diversion of fluid and contaminants (Figures 52b, c, and d) increase as the reduction factor is lowered.

The introduction of a term to induce lateral diversion and perched water at interfaces between hydrogeologic units is a new approach that is presented here to suggest an avenue for further model development. The exact means for incorporating the parameter into model calibration and sensitivity studies has not been developed, and results are available only for the two-dimensional model. We believe that the primary impact of this approach will be in the area of contaminant transport, rather than the calibration of the flow against water content data. Since this report focuses primarily of flow, the lack of a complete set of model runs with the new parameter is not a significant limitation. In the follow-on study of contaminant transport planned for next year, a more complete study of this approach and extension to the three-dimensional model will be performed.

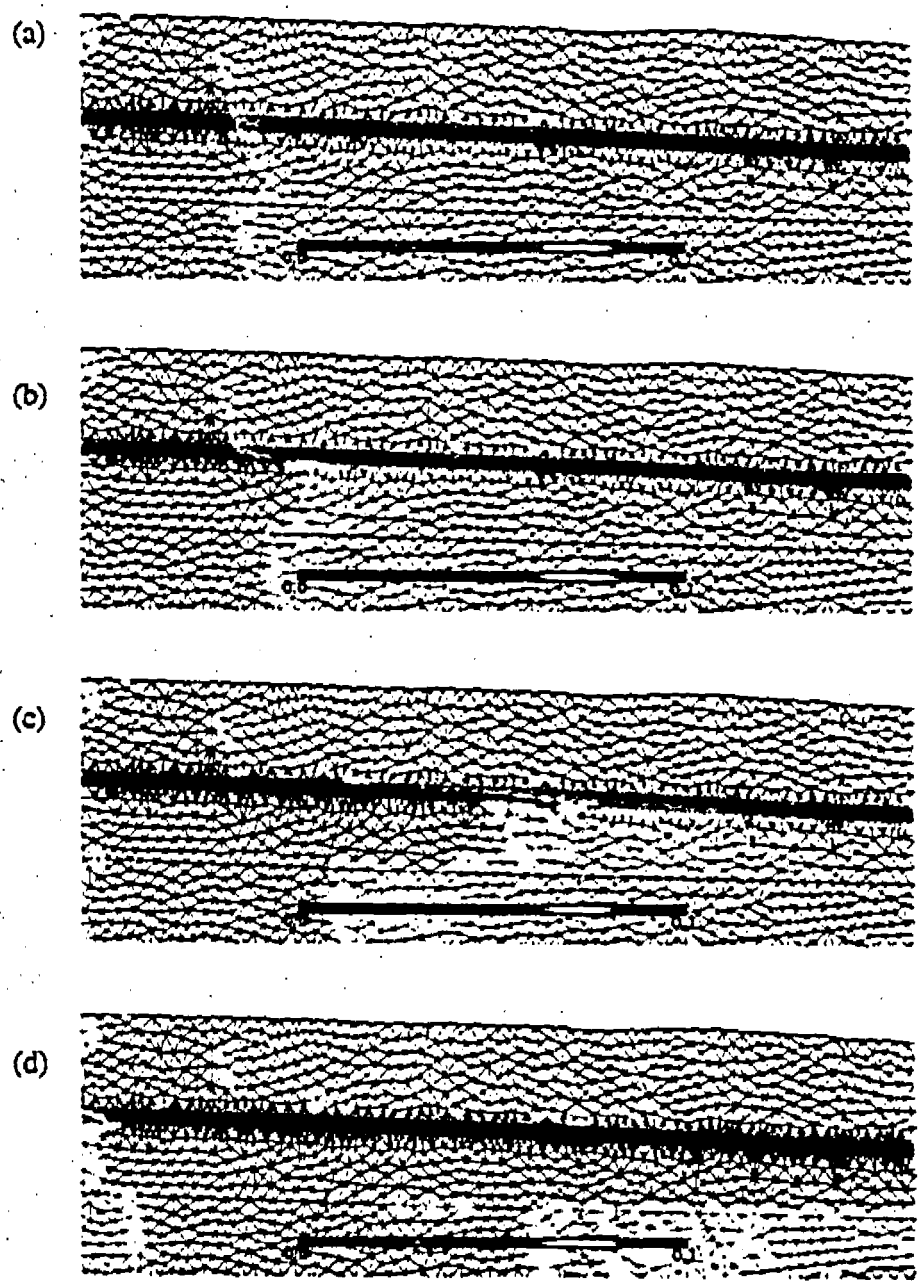

FIGURE 52. Particle tracking simulations for mass released in the vicinity of the Guaje Mountain fault. a) base case. b) reduction factor = 0.01. b) reduction factor = 0.003. b) reduction factor = 0.001

7.0 Three-dimensional flow model results

In this section we present the results of three-dimensional flow simulations. The numerical grid, consisting of 301,436 nodes, presents a very large challenge from the standpoint of computational run times, file management, and graphical output. Therefore, there are practical limitations to the number of simulations that can be performed and reported. The strategy adopted in this modeling study is to perform the sensitivity analyses that do not require the full three-dimensional treatment to be carried out using the two-dimensional model, reserving for three dimensions only those calculations that cannot be studied with the smaller model.

7.1 Three-dimensional model implementation issues

Most of the model implementation issues in three dimensions are the same as those previously discussed in the two dimensional model development (Section --), including: 1) the setting of hydrologic properties; 2) the implementation of the water table as the bottom boundary of the model; and 3) the process for obtaining a steady state model result. The only significant difference in the two models is in the method for determining recharge as a function of spatial location.

The primary reason that three-dimensional calculations are needed is to capture effects such as spatially dependent recharge rates in the model area. In addition to the recharge along the canyon, large portions of the ground surface correspond to mesas or other locations where recharge rates are expected to be low. In this model, we employ a strategy similar to that used in the two-dimensional model for applying recharge to the canyon. However, in three dimensions, the lateral extent of the alluvium/bedrock interface defines the area over which the canyon recharge is applied. This area was provided in digital form by Gray (personal communication, 1999), the result of mapping studies performed in Los Alamos canyon. A polygon was drawn around the mapped alluvium within the canyon, and this domain was overlain on the top surface of the three-dimensional grid to determine the node numbers on the grid that are to be flagged as recharge nodes. The appropriate flux is then computed for each node based on the normal area of that node, as in the two-dimensional procedure. For all top nodes of the grid that are not identified as canyon recharge nodes, a constant recharge rate of 0.5 mm/y is applied. This value, some two to three orders of magnitude lower than the recharge rate along the canyon, represents a recharge rate believed to be appropriate for mesas on the Pajarito Plateau. Values similar to this have been used by Birdsell et al. (1999) in modeling of the MDA G low-level waste site. Different and more complex recharge scenarios can be studied in future versions of this model, as time and data availability warrants.

7.2 Three-dimensional base-case flow simulations and sensitivity analyses

The three-dimensional model allows for the comparison with water content information from an additional well, LADP-4. This well is located in DP canyon, which for the three-dimensional base case solution, has a recharge rate of 0.5 mm/y, the background recharge rate assumed for all model locations except Los Alamos canyon itself. Figure 53 shows the fluid saturation profiles in series of two-dimensional slices through the three-dimensional model. As with the two-dimensional model, this model result

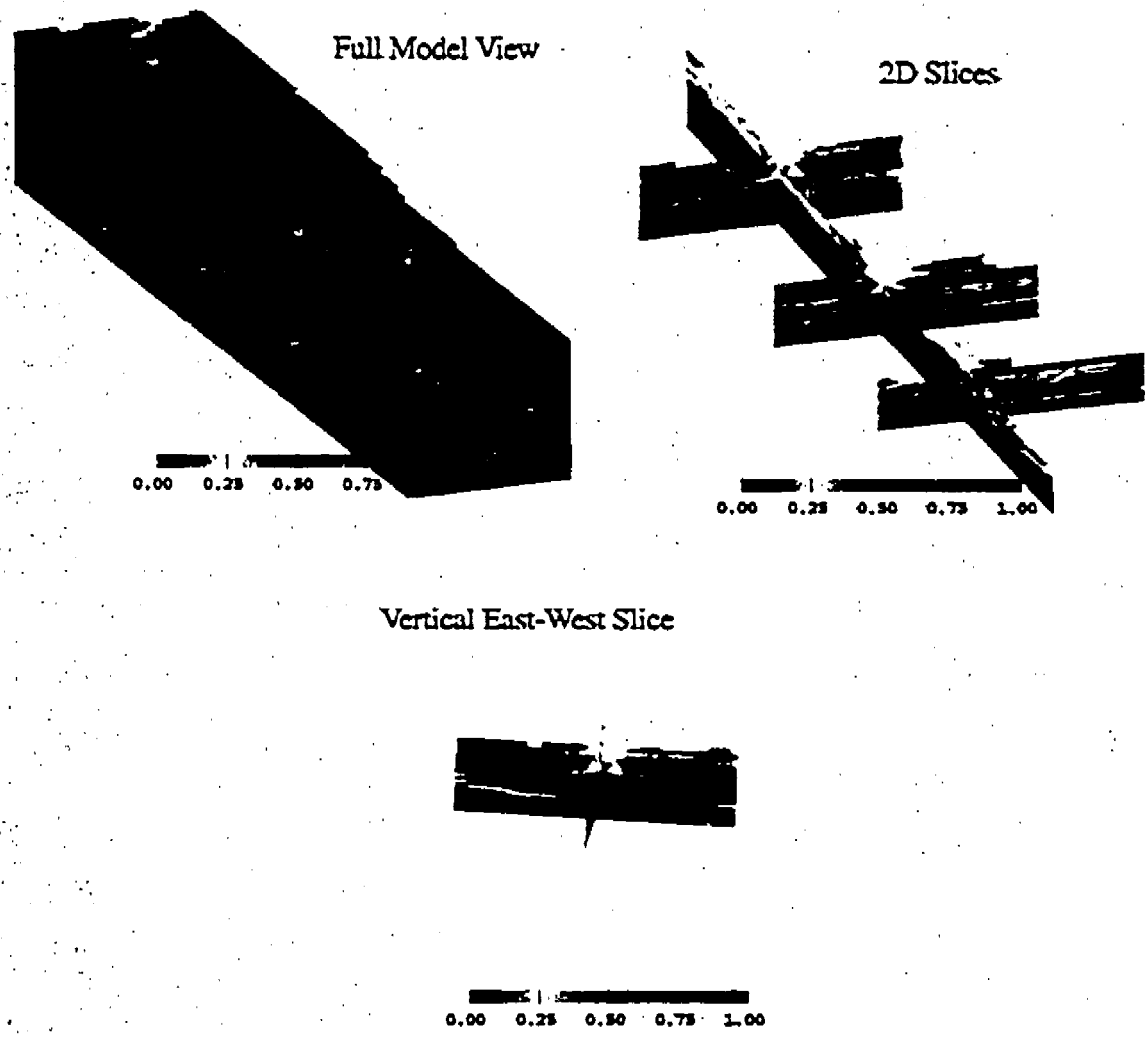

FIGURE 53. Three-dimensional base case model prediction of fluid saturation.

shows the over-riding importance of the stratigraphy in controlling the water contents in the rock. The local recharge rate also exerts a strong control on the results. Directly beneath the canyon, fluid saturation is much higher within a given stratigraphic unit than in other parts of the model domain, a reflection of the high recharge in the canyon.

The quantitative comparisons of model and data at the various observation wells are now presented. The fits to the data at LADP-3 (Figure 54), LAOI(A)-1.1 (Figure 55), LADP-4 (Figure 56), and R-9 (Figure 57) are presented for the base-case recharge map

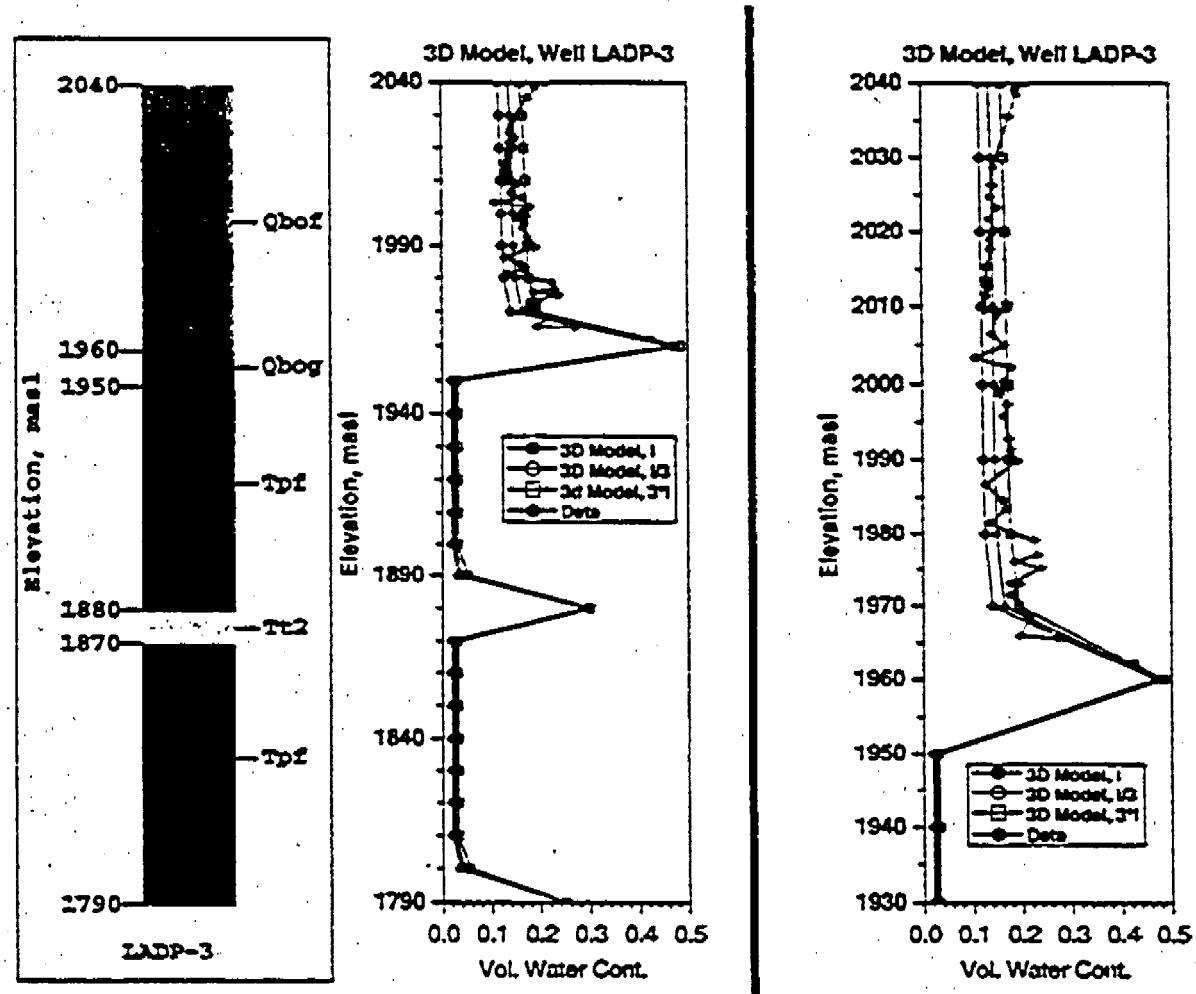

FIGURE 54. Comparison of data and three-dimensional model predictions for water contents in well LADP-3

I, a map with recharge scaled down by a factor of three (*I*/3) from the base map, and a map 3**I* with recharge scaled up by a factor of three. The recharge rate ranges selected now straddle the base estimate because in three dimensions, the total flux into the model now has a well-defined meaning that is not complicated by issues related to flow outside of the plane of the canyon in two dimensions (see Section 6.2). The base recharge map does an adequate job of jointly matching the water content profiles in all wells, despite the different stratigraphy and position relative to the canyon bottom. For example,

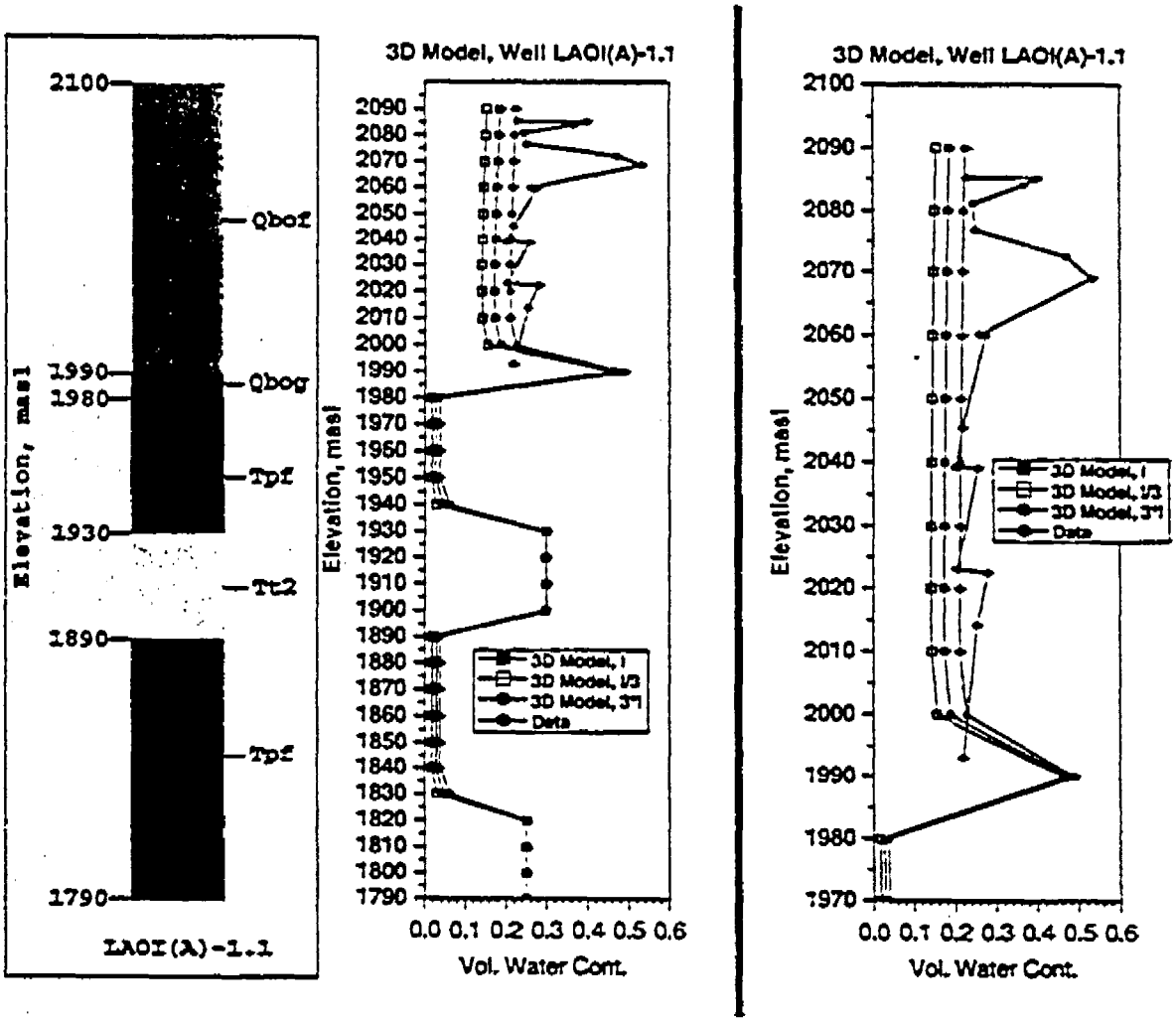

FIGURE 55. Comparison of data and three-dimensional model predictions for water contents in well LAOI(A)-1.1

LADP-3 and LAOI(A)-1.1 fits are improved somewhat over the results of the two-dimensional simulations in that the water contents are somewhat underpredicted in LAOI(A)-1.1, but match the LADP-3 measurements very closely. The good fit for LADP-4 illustrates the adequacy of the model in capturing the fluid saturations in the Tshirege member (not present in the two-dimensional model), as well as in a region where recharge rates are taken to be significantly lower than in Los Alamos canyon. The need to apply significantly lower recharge near LADP-4 is best understood by compar-

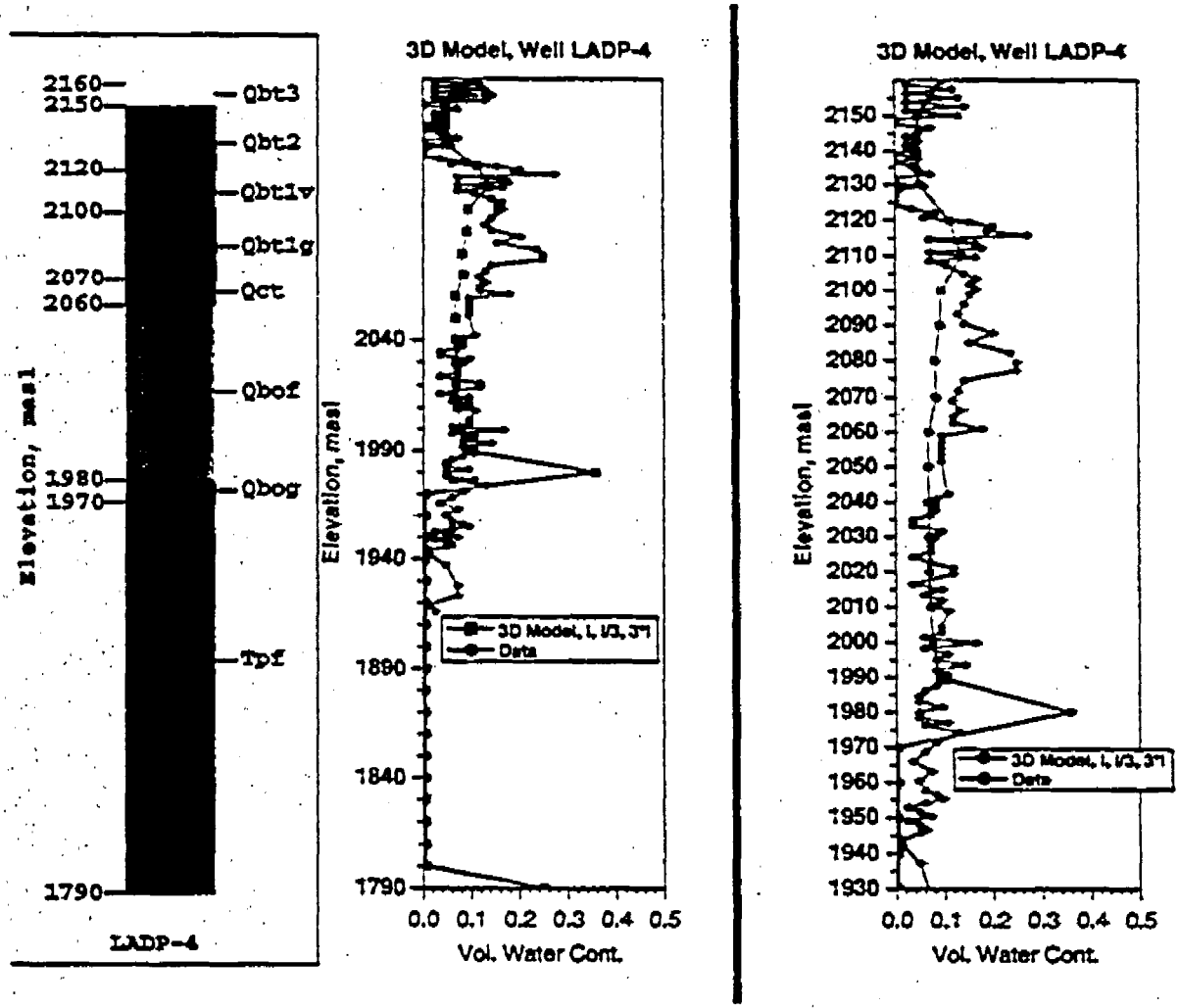

FIGURE 56. Comparison of data and three-dimensional model predictions for water contents in well LADP-4

ing the water content model and data for these two wells. The significantly wetter conditions in LADP-3 are simulated in the three-dimensional model through the setting of high recharge in the canyon. Finally, well R-9 suffers from the difficulty of the inadequacy of the conceptual model, as discussed earlier. Nevertheless, the water contents in the Puye formation are fairly well matched, and the lowering of permeability by an order of magnitude would improve this fit, as it did in the two-dimensional model.

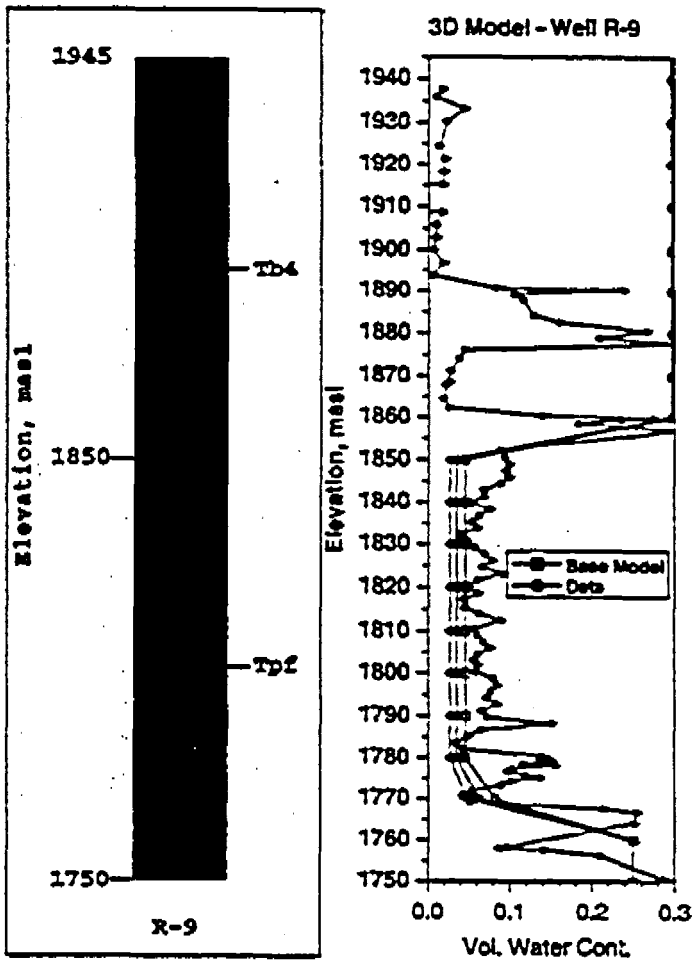

FIGURE 57. Comparison of data and three-dimensional model predictions for water contents in well R-9

Figure 58 shows the influence of applying a high recharge (200 mm/y) as a line source along two segments of DP canyon. The line segments were selected based on the mapped extent of alluvium within the canyon. The these zones were much narrower than for Los Alamos canyon, so applying the same flux to the top of the model results in only a small amount of additional water being input, compared to the base case. The figure shows that the saturation profiles are virtually unchanged from the base-case values, even in LADP-4 which might have been expected to exhibit some increased wetness.

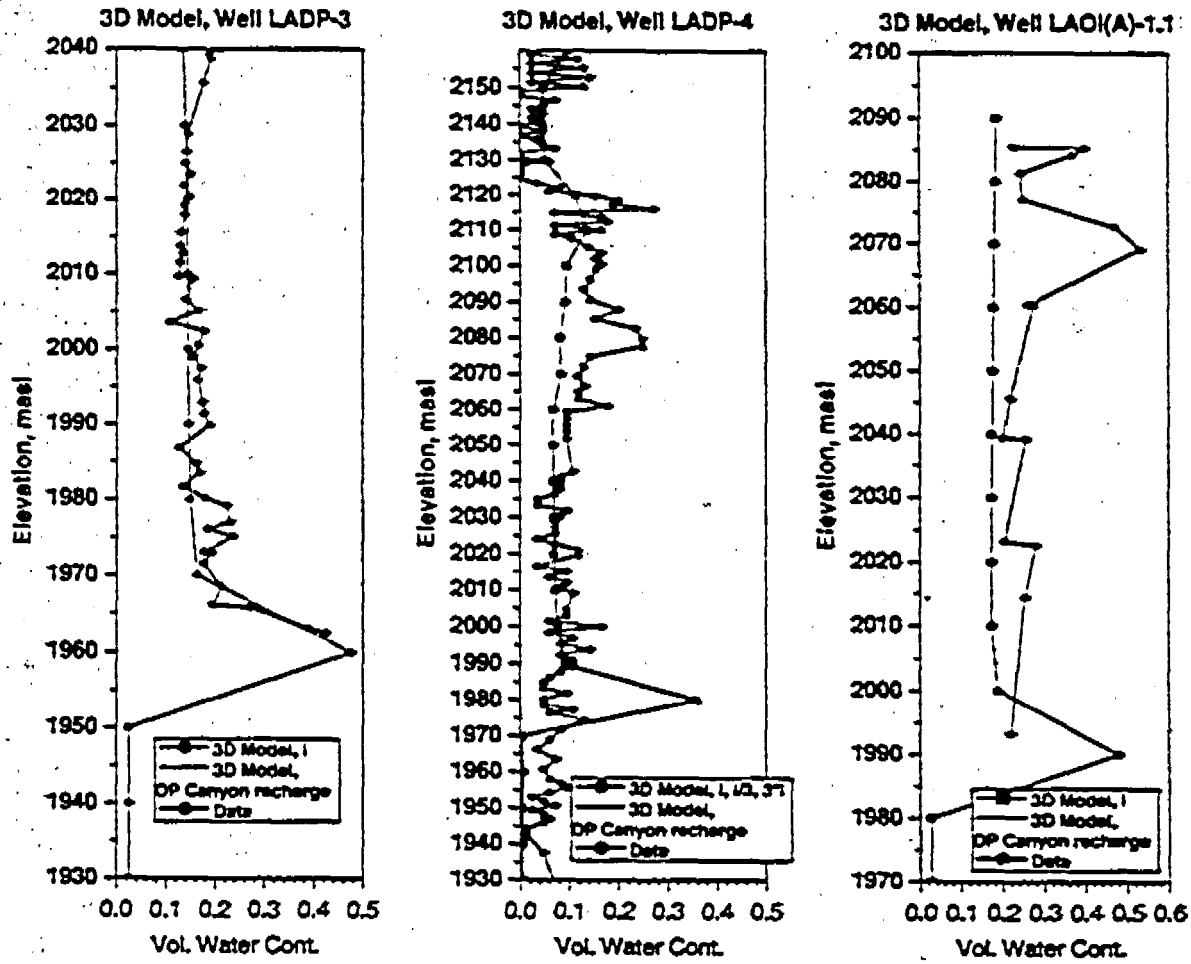

FIGURE 58. Comparisons of data and three-dimensional model results for water contents assuming enhanced recharge in DP Canyon

from water applied in DP canyon. In future simulations, we will attempt to use more direct estimates of recharge in DP canyon obtained from water budget studies, should the field results become available. The recharged fluid can be applied as a total quantity of fluid (per time), and if the recharge is high enough, the model results should reflect the increase through higher water contents beneath DP canyon. Further improvements to the model in this area await the collection and interpretation of water budget data in this canyon.

8.0 Transport Model Results

Having developed a series of flow model simulations in two and three dimensions that adequately captures the available data at observation wells, we may now apply the models to the calculation of contaminant transport in the vadose zone beneath Los Alamos Canyon. Numerical modeling of flow and transport is an appropriate method for determining which uncertainties are most important, and to eventually develop a simulation model that matches enough observations of flow and contaminant movement to become reliable as a predictive tool. The first step in this process is to construct a valid flow model. This effort has been the primary focus of the present study. As the flow model was being developed, a parallel effort was initiated to reconstruct the history of discharges of water and contaminants into Los Alamos canyon and the surrounding mesas. This effort, summarized in Section –, suggests that the history of discharges is complex and uncertain. This uncertainty applies to the timing and concentrations of discharges and unplanned emissions, as well as the total contaminant mass loadings to the environment.

Although a more complete modeling of the migration of contaminants in the Los Alamos canyon study area is planned for the future, this section summarizes results of initial simulations of tritium transport. Tritium, in the form of tritiated water, is among the simplest chemical constituents to model because its chemical state as a water molecule implies that it is a tracer for water. Other contaminants may undergo sorption, precipitation, and complex speciation processes that complicate the transport simulation. Therefore, its was decided to focus attention on the simulation of tritium transport as part of the overall flow model development. Combining the results of flow modeling with simulations of tritium transport provides the foundation for future modeling efforts examining the migration of more complex contaminants.

8.1 Transport Model Implementation Issues

There are potentially several ways that contaminants can be introduced into a numerical model. If the total quantity of mass introduced into the subsurface is known, this mass can be input as a mass flux into the appropriate nodes of the model. This approach would be appropriate in cases such as the discharge of known quantities of fluid with a known concentration-time history. The nature of effluents such as tritium in Los Alamos canyon is not certain enough to apply such a technique. Fortunately, the concentrations of tritium in the shallow alluvial aquifer forms a legitimate basis for introducing tritium into the model. Concentration-time histories of tritium are available (Section –), and these measurements apply to the fluid introduced along the canyon bottom as focused recharge. Therefore, instead of loading contaminant mass to the system in the quantities measured at the discharge "pipeline," we can consider the alluvial aquifer to be our "pipeline," i.e., the location in the model domain where the concentration history is known to a reasonable degree of accuracy. The measured concentration-time history of this fluid, combined with our estimates of recharge along the canyon bottom, provides a reasonable constraint on the overall quantity of tritium introduced into the model.

To incorporate the data from the alluvial aquifer wells into the transport model, we must decide which time-varying input concentration curve enters each section of the numerical model. Since the recharge map is discretized based on the location of the alluvial

wells, we decided to take a similar approach for tritium. The available data from the alluvial wells was employed in the following manner:

- From the Western most edge of the model to LAO-0.6, tritium measurements from LAO-C are assumed. This approach assumes that fluid of background tritium concentrations are introduced with the recharge fluid. This assumption is thought to be valid, as the first significant tritium release occurs downstream of this location.
- From LAO-0.6 to LAO-1, concentrations measured at LAO-1 are used. This section contains tritium releases from the Omega West Reactor.
- From LAO-1 to LAO-3, the concentrations at LAO-3 are used. This concentration applies to the section of Los Alamos Canyon from LAO-1 to the confluence of Los Alamos and DP canyons.
- From LAO-3 to the Easternmost edge of the model, the concentrations at LAO-4.5 are used. This well captures the concentration in the alluvial aquifer fluid downstream of the tritium sources in Los Alamos canyon DP canyons, including TA-21 discharges into DP canyon.

To simulate the tritium concentration versus time, the time varying concentrations for each source region were placed on the same time axis by processing the measured data in Figures 34 to 37 by interpolation onto a uniform, 50 day time step. This table of concentrations was then used as an input function in FEHM, which performs a table lookup at each time to obtain the appropriate concentrations. Tritium is modeled as a non-sorbing solute that undergoes radioactive decay with a half-life of 12.2 years. The calculation is performed by running a background simulation in which a constant, background concentration of tritium of 100 pCi/L is injected with the recharge fluid. After several pore volumes of fluid are displaced in this calculation, an appropriate background concentration field is established. This field generally has decreasing concentrations with depth due to radioactive decay of the tritium. Then, time 0 of the simulation was assumed to be January 1, 1967, which, according to the alluvial well tritium data, precedes the releases of significant tritium mass into Los Alamos canyon. Concentrations within the system are monitored during the simulation and output as concentration fields in the model and as time-varying concentrations at particular nodes in the grid.

Figure 59 shows a series of snapshots of concentration in the model for the base case flow field and hydrologic parameters. The concentrations are plotted as log10 of the concentration in pCi/L on a range from 1 to 10,000 pCi/L. The most concentrated inputs of tritium into Los Alamos canyon occurred starting in about 1970. The tritium plume appears in the subsurface at this time. Transport velocities predicted by the model are such that the majority of the released tritium stays within the vadose zone, where it undergoes natural attenuation by radioactive decay. However, the model does result in transport of a small fraction of the tritium reaching the regional aquifer. The regions where deepest transport occur are those zones of highest recharge, particularly the high-recharge zone corresponding to the Guaje Mountain Fault. This result is consistent with observations of anthropogenic tritium detected in the regional aquifer, albeit at low concentrations. The significant finding of this model is that this tritium appears to be a small fraction of the total amount released: according to the model, most tritium still resides in the vadose zone or has decayed.

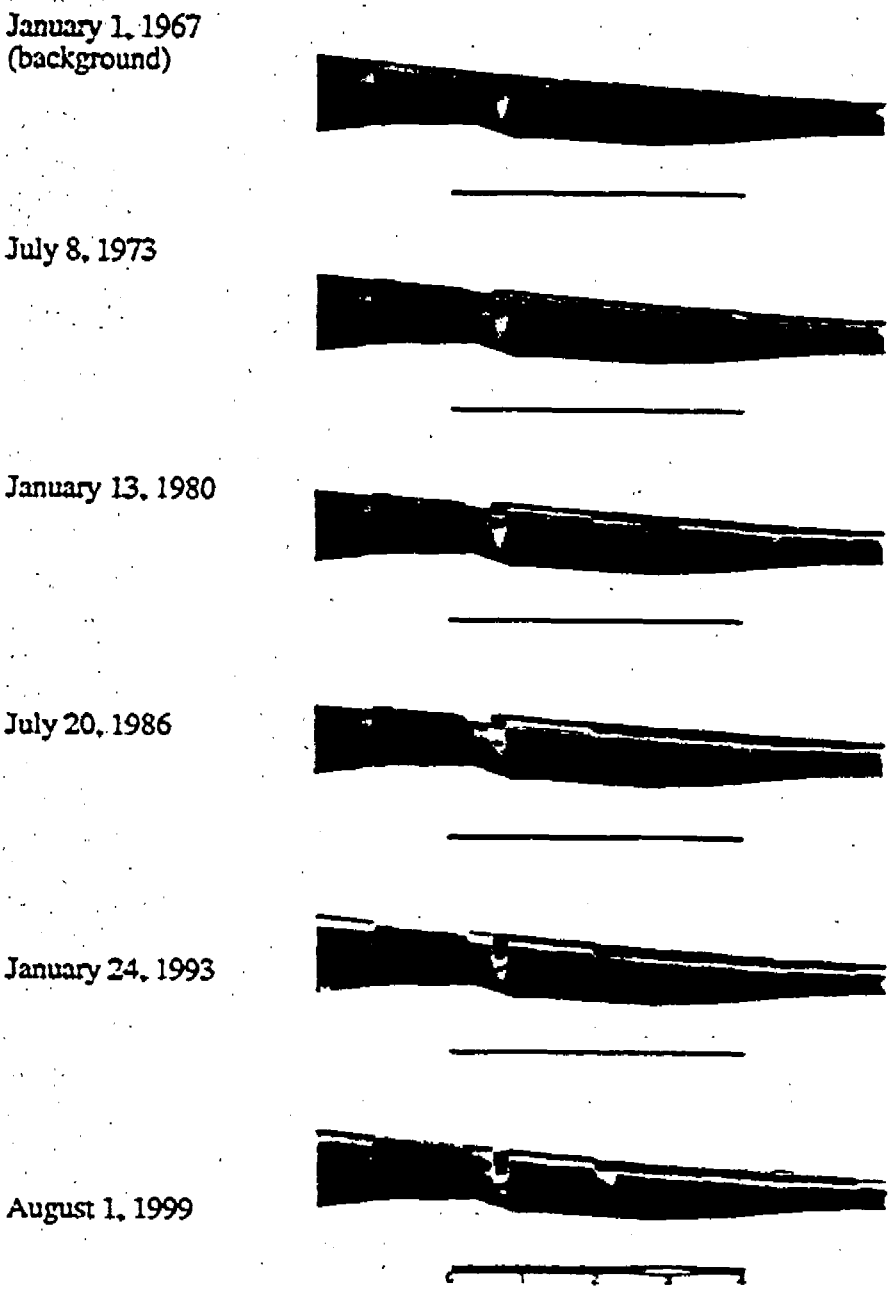

FIGURE 59. Tritium concentrations in the two-dimensional base case model at various times. log10 concentration units used, values in pCi/L.

In recent years the quantities of tritium emitted from Laboratory operations has been curtailed by the cessation of operation of the Omega West reactor and by the improvement of Laboratory operations. The impact of these changes is beginning to be reflected in the lowering of concentrations within the vadose zone, as radioactive decay and dilution with cleaner recharge fluid take effect. The present-day maximum concentration predicted by the model is about 5000 pCi/L, and occurs in the Guaje Pumice Bed. This concentration is consistent with the measured value of 6000 pCi/L found in the perched water of the Guaje Pumice Bed in LADP-3. This result suggests that we probably should not expect to find significantly higher concentrations in samples collected in future wells, and that the zones of highest concentration should be expected at this horizon. Future well drilling and sampling can be used to test this result.

Previously, we showed that the perched water scenario can exert a strong control over the detailed flow paths in the subsurface. Figure 60 shows the predicted tritium concentrations for the lateral diversion scenario with reduction factor of 0.001. Note that in contrast the previous figure for the base case, these figures use a 3X vertical exaggeration, and only the portion of the model from the Guaje Mountain fault to just past the confluence of Los Alamos and DP canyons are displayed. The influence of lateral diversion at the Guaje/Puye interface can be detected, but the overall results are not that dissimilar from the base-case results. Contrary to the conceptual model of lateral diversion causing a "fast path" to the regional aquifer, this model predicts somewhat slower downward transport than the base case. This is seen more clearly in Figure 61, a side-by-side comparison of the predicted present-day concentration fields for the two models. Lateral diversion results in longer travel pathways, and hence longer travel times to the regional aquifer.

We now use these two models to predict future tritium transport through the vadose zone. For this calculation we assume that current low concentrations of tritium in the alluvial water will continue indefinitely, the result of actions taken by the Laboratory to reduce emissions. Forward simulations for the next century are displayed in Figures 62 (base case) and 63 (lateral diversion scenario). The natural processes of dilution, radioactive decay, and arrival at the regional aquifer are expected to reduce the concentrations to historical background levels in the next 50 to 100 years. There seems to be little difference in the two simulations with respect to this "bottom-line" conclusion, although there are differences in the details. This calculation illustrates the time scale over which vadose zone transport occurs in this wet canyon setting. Travel times are of the order of decades through large portions of the vadose zone.

Another way to understand the results of the tritium transport simulations is to examine the overall mass input and output of tritium from the model. The input enters in the recharge fluid, and the output leaves the vadose zone at the regional aquifer water table. Figure 64 shows the results of this analysis for the base case simulation, and Figure 65 is the same plot for the lateral diversion case (reduction factor of 0.001). The plots begin on January 1, 1967, and extend to the present time (the black curves), and then the future predictions are in blue. The total input over the past thirty years has been two to three orders of magnitude higher than the background, but has declined recently due to changes in laboratory operations. The model results suggest that only recently has a significant quantity of tritium reached the regional aquifer (the dotted curves). Under the assumed future release scenario, tritium mass flux reaching the water table should peak some thirty years from now. This implies that the majority of the tritium that has not

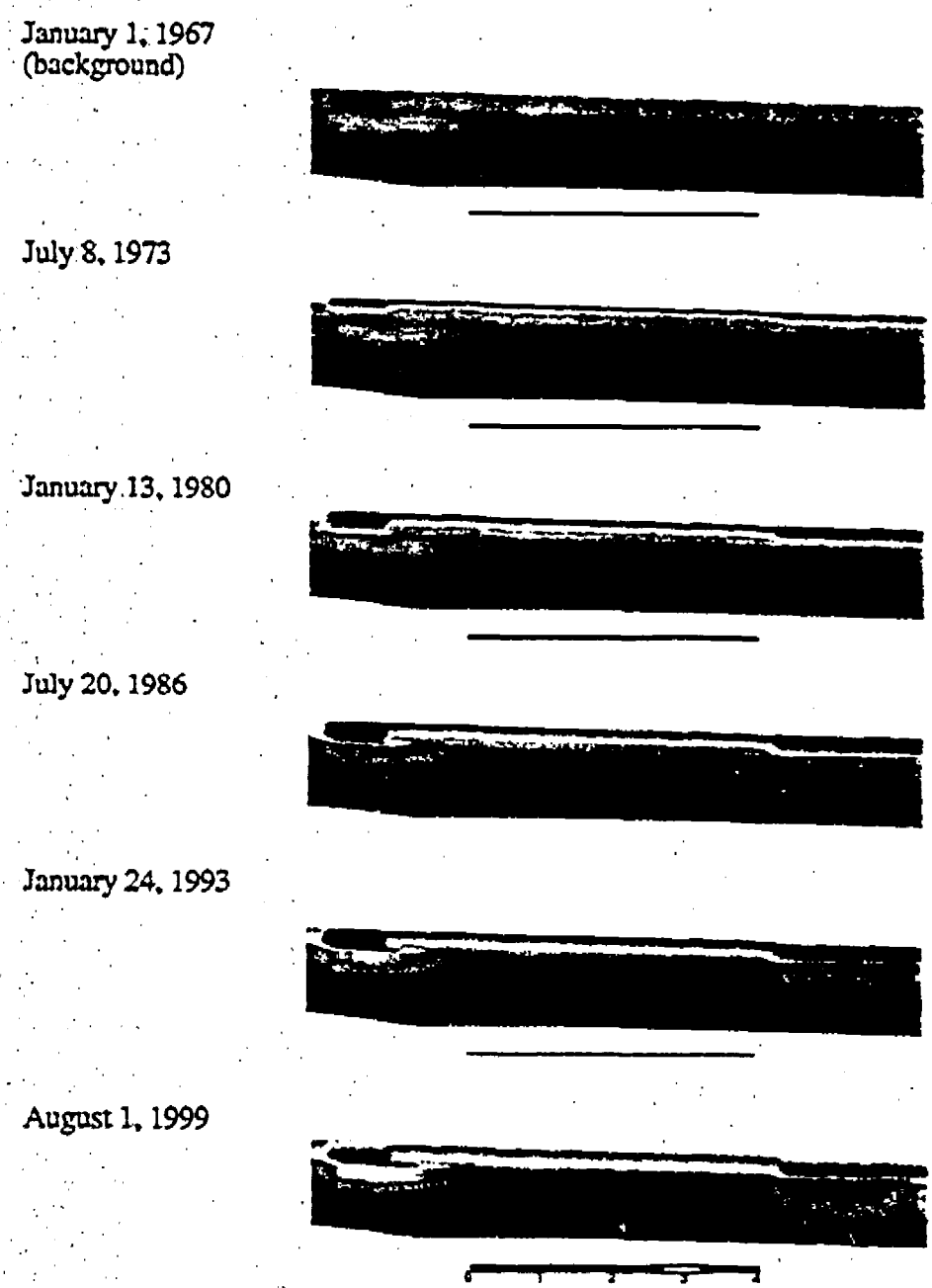

FIGURE 60. Tritium concentrations in the two-dimensional model, lateral diversion, reduction factor = 0.001, at various times. log10 concentration units used, values in pCi/L.

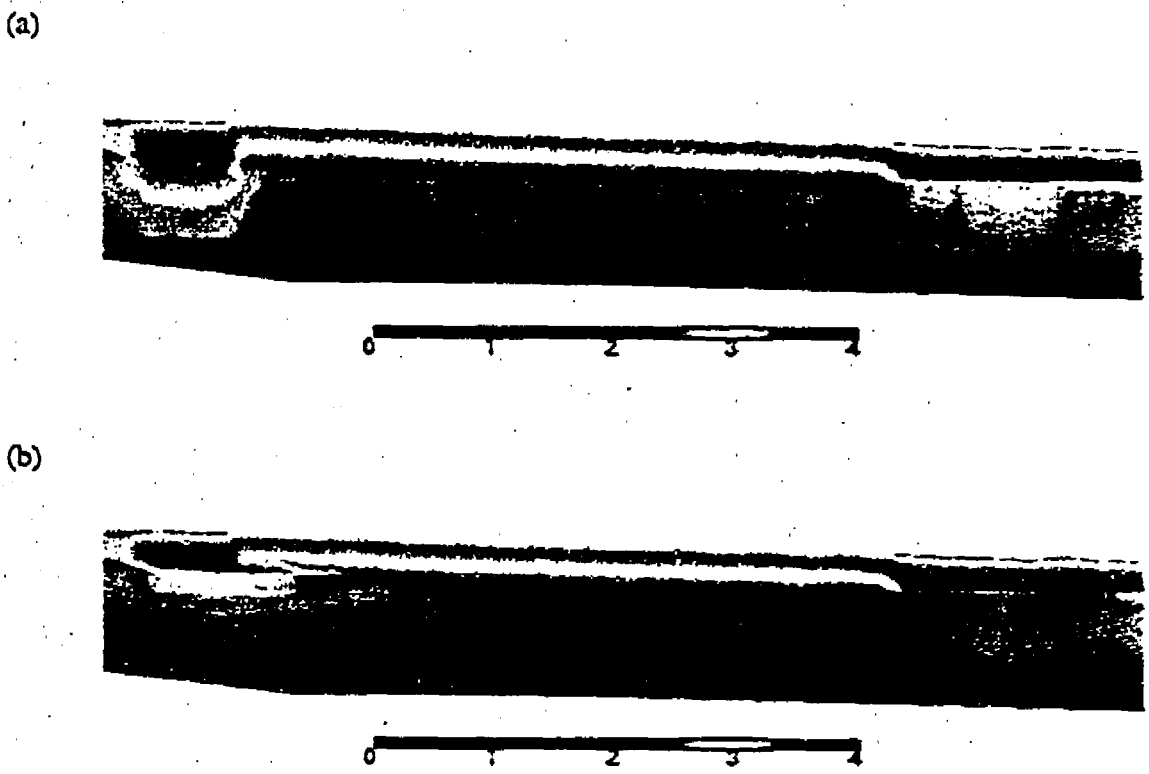

FIGURE 61. Comparison of the tritium transport results for the base case and the lateral diversion case. The region plotted is in the vicinity of the high recharge zone near the Guaje Mountain fault.

decayed still resides in the vadose zone. Note also that the peak mass flux leaving the vadose zone model is three orders of magnitude lower than the peak input mass loading. This implies that the vadose zone provides enough of a barrier to downward migration that the majority of the mass decays or is diluted by clean water residing in the vadose zone before reaching the regional aquifer. As a final observation, note that the base case and lateral diversion scenarios seem to yield only slightly different results with respect to the overall mass flux and travel times through the vadose zone in Los Alamos canyon. The lateral diversion case yields somewhat longer travel times to the water table, and hence somewhat lower mass flux values for tritium.

The final result from these runs the predicted time history of concentration at a point selected in the Guaje Pumice Bed within the high recharge zone associated with the Guaje Mountain fault. Figure 66 shows the predicted concentration-time history of tritium concentration at this location for the base case. The model predicts that the maximum concentration, due to the high mass flux inputs in the early 1970's is just now in the Guaje Pumice bed. Thus, the bulk of the undecayed mass is still in the vadose zone.

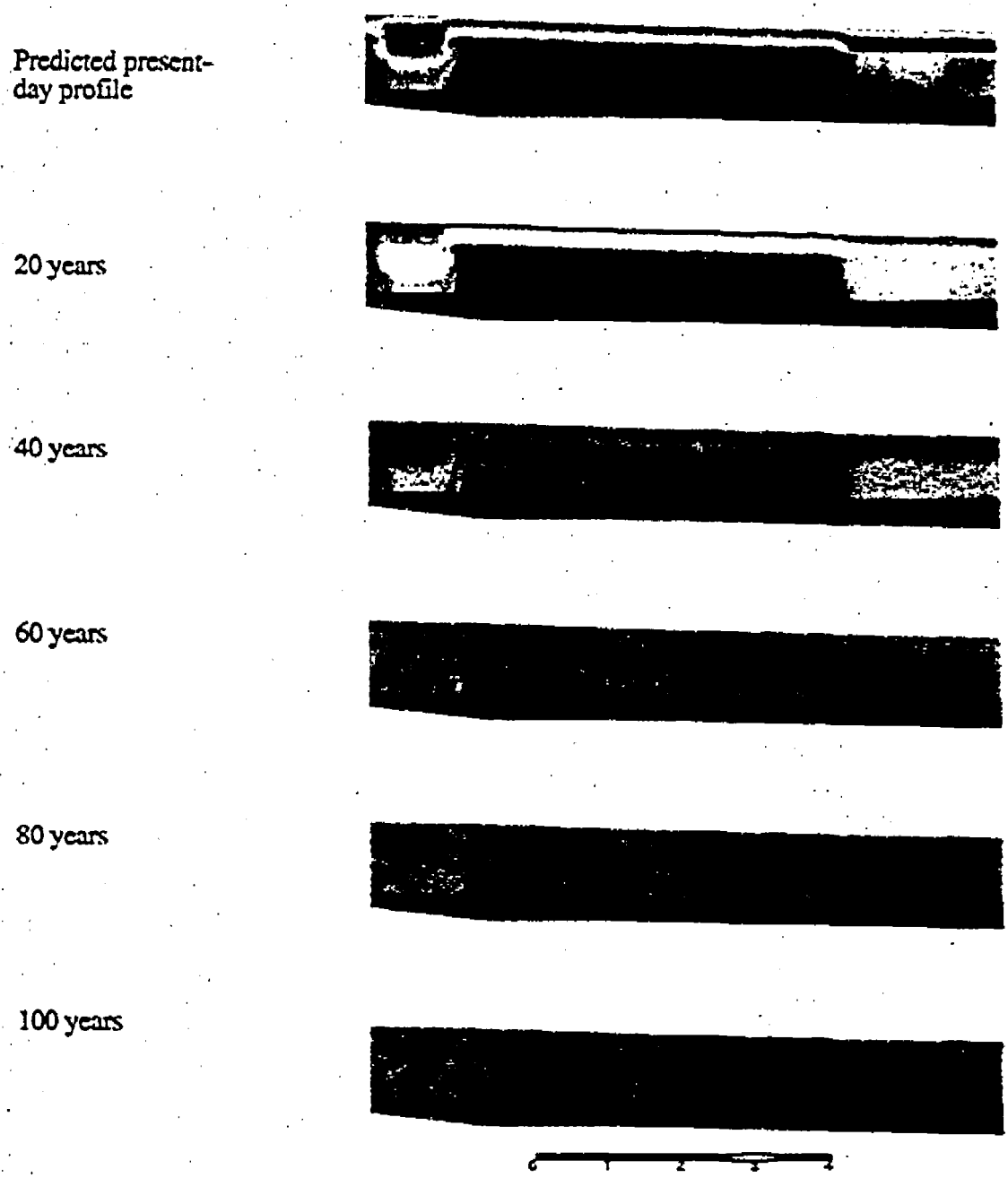

FIGURE 62. Future predictions of tritium transport for the two-dimensional, base-case model.

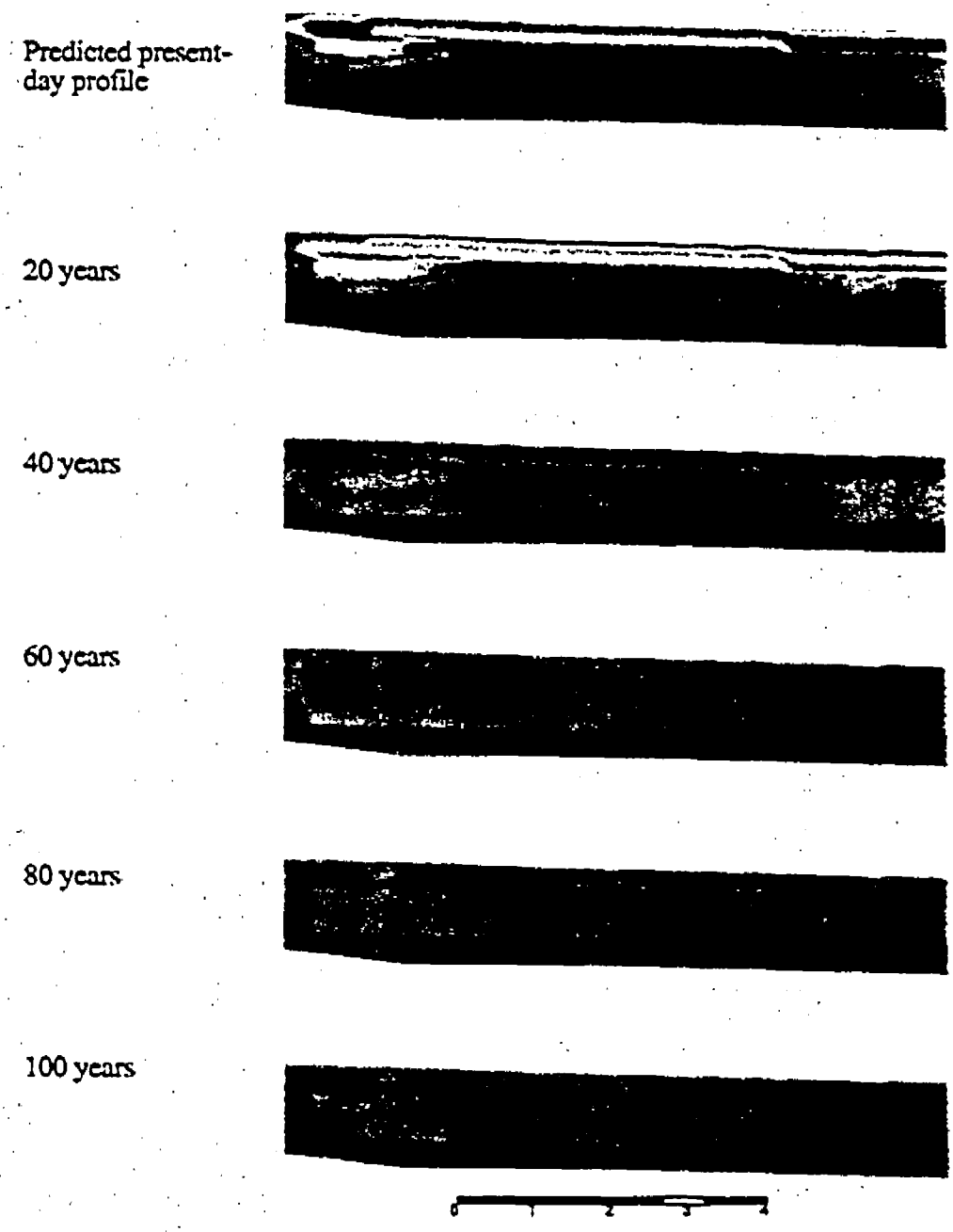

FIGURE 63. Future predictions of tritium transport for the two-dimensional, lateral diversion model.

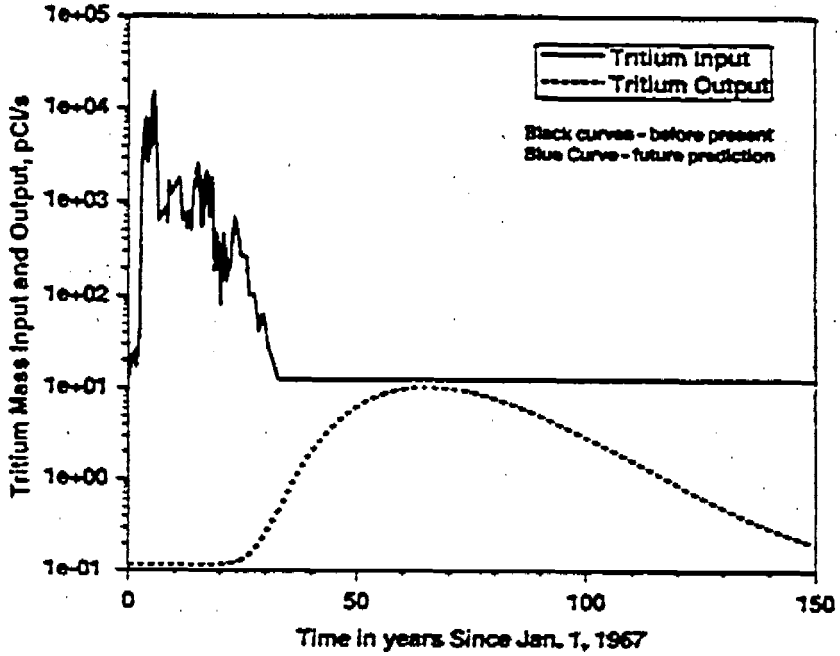

FIGURE 64. Predicted input and output tritium mass flux from the model for the base-case simulation. Black curves - past simulation. Blue curves - future simulation.

as stated earlier. The present-day concentration at this location is about 3650 pCi/L, less than the maximum in the model by almost a factor of two, but in line with the value detected in the LADP-3 sample. We can also use such a simulation to design a sampling scenario assuming that intermediate wells are drilled to monitor contaminant concentrations. The tritium breakthrough curve predicted by the model implies that only very small changes in concentration are likely to occur in the time frame of months to a year. One would only expect significant changes to occur over decades of sampling at depth. This factor should be considered in the design of a long-term monitoring system to assess the impact of Laboratory contaminants on the groundwater.

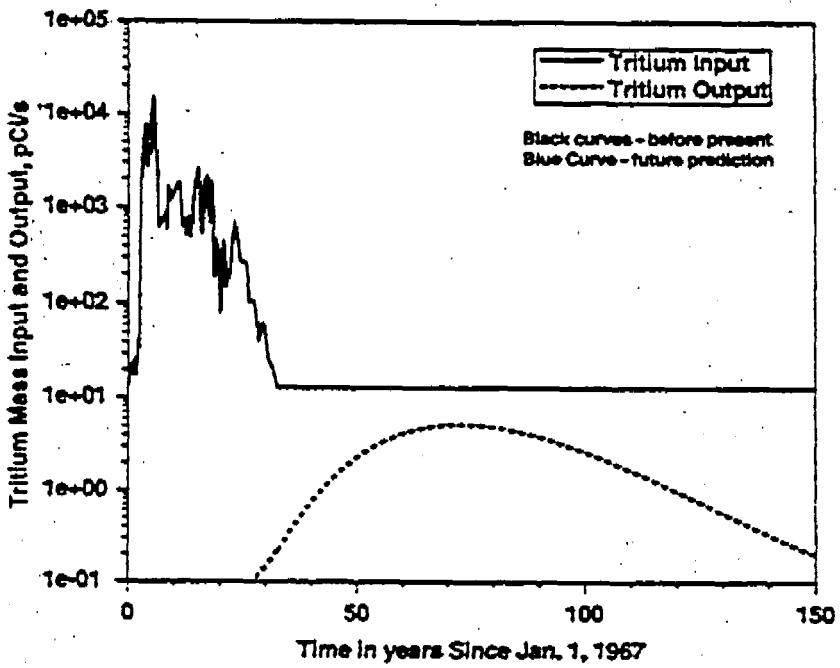

FIGURE 65.

Predicted input and output tritium mass flux from the model for the lateral diversion simulation, reduction factor = 0.001. Black curves - past simulation. Blue curves - future simulation.

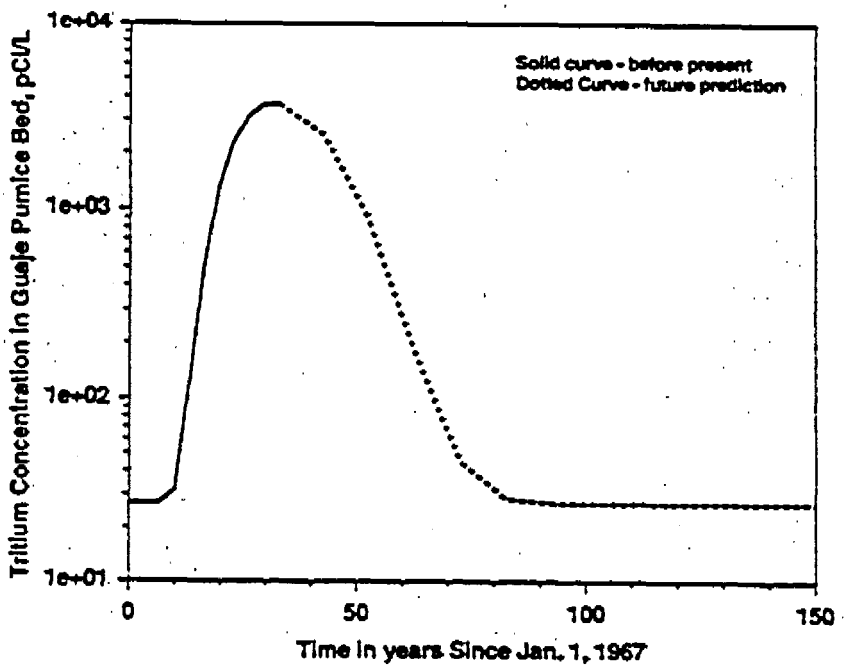

FIGURE 66. Predicted concentration-time history of tritium concentration in the Guaje Pumice bed in the region defined as high recharge (Guaje Mountain Fault zone).

9.0 Acknowledgements:

This work was performed under the auspices of the Department of Energy, Los Alamos Environmental Restoration Project. We thank Dave Broxton and Diana Hollis for supporting the effort. We also thank the following individuals for their assistance in various aspects of the technical work: Bob Gray for his assistance in supplying information and recommendations on the use of his recharge study for Los Alamos canyon; David Rogers for useful discussions on hydrology and modeling issues for the Pajarito Plateau, and for assistance in obtaining data files for hydrologic parameters for the Otowi member; Everett Springer, Dave Broxton and Pat Longmire for supplying us unpublished hydrologic and test well data; Bill Stone for useful discussions and assistance in tracking down data sources; Greg Cole and Bill Carey for providing the stratigraphic framework model in a form suitable for grid development; Carl Gable for technical guidance during the grid generation process; Andy Wolfsberg for his help in the generation of some of the graphics; Gilles Bussod for helpful discussions in the transport model development; Elizabeth Keating for providing the water table map used for the bottom boundary condition of the models; and Marcia Jones for producing a map of the test wells and for performing a variety of tasks needed to complete the model development.

10.0 References

W.V. Abeele, M. I. Wheeler and Burton, Geohydrology of Bandelier Tuff, LA-8962-MS, 1981.

AquaLab CX-2T Technical Information via Decagon Devices, Inc., Pullman, WA 99163 509/332-2756 FAX 509/332-5158.

G.W. Gee et al. Soil Science Society of America Journal, 56, #4, July-August, 1992.

D.E. Broxton et al. Earth Science Investigations for Environmental Restoration - Los Alamos National Laboratory Technical Area 21, LA-12934-MS, 1995.

C. J. Elliott, Initial analysis of infiltration through select samples of the Otowi member in the Pajarito Plateau of Los Alamos County, New Mexico, Los Alamos National Laboratory EES-5 internal report, August, 1999.

R. Allen Freeze and John A. Cherry, Groundwater, Prentice Hall, Inc., 1979.

R. N. Gray, Hydrologic budget analysis and numerical simulations of groundwater flow in Los Alamos canyon near Los Alamos, New Mexico, Master's Thesis, University of New Mexico, Albuquerque, New Mexico, May 1995.

A. Klute, ed., Methods of Soil Analysis, Part 1 - Physical and Mineralogical Methods, Second Edition, American Society of Agronomy, Inc, Soil Science Society of America, Inc., Agron. Monogr. 9 ASA and SSSA, Madison WL [LANL lib S593.B65 1982 pt.1] 1986. S.L. Rawlings and G.S. Campbell, Water potential: Thermocouple psychrometry, p. 597-618.

P. M. Kearl, J. J. Dexter, M. Kautsky, unpublished report, Los Alamos National Laboratory,1986 (cited by Rogers et al., 1996 as obtained by Bendix in 1986).

LANL, Hydrogeologic Workplan, Revision 1.0, Los Alamos, New Mexico, December, 1996.

LANL, Inerim completion report for characterization well R-9, Los Alamos National Laboratory Environmental Restoration Project report, March, 1999.

David B. Rogers and Bruce M.Gallaher, The Unsaturated Hydraulic Characteristics of the Bandelier Tuff, LA-12968-MS, 1995.

David B. Rogers, Bruce M. Gallaher and E. Vold, Vadose Zone Infiltration Beneath the Pajarito Plateau at Los Alamos National Laboratory, LA-UR-96-485, September, 1995.

E. P. Springer, G. J. Langhorst and E. S. Hamilton, "Hydrogeologic Properties of the Bandelier Tuff and Groundwater Occurrence at DP Mesa" "TA-21, Los Alamos National Laboratory, Los Alamos, NM", preprinted July, 1999.

Daniel B. Stephens and Associates, Inc., Laboratory Analysis of Soil Hydraulic Properties of TA-2 Soil Samples, April 1995.

E.A. Sudicky, A Natural Gradient Experiment on Solute Transport in Sand Aquifer: Spatial Variability of Hydraulic Conductivity and Its Role in the Dispersion Process. Water Resources Research 22 #13 2069-2082, 1986

Interim Completion Report for Characterization Well R-12 TABLE C-1 p. C-1, March 1999, Canyons Focus Area: David Broxton, Rick Warren, Andy Crowder, Mark Everett, Robert Gilkeson, Patrick Longmire, Jon Marin, and David Rogers.

M. Th. van Genuchten, 1980, A closed-form equation for predicting the hydraulic conductivity of unsaturated soils, Soil Science Society of America Journal, 44 892-898, 1980.

Mualem, 1976, A new model for predicting the hydraulic conductivity of unsaturated porous media, Water Resources Research, 12, 513-522.

G. A. Zyvoloski et al., Summary of the models and methods for the FEHM application - a finite element heat- and mass-transfer code, Los Alamos National Laboratory report LA-13307-MS, July, 1997.

11.0 Appendix 1. Summary of effluent sources and contaminants to Los Alamos and DP Canyons

Leslie Dale

Richard Koch

SAIC, Inc.

TA-43 Health Research Laboratory

Established in 1953 with the opening of the Health Research Laboratory (TA-43-1). Industrial waste lines carried liquid waste to the TA-45 wastewater treatment facility from 1953 to 1963. The TA-43 system was diverted to the LA County sanitary sewer system's Bayo Plant in 1963. The lines were diverted to the TA-3 sanitary treatment plant in 1981, which in turn was decommissioned and rerouted to the TA-46 WWTP in 1993. In 1975, the practice of pouring low level radioactive waste down the drain was discontinued and containers for the transfer of contaminated liquid wastes to the treatment plant at TA-50 were placed in laboratories. Summaries are from the *RFI Work Plan for Operable Unit 1136* (LANL 1994, ER ID ?) Chapter 2, 5 and 6 - Outfalls.

PRS 43-001(b$_2$) - permitted as NPDES 03A040 in the mid-to-late 1970s; discharged from 6 floor drains in the sub-basement of the HRL (TA-43-1), evaporative cooler blowdown, and stormwater from 13 roof drains on the west side of the HRL. May have received potentially radioactive once-through cooling water prior to permitting.

PRS C-43-001 – storm drain outfall that drained a dock area of the HRL and doubled as an overflow line for the lift station (TA-43-10) [which was part of PRS 43-001(a1), a sanitary sewer line]. No records of routine releases to the storm drain, however the outfall may have received potentially radioactive, nonsanitary cooling water.

PRS 43-001(b$_1$) – outfall pipe that discharged from a drinking fountain located in transportable building TA-43-24. No hazardous constituents were managed or released from this site.

TA-1 Townsite

Summaries are from the *RFI Work Plan for Operable Unit 1078* (LANL 1992, ER ID 43454) Chapter 6 - Septic Systems, Storm Drains, and Outfalls.

Aggregate A – Sigma Building

PRS 1-006(m) – TA-1-56, -74 storm drain and outfall – three storm drains that drained areas around the Sigma Building and had outfalls north of Sigma Building (may have drained to Hillside 140 area given historical topography). Sigma Building used for plutonium, uranium and thorium machining, casting, and powder metallurgy – operated from early 1940s to Dec 1965. Suspected contaminants: ^{239}Pu, ^{235}U, ^{238}U, thorium, toluene, solvents, metals. No effluent volumes reported.

PRS 1-006(t) – TA-1-5 storm drain and outfall – drained an area near C Building (probably toward Bailey Canyon). No record of contamination from sampling conducted during the 1974-1976 rad survey. Suspected contaminants: ^{239}Pu, ^{235}U, ^{238}U, thorium. No effluent volumes reported.

Aggregate B – Bailey Bridge

PRS 1-001(a) – Septic Tank 134 - served Warehouse 19 and the Sheet Metal Shop. Tank was active from 1949 to 1964 and was removed in 1975. The outfall from the tank discharged over the rim of Bailey Canyon. Suspected contaminants: ^{238}U, unspecified hazardous chemicals. No effluent volumes reported.

PRS 1-001(e) – Septic Tank 139 – served the D-5 Sigma Vault and I Buildings from approximately 1947 to 1965. Discharged to the head of Bailey Canyon. Suspected contaminants: ^{239}Pu, ^{235}U, beryllium, ^{137}Cs and unspecified metals. No concentrations or effluent volumes reported.

PRS 1-001(n) – Septic Tank 276 – served Theta Building from 1944 to 1946. Discharged to the head of Bailey Canyon. Tank assumed to be free of contamination. Suspected contaminants: ^{239}Pu. No effluent volumes reported.

PRS 1-001(o) – Sanitary Waste Line from Buildings J and ML – discharged directly into Bailey Canyon. Partially removed in 1959; remnants found and subsequently removed during 1974–1976 cleanup. In 1959, the drain from J and ML buildings was contaminated with between 500 to 4,000 cpm alpha. Suspected contaminants: ^{239}Pu, ^{235}U, metals. No effluent volumes reported.

PRS 1-006(o) – TA-1-1, -2, -5, -26, -61 Storm Drain and Outfall - Served Buildings A, B, C, H, and Sigma 4 and discharged to the head of Bailey Canyon. The storm drainage system was found to be contaminated with up to 74 pCi/g of gross alpha activity. Suspected contaminants: ^{235}U, ^{238}U. No effluent volumes reported.

PRS 1-006 (r) – TA-1-34, -79 Storm Drain and Outfall – Drained areas around J and X Buildings; discharged just south of J-7 Building toward Bailey Canyon. No rad contamination found in drain or outfall area during 1976 survey. Suspected contaminants: Radioactive targets, metals. No effluent volumes reported.

PRS 1-003(a) – Bailey Bridge Landfill – began receiving radioactively contaminated concrete and building debris in 1964; disposal was not allowed by outside contractors. Massive quantities of concrete and debris contaminated with low levels of natural and enriched uranium was deposited into Bailey Canyon and covered with fill. General criteria was <2500 cpm surface alpha contamination. Much of this debris resulted from the 1974 to 1976 cleanup of TA-1. Suspected contaminants: ^{239}Pu, ^{235}U, ^{238}U, thorium, metals.

Aggregate C – Hillside 140

Hillside 140 is located west of the Ridge Park Village Condominiums.

PRS 1-001(b) – Septic Tank 135 - served Building M1, a shop for machining lithium and possibly ^{238}U, from 1950 to 1964. Discharged to Los Alamos Canyon just east of Hillside 140 tributary. Tank was removed during 1974–1976 cleanup. No rad contamination found in tank or lines. No effluent volumes reported; no contaminants suspected.

PRS 1-001(f) – Septic Tank 140 – served Buildings HT and FP from approximately 1945 to 1965 and discharged into the Hillside 140 tributary. Although a sanitary system, it received radioactive waste from heat treatment facility operations. 1974–1976 sludge samples from tank contained 60,000 cpm U activity; tank, inlet and outlet lines also contaminated. Tank, inlet and outlet lines, and 351 yd^3 of surrounding soil (max U concentration 3000 pCi/g) removed in 1975. Suspected contaminants: ^{239}Pu, ^{235}U, ^{238}U, nonferrous metals. No effluent volumes reported.

PRS 1-006(p) – TA-1-29, -98 Storm Drain and Outfall – drained southwest side of HT Building and discharged to Los Alamos Canyon. 1976 survey showed no contamination of drain or outfall. Suspected contaminants: ^{239}Pu, ^{235}U, ^{238}U, nonferrous metals. No effluent volumes reported.

Aggregate D – J-2/TU Area

The J-2/TU Area housed fission product radiochemistry operations, plutonium tracer experiments, and uranium processing. The area is located beneath present day Ridge Park Village.

PRS 1-001(i) – Septic Tank 143 – served J Division Annex (used for storage and film calibration) and TU Building from early 1940s to approximately 1964; probably discharged to Hillside 140 tributary. Tank removed during 1974–1976 cleanup; rad survey showed no contamination in tank sludge. Suspected contaminants: uranium, metals, solvents. No

effluent volumes reported.

PRS 1-001(k) – Septic Tank 268 – served TU Building from early 1940s until removed in 1964. Discharged to Hillside 140 tributary. Suspected contaminants: uranium, metals, ^{137}Cs. No effluent volumes reported.

PRS 1-006(f) – TA-1-76 Storm Drain and Outfall – drained Warehouse 4 area (used for non-rad, non-haz storage). Probably discharged to Hillside 140 tributary. Low level U contamination found in outfall area during 1974-1976 survey (gross alpha max 44 pCi/g). Suspected contaminants: uranium. No effluent volumes reported.

PRS 1-006(k) – TA-1-75, -76 Storm Drain and Outfall – drained area between Warehouse 4 and the J Division Annex. Probably discharged to Hillside 140 tributary. 1974-1976 survey found "uranium contamination" near the storm drain outfall that was believed to have originated from the TU and TU-1 Buildings. Suspected contaminants: uranium. No effluent volumes reported.

PRS 1-006(l) – TA-1-74, -75 Storm Drain and Outfall – drained area between Warehouse 2 (used for non-rad storage) and the J Division Annex. Probably discharged to Hillside 140 tributary. 1976 survey indicated no rad contamination. Suspected contaminants: solvents. No effluent volumes reported.

Aggregate E – Cooling Tower 80

Cooling Tower 80 served Building X, which housed the Harvard cyclotron where many radioactive targets were tested. Area is located east of Bailey Canyon.

PRS 1-001(c) – Septic Tank 141 – served Building X and discharged to Los Alamos Canyon. Removed during 1974-1976 cleanup; no rad detected in tank, sludge, or surrounding soil. Suspected contaminants: ^{239}Pu, ^{235}U, ^{238}U, metals. No effluent volumes reported.

PRS 1-006(a) – TA-1-80 Drain Line and Outfall – may have discharged chromium; one 1980s soil sample indicated no metal, organic compound or rad above background. Discharged to Los Alamos Canyon. Suspected contaminants: ^{239}Pu, ^{235}U, ^{238}U, metals. No effluent volumes reported.

PRS 1-006(e) – TA-1-79, -42, -49, -6, -10, -13 Storm Drain and Outfall – served Buildings X, M, Q, D, D-4, and D-7. Discharged to Los Alamos Canyon. Suspected contaminants: ^{239}Pu, ^{235}U, ^{238}U, metals. No effluent volumes reported.

Aggregate F – Hillside 138

Hillside 138 is located south of present day MK/PMC office building and west of Los Alamos Inn.

PRS 1-001(d) – Septic Tank 138 – served Buildings K (chemical stock room), V (uranium and beryllium machine shop), and Y (physics laboratory that handled tritium, ^{238}U, and ^{210}Po) from early 1940s to approximately the mid 1960s and discharged to Los Alamos Canyon. Mercury spills of unspecified amounts were reported in Building K. In 1946, high alpha and gamma radiation were confirmed at the waste outlet of Y Building; polonium was observed at the drain exit, but no plutonium was detected. The 1974-1976 rad survey found ^{239}Pu on the hillside below tank 138 at maximum concentrations of 3,600 pCi/g on the upper level of the slope and 8,900 pCi/g on the lower level. 137Cs also listed as a principal contaminant (no concentrations reported). Suspected contaminants: ^{239}Pu, ^{235}U, ^{238}U, ^{137}Cs, beryllium, barium, chloride, mercury, tritium, solvents. No effluent volumes reported.

PRS 1-006(h) – TA-1-50, -81 Storm Drain and Outfall – served the northwest side of Building R (model, glass, carpentry and plumbing shops), and the east side of Building Y. The outfall was located 25 ft south of Building Y near the north edge of the perimeter road adjacent to Hillside 138. During the 1974-1976 rad survey, puddles of elemental mercury (quantity not specified) were present in the drain line; the mercury and drain were removed. Suspected contaminants: ^{239}Pu, ^{235}U, ^{238}U, mercury, tritium. No effluent volumes reported.

Aggregate G – Hillside 137

Hillside 137 is located south of present day Los Alamos Inn. Structures in this aggregate were vacated in the mid 1950s

PRS 1-001(c) – Septic Tank 137 – Installed in 1945, one of the drain lines associated with the former laundry in Building D-2 was connected to the tank at that time. Is likely that most of the contamination present on Hillside 137 is due to laundry operations and not to septic tank discharges. In 1975, septic tank 137 was relocated and investigated as the source of plutonium contamination found in the run-off area below the outfall pipe from the tank. Tank removed in 1975. Low levels of activity detected in soil along sidewalls of tank excavation. Suspected contaminants: ^{241}Am, ^{239}Pu, ^{235}U, ^{238}U, metals. No effluent volumes reported. See PRS 1-007(b).

PRS 1-006(b) – TA-1-6 Drain Line and Outfall – served D Building (plutonium processing – converted plutonium nitrate solution into a purified metallic form) and discharged to Los Alamos Canyon. The types and quantities of fluids handled by this drain line are unknown. Suspected contaminants: ^{239}Pu, ^{235}U.

PRS 1-006(c) – TA-1-8 Drain Line and Outfall – consisted of three drain lines and outfalls that served D-2 Building and discharged directly on to Hillside 137. Suspected contaminants: ^{241}Am, ^{239}Pu, ^{235}U. Effluent types and volumes not reported.

PRS 1-006(d) – TA-1-9 Drain Line and Outfall – served D-3 Building (rad counting lab) and discharged to Hillside 138 in the same area as the D-2 Building drain lines (laundry outfalls – see PRS 1-007(b). Suspected contaminants: ^{239}Pu, ^{238}U. Effluent types and volumes not reported.

PRS 1-006(n) – TA-1-6 Storm Drain and Outfall – served southeast side of D Building and discharged to Los Alamos Canyon. Suspected contaminants: ^{239}Pu, ^{235}U, ^{238}U. No effluent volumes reported.

PRS 1-007(b) – Soil contamination – D-2 Building was used as a rad laundry (contaminated equipment and clothing) facility for 2 years (in 1945, laundry moved to DP site). Drain lines from the laundry facility discharged directly onto Hillside 137. In 1945, Building D-2 was converted to an electronics shop and the drain line was extended southward and buried to contain contamination. At that time, septic tank 137 was installed and one of the waste drain lines was connected to the septic tank. In 1975, surveillance trenching activities found significant contamination at the ends of two outfall pipes extending from the laundry; both pipes were contaminated with ^{239}Pu and ^{241}Am. Suspected contaminants: ^{241}Am, ^{239}Pu, ^{238}U, metals.

Aggregate H – Surface Disposal Site Southeast of Los Alamos Inn

PRSs 1-001(h), 1-001(i), and 1-001(l) – Septic Tanks 142, 149, and 269, respectively. No known fugitive discharges. No contaminants suspected – all recommended for no further action (NFA) in the work plan. No effluent volumes reported.

PRSs 1-006(i), 1-006(j), and 1-006(q) – Storm Drains and Outfalls serving TA-1-54 and –50, TA-1-53, and TA-1-64, respectively. No known fugitive discharges. No contaminants suspected – all recommended for NFA in the work plan. No effluent volumes reported.

Aggregate I – Can Dump Site

PRS 1-001(m) – Septic Tank 275 – served Warehouse 13 (Zia Company Operations site) from approximately early1940s until mid to late 1950s and discharged to Los Alamos Canyon (or more likely, to the small tributary to Los Alamos Canyon in this area). Location is near storage buildings south of present day Sonic Drive-In. Bulldozed into tributary of Los Alamos Canyon prior to 1974-1976 cleanup. No contaminants suspected. No effluent volumes reported.

TA-41 Weapons Development Facility

TA-41 was used, starting in the early 1940s, for nuclear weapons development and long-term studies on weapon subsystems. Summaries are from the *RFI Work Plan for Operable Unit 1098* (LANL 1993, ER ID 21404) Chapters 3 and 7-Outfalls, Drains, and Accidental Releases.

PRS 41-001 – abandoned septic tank – discharged to a single drain tile line. Believed to have served a single bathroom from the TA-41-2 guard shack from 1949 to 1953. However, one report (Balo and Warren 1986, 0022, cited in work plan) indicated that the tank was radioactively contaminated with low levels of plutonium, uranium, and tritium. Discharge volumes not reported.

PRS 41-002 – Sewage Treatment Plant – built in 1951, consists of and Imhoff tank and an 800 ft^3 chlorinator, a contact tank, and a drying bed. Handled sanitary waste from TA-41 from 1951 and from TA-2 from the early 1970s until 1987 (then rerouted to TA-3). When in use, discharged to NPDES SSS06S in Los Alamos Canyon. Liquid and sludge effluent data from the treatment plant was collected periodically during 1978 to 1986 (Rad Data 1992, 14-0043, cited in work plan). Data summary: Liquid – alpha generally <2 pCi/L with 7 pCi/L measured in Feb 1984, beta average 6 pCi/L with a peak of 156 pCi/L in Jan 1983, gamma average 50 pCi/L with peak of 1443 pCi/L in Dec 1979, tritium highly variable ranging from about 100 to 5,000 pCi/L. Sludge showed elevated alpha/beta, gamma, and tritium. Effluent volume not reported.

PRS 41-003 – sump pit – served TA-41-1, handled storm water and water used to hose out the storage tunnel at TA-41. Tunnel built in 1948, sump removed in 1988. Tunnel used to store TRU wastes and tritium, but past releases unknown.

PRS C-41-004 – storm drainages – consists of several drainages and catch basins/manholes around TA 41-4. No evidence of intentional discharges other than storm water, however the stack between buildings TA-41-1 and TA-41-30 is known to have had operation releases of tritium. Surface contamination of the drains might have resulted from these operational releases. No monitoring of the drains or outfall conducted in the past and no discharge volumes reported.

TA-2 Omega West Reactor Site

TA-2 was used since 1943 to house a series of research reactors. Early reactors were fueled by aqueous uranyl solutions, whereas other reactors (including the OWR) were fueled by solid fuel elements. The earliest of these reactors consisted of three successive homogeneous liquid-fueled reactors, including the first ever of that type (water boiler) which was assembled in late 1943. These reactors were fueled by aqueous solutions of a uranium salt, enriched in 235U; the last modification was deactivated in 1974. The first of the solid fuel reactors involved a now-decommissioned plutonium-fueled, mercury-cooled reactor. The reactor system was self contained and operated from 1946 to 1953. Since 1956, TA-2 has been the operating site of OWR and 8-MW, a water-cooled research nuclear reactor fueled by highly enriched uranium contained as solid fuel. Summaries are from the *RFI Work Plan for Operable Unit 1098* (LANL 1993, ER ID 21404) Chapters 3 and 7-Outfalls, Drains, and Accidental Releases.

PRS 2-003(a-e) – the Water Boiler Reactor and associated lines and a holding tanks– operated from 1944 to 1974, and underwent D&D in 1986-1987. Secondary reactor cooling water, which contained small amounts of fission products, was routinely discharged to Los Alamos Creek. In 1964, a water hold-up tank [PRS 2-003(e)] and alarm was installed to collect secondary cooling water in the event a break occurred in the reactor cooling coils with subsequent infiltration of primary reactor solution into secondary cooling water. Prior to 1964, if such a break occurred, primary cooling water containing uranium and fission products would have been discharged into Los Alamos Creek with the secondary cooling water. Effluent volumes and gross beta activity released in effluent reported for the Water Boiler Reactor for 1967 through 1969 is located in Excel file LA-DP Effluent Discharge Records.xls as reported per Whipple 1970 (ER ID 8750).

PRS 2-004(a-g) – the OWR and associated USTs, underground pits, etc. - Accidental releases documented in DOE 1987, 0264:
In February 1964, 125 gallons of slightly acidic liquid waste of short-lived isotopes was discharged from the OWR storage tanks into Los Alamos Canyon. The discharge contained 2 mCi ^{51}Cr, 0.43 mCi ^{124}Sb, 0.2 mCi ^{59}Fe, and 0.2 mCi ^{54}Mn.

In May 1964, 1000 gallons of liquid from the resin bed regeneration was discharged. It contained short-lived radionuclides and 2.5 mCi of ^{54}Mn.

In 1970, a monitoring report stated that water from the acid pit [PRS 2-004(e)] was pumped into the creek through a concrete trench. Before decontamination, radiation levels as high as 30 mR/h were measured in the trench.

In 1972, water was reported to have been dumped into a floor drain that emptied into the creek. Radionuclides ^{24}Na, ^{56}Mn, and ^{64}Cu were identified in the dump.

Effluent volumes and gross beta released in effluent from the OWR for years 1967 through 1969 is located in Excel file LA-DP Effluent Discharge Records.xls as reported per Whipple 1970 (ER ID 8750).

Tritium release from leak at OWR – Releases of tritium resulted from a leak in the primary cooling water system at OWR. The leak occurred from a break in a weld seam in a section of the delay line running from building TA-2-1 to the surge tank. This release was discovered in January 1993 and was within the Guaje Mountain fault zone. Tritium was leaking from the delay line at a rate of up to 70 gal/day until March 1993 when the cooling water was drained from this line. Typical concentrations of tritium in the cooling water ranged from 15.7×10^6 to 20.2×10^6 pCi/L. The duration of the leak is not documented, however tritium concentrations in groundwater sampled from alluvial well LAO-1 (located at the eastern boundary of TA-2) suggest that the leak may have begun between November 1969 and January 1970. OWR was permanently shut down in 1994. Alluvial groundwater tritium data is located in Excel file ESH-18 H-3.xls.

PRS 2-005 – cooling water drift loss - From 1957 to the mid 1970's, potassium dichromate was added to the cooling water in the OWR cooling tower (TA-2-49) to prevent corrosion of the aluminum heat exchangers. In 1971, measurements indicated that 0.05 lb of hexavalent chromium per hour of operation (120 hours/week) was being lost due to cooling tower operations. Calculations based on archival data indicate that approximately 5000 lbs of chromium may have been discharged over a 17-yr period to the soil and sediments adjacent to TA-2-1. Potassium dichromate used was discontinued in the mid-1970s when the aluminum heat exchangers were replaced by stainless steel heat exchangers.

PRS 2-006(b) – acid waste line – discharged chemical waste to Los Alamos Creek, abandoned in place at least 25 years ago. Effluent composition not reported.

PRS 2-006(e) – drain from floor and mezzanine for the OWR reactor room – drain discharged to a sump that overflows to the creek. Spills in the room included primary coolant water that contained long-lived fission products.

PRS 2-007 – decommissioned septic system – consisted of tank (TA-2-43) and leachfield that operated from the 1950s and was removed in 1986. 1967 sludge samples from the tank contained 28,000 pCi/L gross alpha (predominantly from ^{235}U); 2,703,000 pCi/L gross beta (6% from ^{90}Sr); and 500,000 pCi/L gross gamma (from ^{137}Cs). Effluent volume not reported.

PRS 2-008(a) – cooling tower outfall [aka PRS 2-011(e)] – discharged secondary cooling water from 1957 to ?. Hexavalent chromium was discharged continuously in water out of this outfall – see PRS 2-005. No quantification of effluent volume or chromium concentration in effluent. Permitted as NPDES 03A020.

PRS 2-008(b) – photoprocessing outfall from TA-2-4. Hazardous chemicals most likely discharged, however effluent volume and specific amounts of chemicals unknown.

PRS 2-008(c) – outfall from TA-2-1 – probably drained water infiltrating into basement. Water may have come in contact with tritium and fission products due to OWR operations and chromium. Effluent volumes not reported.

PRS 2-011(a) – consists of 11 drains associated with TA-2-1 – all either handled stormwater exclusively or are duplicates of PRSs addressed above.

PRS 2-011(b) – two drains associated with TA-2-19, the stack gas valve house – no operational or discharge history

PRS 2-011(c) – drain in TA-2-44 that discharged to PRS 2-011(d) – outfall - pipe and outfall are likely the route through which liquid effluent from an ion exchange system in TA-2-44 was discharged. Periodically, the ion exchanger would be regenerated by flushing with clean water. The flushed water was discharged directly to the creek from 1957 until 1963. The regenerated effluent water's principal activity is the 15-hour half-life of ^{24}Na, with small amounts of ^{51}Cr (28 day), ^{65}Zn (244 day), ^{124}Sb (60 day). ^{60}Co (5.3 yr) and ^{56}Mn (2.6 hr) have also been documented in regenerate effluent. During this 6-yr period, a maximum rate of about 15 Ci/yr was released through effluent water discharged directly to the creek.

PRS 2-011(d) – outfall – reported in SWMU Report as NPDES 03A019, is not currently permitted per LANL 1993 (ER ID 21404). Engineering drawings indicate that outfall handles stormwater. 03A is the category for cooling tower discharge, however more specific information regarding the discharge history of PRS 2-011(d) is lacking.

TA-32 Medical Research Facility

TA-32 was operated from 1944 to 1954. Located south of the County Annex and southeast of Knecht Street along the north rim of Los Alamos Canyon. Conducted first medical surveillance program on employees (urinalysis). Organic chemistry, radiobiology (radiation effects on tissue), and biochemistry (radionuclide toxicity) studies were performed at TA-32. Summaries are from the *RFI Work Plan for Operable Unit 1079* (LANL 1992, ER ID 7668) Chapter 3 - Septic Tanks

PRS 32-002(a) – Septic Tank – uncertain which TA-32 structures were served. Located near the mesa edge and discharged to Los Alamos Canyon. Radionuclides were used in the TA-32 laboratories and there was no connection to the industrial waste line, therefore contaminants were possibly disposed of through septic system. Septic tank (TA-32-7) was constructed of wood (unusual). No effluent volumes reported.

PRS 32-002(b) – Septic Tank - uncertain which TA-32 structures were served. Located near the mesa edge and discharged to Los Alamos Canyon. Radionuclides were used in the TA-32 laboratories and there was no connection to the industrial waste line, therefore contaminants were possibly disposed of through septic system. Septic tank (TA-32-8) was constructed of concrete. No effluent volumes reported

TA-0

The following summaries are from the *RFI Work Plan for Operable Unit 1071* (LANL 1992, ER ID 7667) Chapters 3, 5 and 6 – Outfalls.

PRS 0-030(i) – Septic system – located south of Trinity Drive and east of 35th St. Information on the buildings served by the tank and its outfall are unavailable; however, the location of the tank suggests that it served residences.

Aggregate 0-B – Zia Warehouses

The Zia Warehouses are located south of the intersection of DP Road and Trinity Drive. The aggregate consists of septic systems believed to have handled only sanitary waste. No effluent volumes were reported.

PRS 0-030(b) – Septic System #1 – located east of the Zia warehouses. Comprised four tanks that served warehouses 1, 2, 5,6, 7, and 8, an office building, the cold storage plant and possibly the eastern portion of TA-1. The tanks discharged to a leach field located east of the warehouses, as well as directly to an outfall in Los Alamos Canyon.

PRS 0-030(m) – Septic system – served an incinerator building in which garbage collected from private residences was burned. This septic system was sometimes called the "grease trap". The outfall line connected with the line from PRS 0-030(b) before discharging into Los Alamos Canyon.

PRS 0-030(1) – Septic system – served warehouses 3 and 4 and discharged through an outfall into Los Alamos Canyon. The system received boiler blow-off which may have contained unspecified descaling chemicals.

Aggregate 0-E – DP Road Storage Area

PRS 0-027 – DP Road Storage site – located at the intersection of Trinity Drive and DP Road (currently the site of the Knights of Columbus Hall). The site was used as a fuel tank farm beginning in 1946 and was converted to a drum storage area in mid-1948. An iron drainpipe(s) may have run under the storage area northward to a discharge point in DP Canyon (conflicting reports on number of drain pipes and if pipes were ever installed). The site was decommissioned in the late 1950s. Suspected contaminants are primary fuel products, including BTEX, VOCs, SVOCs, TPH, metals, and PCBs. 1996 RFI soil samples indicated the presence of 5 inorganic chemicals (antimony, copper, mercury, nickel, and zinc) and 41 organic chemicals at concentrations exceeding background screening values. TPH was detected in several samples at concentrations greater than 4000 mg/kg; benzene was detected at a maximum concentration of 8 mg/kg. 1996 RFI data from draft *RFI Report for PRS 0-027* (LANL 1998, ER ID?).

PRS 0-030(a) – Septic system – located north of the DP Road Storage site. Consists of a single septic system that handled sanitary wastes discharged by the DP Road storage area fuel dispatch office from the early 1940s to approximately the late 1950s. The septic tank outfall discharged to the head of DP Canyon. 1996 RFI Soil samples indicate the presence of tritium (0.11 pCi/g) and $^{239/240}$Pu (0.445 pCi/g) in the soil sample collected at the location of the septic tank outlet. 1996 RFI data is from the *VCA Report for SWMU 0-030(a)*, (LANL 1996, ER ID?).

PRS 0-031(a) – Soil contamination beneath former service station – Former government service station (operated by Zia Company) located at present-day northeast parking lot of Hilltop House Hotel; leased to private operator (Mobil) from 1967 to 1974. Property sold to Hilltop House in 1974 and continued to operate as a service station. Hilltop House made renovations in 1988 and 1989 and removed the original USTs (beneath what is presently the NE parking lot at intersection of 4th St and Trinity) and installed new pumps and tanks north and northwest, respectively, of the hotel convenience store. Site is located north of Trinity Drive near head of DP Canyon. Potential contaminants include BTEX (leaded gasoline), solvents, oils, and greases.

PRS 0-017 - Waste lines – the contaminated waste line through Los Alamos Canyon and one manhole (ULR-33) were removed in between 1981 and 1985. Releases occurred from some of the sumps as a result of processes used during decommissioning. An area of contamination was found in the vicinity of manhole ULR-33, located north of Omega Road in Los Alamos Canyon. ^{241}Am and ^{137}Cs were identified; ^{239}Pu was suspected. Cleanup action was recommended, however no documentation has been located on decontamination of the site. In 1977, a 17 m section of exposed, partially cracked waste line was removed from beneath the north end of Omega Bridge and "some" soil contamination was found under the cracked pipe. The area was reportedly cleaned to equal to or less than 25 pCi/g. Releases of acids and other chemicals are not recorded. No information is available on releases of other potential contaminants.

Aggregate 0-A

PRS 0-012 - Western Steam Plant – located west of and adjacent to the DOE LAAO office. Began operating in 1949 and was on stand-by status until 1990. The Zia Company's wastewater laboratory operated as part of the Western Steam Plant between 1976 and 1983. Blowdown from the steam plant was routed to an underground filtration tank (to remove solids) before effluent was discharged through a drain line to an outfall (NPDES permit number 108). Possible contaminants include waste oil and algicides, which may have been used to treat the water in the boiler. Four drain lines assumed to serve floor drains in the plant extend from the south wall and discharge to the mesa top – any discharge would flow into Los Alamos Canyon. Various chemicals used by the Zia wastewater laboratory are assumed to have been disposed via the floor drains; there is no information on the types of chemicals used. No effluent volumes reported.

TA-26 D-Site

TA-26, D-Site, was established for CMR division; operated from 1946 to approximately 1965; stored radioactive materials in a concrete storage vault. Located southeast of East Gate on SR 502 on mesa edge above north rim of Los Alamos Canyon. Summaries are from the *RFI Work Plan for Operable Unit 1071* (LANL 1992, ER ID 7667) Chapters 3, 5 and 6 – Outfalls.

PRS 26-001 – Canyonside disposal area – consists of debris from a five-room concrete storage vault that was decommissioned and dismantled in 1966 and possibly a septic tank. A pre-decommissioning survey found alpha contamination on the structure of up to 10,000 cpm; contaminants suspected to be enriched ^{233}U and ^{235}U and possibly plutonium. No information documenting the disposition of the radioactive materials stored in the vault are reported.

PRS 26-002(a and b) – Sump system and drains from the vault's equipment room – operated from approximately 1946 to 1965. System was associated with the highly contaminated south center room of the storage vault and is assumed to be contaminated with radionuclides and possibly acids. Consisted of a collection sump and outfall for discharge into Los Alamos Canyon. No effluent volumes reported.

PRS 26-003 – Septic system - consisted of 250 gal steel tank and outfall for discharge to Los Alamos Canyon. It served sanitary facilities located in the east room of the vault from 1948 to 1965. Because radioactive contamination was found in vault, it is possible that contaminants were introduced to the system. Tank may have been disposed over the edge along with the vault debris. No effluent volumes reported.

TA-21 DP Site

The following summaries are from the *Phase Report 1C, TA-21 Operable Unit RCRA Facility Investigation: Outfalls Investigation* (LANL 1994, ER ID?) Chapters 3-10 - Outfalls

PRS 21-004(d) – Drain Line and Outfall – received overflow discharges from an acid waste pumping station (TA-21-223) located at the north side of DP East and occasionally discharged into DP Canyon from 1945 to 1979. Outfall may have received diluted laboratory and chilled water system waste liquids which may have contained mercury, tritium, polonium, actinium, and $^{239/240}Pu$. Tritium was detected at a maximum concentration of 1,700 nCi/L in 1992 RFI soil samples collected below the outfall and in the drainage. No effluent volumes reported. This outfall shares a common drainage pathway with PRS 21-024(h).

PRS 21-006(h) – Underground Seepage Pit and Drain Line/Outfall – received acid wastes from building TA-21-2, located on the south side of DP West. The system was built to accept waste from the ethyl ether extraction process, which was part of an early plutonium purification process at TA-21. The discharge point is approximately eight feet above the bench, immediately below the Los Alamos Canyon edge. No effluent volumes reported. 1992 RFI soil sample analytical results indicate no constituents present above "process area baseline" levels.

PRS 21-011(k) – Industrial Waste Treatment Plant Outfall - NPDES 050050 – outfall discharge line carried treated industrial waste water from the "old" (TA-31-35) and "new" (TA-21-257) industrial waste treatment plants to a discharge point on the south slope of DP Canyon from approximately 1952 to 1985 (effluent routed to TA-50 in 1985). Effluent monitoring records summary for years 1952 to 1961 (years of TA-21-35 operation) which includes discharge volume and gross alpha and plutonium (cpm/L) in effluent is located in Excel file LA-DP Effluent Discharge Records.xls as reported in (no author, no date, ER ID 385). Effluent monitoring records summary for years 1967 to 1985 (years of TA-21-257 operation) which includes discharge volume and contaminant mass released is located in Excel file LA-DP Effluent Discharge Records.xls as reported in SAIC 1998 (ER ID 58719). A 1970 SOP for the DP-257 Waste Treatment Plant states "if gross alpha activity is less than 2,500 c/m/l and there is a shortage of storage capacity in the DP-West tanks, the DP-East tank contents may be discharged to the canyon" in (no author 1970, ER ID 422). In 1972, samples of treated waste from DP-257 (collected from storage tanks) were collected weekly and analyzed for tritium; the volume of waste treated and resultant tritium concentration per week is reported in Christenson 1972 (ER ID 425).

Additional information on the 21-011(k) outfall from Chapter VI in Purtymun 1975 (ER ID 11787):

Industrial Treatment Plant Bldg 35 – 1952 to 1967 – The major contaminates treated were plutonium and americium. Many wastes from this area contained high concentrations of inert salts that would interfere with the usual treatment of plutonium and americium wastes. These wastes were treated separately. Chemical wastes, such as hydrofluoric acid used in processing plutonium, were neutralized and discharged with other effluents from the plant into DP Canyon. The annual discharge into DP Canyon ranged from 7.5×10^3 m^3 to 15×10^3 m^3.

Industrial Treatment Plant Bldg 257 – 1967-1985 – Had a greater capacity for treatment of effluents than Bldg 35. Effluent volume not available.

Data available for Bldgs 35 and 257 include: Analyses of the chemical quality of industrial effluents, average annual concentrations of gross α, gross β, total Pu, tritium, ^{137}Cs, ^{89}Sr and ^{90}Sr in effluents released, and the annual amounts of radionuclides released with effluents (gross α, gross β, total Pu). Radionuclides for which data are available vary by year.

PRS 21-016(a and b) – MDA-T

MDA T comprises seepage Pits (Absorption Beds) for Industrial Effluent. These four absorption beds near Building 35 are the oldest used for the disposal of liquid wastes at Los Alamos. Wastes from the processing of plutonium at TA-21 were released into the beds during the period 1943 to 1952. The use of the beds was reportedly discontinued in 1952 when the Industrial Treatment Plant Building 35 was installed, however discharge volume data to the beds is available for years 1945 to 1967 which suggests that the beds continued to receive waste after 1952 (see below). The source of all waste disposed in MDA T was plutonium-processing waste from DP West, wit the exception of waste from DP East added to the beds from 1965 to 1967. Chemical and radionuclide data for waste discharged to the beds are located in Excel file LA-DP Effluent Discharge Records.xls. In addition, 39.5 m^3 of effluent highly concentrated with ammonium citrate was released into the pits from June 1951 to July 1952. A summary of the citrate waste composition is also located in Excel file LA-DP Effluent Discharge Records.xls. According to Purtymun 1975 (ER ID 11787), the pits were not used from 1952 to 1965. However, the TA-21 Operable Unit Work Plan (LANL 1991, ER ID 7529, Table 16.3-IV) provides a summary of waste volumes discharged to the absorption beds from 1945 to 1967. This discharge summary is located in Excel file LA-DP Effluent Discharge Records.xls. Sources: Purtymun 1975, ER ID 11787, Chapter VI and LANL 1991, ER ID 7529, Chapter 16.3.

Christenson 1973 (ER ID?) estimates a total of 9.82 Ci of Pu was released to MDAs T and V between 1945 and 1951, but does not differentiate the quantity released to each MDA. In addition, estimated quantities of nuclides (tritium, ^{89}Sr, ^{90}Sr, and Pu in Ci) released to Acid, DP, Mortandad, and Ten Site Canyons from 1945 to 1972 are provided, however the estimates represent totals released to the canyons as a whole and do not differentiate releases to each canyon.

PRS 21-017(a through c) – MDA U

MDA U covers an area of 1,200 m^2 (0.2 acre) and contains two absorption beds [PRSs 21-017(a and b)] that were used for subsurface disposal of radioactively contaminated liquid wastes from 1948 to 1968 from DP East operations. PRS 21-017(c) is a sump located between the two beds. The two beds have a surface area of approximately 167 m^2 (1800 ft^2) with an estimated volume of about 510 m^3 (18,000 ft^3). Historical records for MDA U are lacking, however it is known that the primary contaminant released was ^{210}Po (half-life 138.4 days) and that about 2.5 Ci of ^{227}Ac were discharged to the beds in 1953 (Christenson 1973, ER ID?). A handwritten note (cited in the work plan) reads, "12/17/85 Purtymun states that liquid effluent used to run down into the canyon and pond in a swampy area there." Source: LANL 1991, ER ID 7529, p. 16-199).

PRS 21-018(a) – MDA V

MDA V covers an area of 3,561 m^2 (0.88 acre) and contains three absorption beds that occupy 1,390 m^2 (15,000 ft^2) and a volume of 4,250 m^3 (150,000 ft^3). The beds were used for liquid waste disposal from a laundry operation (TA-21-20 [PRS 21-018(b)] and were in continuous use from October 1945 to 1961. The laundry handled all known and "suspect"

contaminated clothing. The average discharge of laundry waste to MDA V during the operating period was 22,710 to 30,280 liters (6,000-8,000 gal) per day. 7.57 million liter per year (2 million gal per year), or about 151.4 million liter (40 million gal) over the used history (Abrahams 1962, cited in work plan). There are no records of tritium being disposed into MDA V.

Christenson 1973 (ER ID?) estimates a total of 9.82 Ci of Pu (mostly ^{239}Pu) was released to MDAs T and V between 1945 and 1951, but does not differentiate the quantity released to each MDA. An additional 0.035 Ci of Pu was released to MDA V between 1952 and 1961. Between 1945 and 1961, 0.35 Ci of ^{89}Sr, 0.034 Ci of ^{90}Sr-^{90}Y, and 2.93 Ci of ^{140}Ba-^{140}La were released to MDA V. In addition, estimated quantities of nuclides (tritium, ^{89}Sr, ^{90}Sr,and Pu in Ci) released to Acid, DP, Mortandad, and Ten Site Canyons from 1945 to 1972 are provided, however the estimates represent totals released to the canyons as a whole and do not differentiate releases to each canyon.

TA-21 Outfalls

PRS 21-022(h) – Acid Waste Lines and Sump/Outfall – NPDES 03A032 – currently discharges treated cooling water; previously discharged industrial wastewater and received discharge from the basemen floor and roof drains of Building TA-21-150 (plutonium fuel service building). Discharges at edge of Los Alamos Canyon. 1992 RFI soil samples from discharge area below outfall indicate the following radionuclides to be present (max concentrations) at three locations in the 0-6 in. interval: ^{241}Am (1.41 pCi/g), tritium (75.2 (nCi/L), ^{238}Pu (14.77 pCi/g), and $^{239/240}$Pu (14.77 pCi/g). No effluent volumes reported.

PRS 21-023(c) – Decommissioned Septic System - served Building TA-21-33 (waste treatment laboratory where research into recovery of plutonium from liquid process wastes was performed) from 1948 to 1965. Outfall discharged either to mesa top or directly into Los Alamos Canyon south of TA-21-33.1988 soil sampling at outfall identified $^{239/240}$Pu and tritium. Other potential contaminants include organic solvents, nitrates, chlorides, mercury, americium, thorium, cobalt, uranium, and zirconium. 1992 RFI soil samples from discharge area below outfall indicate the following radionuclides to be present (max concentrations) at multiple locations at the 0-6 in. interval: ^{241}Am (344 pCi/g), ^{238}Pu (1.8 pCi/g), $^{239/240}$Pu (260 pCi/g), ^{90}Sr (0.9pCi/g), and total U (8.6 ppm). 1988 soil sample data indicating similar concentrations are reported in the *Phase Report 1C, TA-21 Operable Unit RCRA Facility Investigation: Outfalls Investigation*, (LANL 1994, ER ID?, Chp 7). No effluent volumes reported.

PRS 21-024(a) – Inactive Septic System and Outfall - routed sewage from Building TA-21-9 (old steam plant) through a concrete septic tank (abandoned in place) to the surface on the north rim of Los Alamos Canyon from approximately the 1940s until 1966. May have released fuel oil from the boiler and blowdown constituents such as sulfite and copper salts. Liquid wastes from the old steam plant may have contained elevated concentrations of cadmium, chromium, copper iron, lead, nickel, and zinc. The following constituents (max concentrations) were detected in 1992 RFI soil samples collected below the outfall from a variety of locations and primarily from the 0-6in. interval: ^{90}Sr (0.9 pCi/g), total U (22.2 ppm), As (7.5 ug/g), Ca (20,100 ug/g), Cd (4.5 ug/g), Cu (424 ug/g), Cr (31.8 ug/g), Fe (24,000 ug/g), Ni (73.6 ug/g), Pb (204 (ug/g), Sr (265 ug/g), and Zn (362 ug/g). No effluent volumes reported.

PRS 21-024(b) – Inactive Septic System and Outfall – routed sewage from Building TA-21-17 (removed in 1969) through a concrete septic tank to a discharge point on the surface south of Building TA-21-5 near the rim of Los Alamos Canyon from approximately the 1940s until 1969. The following constituents (max concentrations) were detected in 1992 RFI soil samples collected below the outfall from three locations and primarily from the 0-6in. interval: ^{241}Am (15.06 pCi/g), tritium (37 nCi/L), $^{239/240}$Pu (324 pCi/g), total U (21 ppm), As (3.8 ug/g), Cr (27.1 ug/g), Ni (24.3 ug/g), Se (0.72 ug/g), and Zn (246 ug/g). 1988 soil sample data indicating similar concentrations are reported in the *Phase Report 1C, TA-21 Operable Unit RCRA Facility Investigation: Outfalls Investigation*, (LANL 1994, ER ID?, Chp 8). No effluent volumes reported.

PRS 21-024(c) – Inactive Septic System and Outfall – routed sewage from TA-21-54 (removed in 1969) through a concrete septic tank and discharged to the surface on the north rim of Los Alamos Canyon from approximately the 1940s until

1966 (tank abandoned in place). The following constituents (max concentrations) were detected in 1992 RFI soil samples collected below the outfall from two locations at the 0-6 in. interval: ^{241}Am (3.24 pCi/g), tritium (7100 nCi/L), $^{239/240}$Pu (13.23 pCi/g), total U (195.5 ppm), ^{90}Sr (0.9 pCi/g), Ag (105 ug/g), As (8.2 ug/g), Cd (3.8 ug/g), Cr (415 ug/g), Cu (1520 ug/g), Ni (43.7 ug/g), Pb (2300 ug/g), and V (53.6 ug/g). 1988 soil sample data indicating similar concentrations are reported in the *Phase Report IC, TA-21 Operable Unit RCRA Facility Investigation: Outfalls Investigation*, (LANL 1994, ER ID?, Chp 8). No effluent volumes reported.

PRS 21-024(d) – Inactive Septic System and Outfall – routed sewage from TA-21-1 (removed in 1965) through concrete septic systems to a discharge point at the cliff on the north rim of Los Alamos Canyon from approximately the 1940s until 1965. The following constituents (max concentrations) were detected in 1992 RFI soil samples collected below the outfall from two locations and primarily from the 0-6 in. interval: ^{241}Am (0.958 pCi/g), tritium (520 nCi/L), $^{239/240}$Pu (33.8 pCi/g), total U (8 ppm), Ag (19.4 ug/g), and Pb (146 ug/g). 1988 soil sample data indicating similar concentrations are reported in the *Phase Report IC, TA-21 Operable Unit RCRA Facility Investigation: Outfalls Investigation*, (LANL 1994, ER ID?, Chp 8). No effluent volumes reported.

PRS 21-024(e) – Inactive Septic System and Outfall – routed sewage from TA-21-20 (contaminated laundry facility removed in 1965) through a steel tank to a discharge point 20 ft from the rim of Los Alamos Canyon from approximately the 1940s until 1965. The septic tank and outfall are located south of MDA V (laundry waste absorption beds). The following constituents (max concentrations) were detected in 1992 RFI soil samples collected below the outfall from two locations at the 0-6 in. interval: ^{241}Am (1.53 pCi/g), tritium (41.7 nCi/L), $^{239/240}$Pu (41.49 pCi/g), total U (37.7 ppm), As (6.6 ug/g), Cd (8.4 ug/g), Cr (31 ug/g), Pb (92.6 ug/g), V (50.3 ug/g) and Zn (275 ug/g). 1988 soil sample data indicating similar concentrations are reported in the *Phase Report IC, TA-21 Operable Unit RCRA Facility Investigation: Outfalls Investigation*, (LANL 1994, ER ID?, Chp 8). No effluent volumes reported.

PRS 21-024(f) – Inactive Septic System and Outfall – routed sewage from TA-21-45 (Safety Training Building, now removed) through a steel septic tank to the surface on the north rim of DP Mesa into DP Canyon from approximately the 1940s until approximately 1965. The following constituents (max concentrations) were detected in 1992 RFI soil samples collected below the outfall from two locations at the 0-6 in. interval: ^{241}Am (0.62 pCi/g), $^{239/240}$Pu (13.9 pCi/g), ^{90}Sr (0.736 pCi/g), Cd (1.6 ug/g), and Cr (21 ug/g). 1988 soil sample data indicating similar concentrations are reported in the *Phase Report IC, TA-21 Operable Unit RCRA Facility Investigation: Outfalls Investigation*, (LANL 1994, ER ID?, Chp 8). No effluent volumes reported.

PRS 21-024(g) – Inactive Septic System and Outfall – routed sewage from TA-21-71 (warehouse) and TA-21-31 (electronics shop) through a concrete septic tank (abandoned in place) to the surface on the north rim of DP Canyon from approximately the 1940s until 1966. The following constituents (max concentrations) were detected in 1992 RFI soil samples collected below the outfall from four locations and primarily from the 0-6 in. interval: ^{241}Am (0.551 pCi/g), tritium (792.7 nCi/L), ^{238}Pu (0.508 pCi/g), $^{239/240}$Pu (19.4 pCi/g), ^{90}Sr (0.9 pCi/g), total U (20 ppm), As (10 ug/g), Cd (5.6 ug/g), Cr (32.3 ug/g), Cu (59.3 ug/g), Mn (503 ug/g), Ni (19.5 ug/g), Pb (73.6 ug/g), Se (0.83 ug/g), V (52.1 ug/g) and Zn (399 ug/g). 1988 soil sample data indicating similar concentrations are reported in the *Phase Report IC, TA-21 Operable Unit RCRA Facility Investigation: Outfalls Investigation*, (LANL 1994, ER ID?, Chp 8). No effluent volumes reported.

PRS 21-024(h) – Inactive Septic System and Outfall – routed sewage from TA-21-151 through septic tank TA-21-163 (abandoned in place) to the surface on the north rim of DP Mesa into DP Canyon from approximately the 1940s until 1966. The following constituents (max concentrations) were detected in 1992 RFI soil samples collected below the outfall from three locations and primarily from the 0-6 in. interval: ^{241}Am (0.677 pCi/g), ^{239}Pu (33 pCi/g), total U (38 ppm), and ^{228}Th (2.87). 1988 soil sample data indicating similar and lower concentrations are reported in the *Phase Report IC, TA-21 Operable Unit RCRA Facility Investigation: Outfalls Investigation*, (LANL 1994, ER ID?, Chp 8). No effluent volumes reported.

PRS 21-024(i) – Inactive Septic System and Outfall – routed sewage from TA-21-152 through a concrete septic tank (abandoned in place) to the surface outside of TA-21-109 near the rim of Los Alamos Canyon from approximately the 1940s until 1965. Cooling tower blowdown was also routed to this outfall [see PRS 21-027(h)]. Previous activities indi-

cate that the outfall may contain low levels of laboratory organics and inorganics due to research that was conducted at TA-21-152. The following constituents (max concentrations) were detected in 1992 RFI soil samples collected below the outfall from three locations and primarily from the 0-6 in. interval: ^{241}Am (1.54 pCi/g), tritium (4200 nCi/L), ^{90}Sr (1 pCi/g), total U (40.4 ppm), As (34.7 ug/g), Ba (1733.4), Cr (157.4 ug/g), Cu (71 ug/g), Ni (34.8 ug/g), Pb (299.4 ug/g), Se (1.28 ug/g), V (127 ug/g) and Zn (1220.5 ug/g). 1988 soil sample data indicating similar concentrations (exception: tritium detected at 13,000 nCi/L) are reported in the *Phase Report 1C, TA-21 Operable Unit RCRA Facility Investigation: Outfalls Investigation*, (LANL 1994, ER ID?, Chp 8). No effluent volumes reported.

PRS 21-024(j) – Inactive Septic System – served TA-21-155 (warehouse/laboratory) from 1961 to 1966. It is not known where (or if) the septic tank discharged overflow to the environment. The function and operation of the laboratory in TA-21-155 is reported as "not determined". Potential contaminants include radionuclides, organics, metals and inorganic lab chemicals. Boreholes were drilled and sampled in 1993, however the data was not received in time for inclusion in the *Phase Report 1C, TA-21 Operable Unit RCRA Facility Investigation: Outfalls Investigation*, (LANL 1994, ER ID?), therefore no data is reported.

PRS 21-024(k) – Inactive Septic System and Outfall – 21-024(k) consists of tank TA-21-194 associated drain lines and a leachfield that routed sewage from TA-21-209 (high-temperature chemistry building) from approximately the 1940s until 1966. The leachfield was located near the mesa edge above Los Alamos Canyon. Potential contaminants include radionuclides, organics, metals and common laboratory chemicals. Boreholes were drilled and sampled in 1993, however the data was not received in time for inclusion in the *Phase Report 1C, TA-21 Operable Unit RCRA Facility Investigation: Outfalls Investigation*, (LANL 1994, ER ID?), therefore no data is reported.

PRS 21-024(l) – Floor Drain and Outfall – received liquid waste from the floor drain of the mechanical room in TA-21-21, which was formerly used as a vault that stored plutonium and uranium metals. The outfall line ran north toward DP Canyon. 1992 RFI soil sampling detected ^{238}Pu to be present above background at only one of six locations below the outfall. 238Pu was detected at a concentration of 12.1 pCi/g at the 0-6 in. interval. A soil sample was collected in 1988 at a location that may not represent the outfall; the data area reported in *Phase Report 1C, TA-21 Operable Unit RCRA Facility Investigation: Outfalls Investigation*, (LANL 1994, ER ID?, Chp 8). No effluent volumes reported.

PRS 21-024(m) – Outfall – exits TA-21-209 (high-temperature chemistry lab). No additional historical/operational information reported. Shares common drainage with PRS 21-027(b); see summary for PRS 21-027(b).

PRS 21-024(n) – Drain and Outfall – received liquid wastes from a drain exiting TA-21-155 (warehouse/laboratory) and discharges northward into DP Canyon. No historical/operational information reported. The following constituents (max concentrations) were detected in 1992 RFI soil samples collected below the outfall from three locations and primarily from the 0-6 in. interval: tritium (14.9 nCi/L), total U (8.8 ppm), and Cr (37.2 ug/g). 1988 soil sample data indicating similar concentrations (exception: tritium detected at 53 nCi/L) are reported in the *Phase Report 1C, TA-21 Operable Unit RCRA Facility Investigation: Outfalls Investigation*, (LANL 1994, ER ID?, Chp 8). No effluent volumes reported.

PRS 21-024(o) – Drain and Outfall – served TA-21-46 (old diesel plant which was converted to a warehouse between 1957 and 1964) and discharges south into Los Alamos Canyon. Additional historical information (e.g., operation dates) not reported. The following SVOC constituents (max concentrations) were detected in 1992 RFI soil samples collected below the outfall from two locations and primarily from the 0-6 in. interval: benzo(b)fluoranthene (580 ug/g), benzoic acid (2450 ug/g), diethyl phthalate (19,000 ug/g), fluoranthene (500 ug/g), phenanthrene (410 ug/g), phenol (1100 ug/g), and pyrene (580 ug/g). 1988 soil sample data indicating low concentrations of inorganics and radionuclides are reported in the *Phase Report 1C, TA-21 Operable Unit RCRA Facility Investigation: Outfalls Investigation*, (LANL 1994, ER ID?, Chp 8). No effluent volumes reported.

PRS 21-026(d) – Wastewater Treatment Plant Outfall – The Eastern Sewage Treatment Plant [PRS 21-026(a)] began operating in 1966 and replaced septic tank/filter field and septic tank/surface discharge systems throughout TA-21. The outfall receives liquid wastes from the sewage treatment plant TA-21-227. The plant treats sanitary wastes and cooling water from TA-21 facilities and has also received water from decontamination activities, janitor's scrub water, and waste from other operations. The outfall is currently permitted as NPDES SSS05S and discharges into DP Canyon. Treatment was designed for sanitary wastes and would not remove tritium or other radionuclides. Flow data from October 1978 through

June 1990 and gross alpha, gross beta, gross gamma, and tritium data for plant effluent from June 1976 through December 1989 are presented in Nyhan 1990 (ER ID 12605) and are located in Excel file LA-DP Effluent Discharge Records.xls.

Additional information on the Eastern Sewage Treatment Plant from Chapter VI in Purtymun 1975 (ER ID 11787):

Eastern Sewage Treatment Plant –The sewage treatment plant treats and releases about 30 x 10^3 m^3 of effluent per year. The plant services the facilities at TA-21 and enters the canyon between sampling stations DPS-3 and DPS-4. Chemical and radionuclide (gross α, gross β, ^{238}Pu, ^{239}Pu, ^{241}Am, ^{226}Ra, tritium) analyses of sewage effluent are available.

The following constituents (max concentrations) were detected in 1992 RFI soil samples collected below the outfall from four locations and primarily from the 0-6 in. interval: ^{241}Am (1.39 pCi/g), tritium (108.4 nCi/L), $^{239/240}$Pu (2.48 pCi/g), Ag (3.5 ug/g), Cd (1.4 ug/g), Cr (182 ug/g), Cu (41.1 ug/g), Ni (127 ug/g), and Zn (148 ug/g). Additionally, many SVOCs were detected at low concentrations representative of nearby asphalt paved areas and are reported in the *Phase Report IC, TA-21 Operable Unit RCRA Facility Investigation: Outfalls Investigation*, (LANL 1994, ER ID?, Chp 8).

PRS 21-027(a) – Surface Discharge – receives liquid wastes from floor drains in room 3A of TA-21-3 that discharge into a ponding area that also received NPDES permitted discharges (03A031) of treated cooling water from cooling tower TA-21-143. Combined effluents collected in the ponding area are routed via a CMP to the mesa edge above Los Alamos Canyon. Additional historical information (e.g., operational dates) not reported. The following constituents (max concentrations) were detected in 1992 RFI soil samples collected below the outfall from 13 locations at the 0-6 in. interval (most constituents were detected at the majority of the 13 sample locations): ^{241}Am (15.82 pCi/g), tritium (2300 nCi/L), ^{238}Pu (25.23 pCi/g), $^{239/240}$Pu (193 pCi/g), total U (231.5 ppm), As (6.9 ug/g), Cd (4.2 ug/g), Cr (1000.4 ug/g), Cu(198 ug/g), Ni (42.3 ug/g), Pb (73 ug/g), and Zn (826.3 ug/g). 1988 soil sample data and DOE Environmental Problem 19 analytical data indicating similar concentrations are reported in the *Phase Report IC, TA-21 Operable Unit RCRA Facility Investigation: Outfalls Investigation*, (LANL 1994, ER ID?, Chp 8). Effluent volume reported as 325,000 gpy in 1971 per Miller 1971 (ER ID 3853).

PRS 21-027(b) – Outfalls – consists of two outfalls: active NPDES 03A034 which discharges treated cooling water from cooling towers 166 and 167 [these towers formerly discharged through the drain line for PRS 21-024(l); and an outfall which apparently received discharges from a cooling tower associated with TA-21-152 (this outfall may have been a NPDES outfall which has been eliminated). Shares a common drainage with PRS 21-024(m); these two PRSs were investigated concurrently. 1992 RFI soil samples indicate no constituents present above background. Effluent volume for outfall from cooling tower TA-21-166 reported as 42,600 gpy in 1971; effluent volume for outfall from cooling tower TA-21-167 reported as 36,500 gpy in 1971; effluent volume for outfall from cooling tower TA-21-152 reported as 16,700 gpy in 1971 per Miller 1971 (ER ID 3853).

PRS 21-027(d) – Outfall – originated in a stormwater catch basin around a fuel tank (TA-21-47) and discharged via a steel drain line toward Los Alamos Canyon from approximately the 1940s until 1965. The following constituents (max concentrations) were detected in 1992 RFI soil samples collected below the outfall from 3 locations at the 0-6 in.: ^{241}Am (0.16 pCi/g), $^{239/240}$Pu (4.6 pCi/g), and Cd (1.4 ug/g). No effluent volumes reported.

NPDES Outfalls Not Identified as PRSs
These are outfalls located at TA-21 that have not been identified as PRSs; no previous data reported in work plan (LANL 1991, ER ID 7529) (except 02A129) and these outfalls are not addressed in the TA-21 *Operable Unit* RFI Phase Report 1 (LANL 1994, ER ID?). Summaries below address potential contaminant discharges prior to permitting and are from the *TA-21 Operable Unit RFI Work Plan* (LANL 1991, ER ID 7529) Chapter 15.10 - NPDES Outfalls

NPDES Outfall 02A129 – discharges boiler blowdown from the stream plant (TA-21-357) into a channel on DP Mesa that carries effluent into Los Alamos Canyon. Effluent potentially contaminated with fuel oil from the boiler and common blowdown constituents, such as sulfite and copper salts in addition to the plutonium, tritium, and uranium identified in 1988 samples. 1988 outfall reconnaissance sampling indicated the presence of the following constituents (max concentrations): ^{137}Cs (0.4 pCi/g), ^{239}Pu (0.2 pCi/g), ^{226}Ra (1.6 pCi/g), ^{90}Sr (0.2 pCi/g), ^{232}Th (1.5 pCi/g), tritium (8 pCi/mL),

^{234}U (1.0 pCi/g), and ^{238}U (1.0 pCi/g).
No effluent volumes reported.

NPDES Outfall 03A035 – discharges treated cooling water from tower TA-21-210 southward toward Los Alamos Canyon. The discharge point is on the mesa top and mostly infiltrates before reaching the mesa edge. Potential contaminants include plutonium, uranium, metals, and organic and inorganic lab chemicals due to association with the plutonium research support building. Flow rate data is given in the work plan as <1 gal/min.

NPDES Outfall 03A036 – discharges treated cooling water from tower TA-21-220 northward into DP Canyon. No information is available to support selection of a source term. Effluent volume reported as 910,000 gpy in 1971 per Miller 1971 (ER ID 3853).

NPDES Outfall 03A037 – runs south from the corridor (TA-21-314) between TA-21-3 and TA-21-4 and discharges at the south rim of DP Mesa into Los Alamos Canyon. Potential source term for this outfall includes plutonium, uranium, mercury, lead, and organic solvents, because it is connected to a corridor that is associated with plutonium processing. No effluent volumes reported.

NPDES Outfall 04A142 – discharges non-contact cooling water from TA-21-149 (the corridor between TA-21-5 and TA-21-150) to the south edge of DP Mesa with effluent running over the rim into Los Alamos Canyon. Potential contaminants include plutonium, uranium, mercury, lead, and organics due to connection with a corridor associated with plutonium processing.

TA-53 LANSCE
The following summaries are from the *RFI Work Plan for Operable Unit 1100* (LANL 1994, ER ID 34756) Chapters 2, 5, and 6 - Outfalls

PRS 53-002(a and b) – Three surface impoundments –North impoundments (2) operated from early 1970s until 1993. Both are bentonite clay lined and each has a liquid storage capacity of 1.6 million gal. Originally planned as retention impoundments for sanitary, industrial, and radioactive wastewaters. They were frequently filled to capacity and had to be discharged. The system was designed to operate in batch mode, discharging 2 to 3 times per year to NPDES outfall 09S (permit issued in 1978), however discharges were more frequent (nearly continuous). An unlined rock ditch served as an overflow system that would have discharged to Sandia Canyon; it is unknown whether discharges to this ditch occurred. The south impoundment was built in 1985 to accommodate excess wastewater from the northern impoundments and operated as such until 1989; from 1985 to 1989 releases to the NPDES outfall from the northern impoundments were reduced from continuous releases to releases every 4 to 6 months. The south impoundment has a 36-mil Hypalon liner and a liquid storage capacity of 2.5 million gal. In 1989, the southern impoundment became a total-retention radioactive liquid waste storage impoundment and the northern impoundments began to receive only sanitary wastes. From 1989 to 1993, discharges from the northern impoundments were continuous. The northern impoundments were taken out of service in 1993; the southern impoundment is still active and receives radioactive liquid waste (as of June 1998; was scheduled to stop receiving radioactive liquid waste by late 1998). The southern impoundment was designed as a retention impoundment, however an overflow system was installed in the event that water reached high levels; the overflow pipe was locked and tagged out in 1989 because discharges would not be covered by the permit and discharges never took place. Facility personnel report that overflows from the southern impoundment have not occurred.

Discharge records are available for October 1978 through January 1993 and simple summation of the records show that a minimum of 60 million gallons of effluent was discharged into the outfall during this time period. The discharge records in the table below are also located in Excel file LA-DP Effluent Discharge Records.xls as reported in LANL 1998 (ER ID 58841). Chemical composition of the discharge is limited to the required permit parameters of pH, TSS, and BOD.

Average Monthly Discharge (Millions of Gallons Per Day) From TA-53 Northern Surface Impoundments PRS 53-002(a)

Year	JAN	FEB	MAR	APR	MAY	JUN	JUL	AUG	SEP	OCT	NOV	DEC
1978	NI	NI	NI	NI	NI	NI	NI	NI	NI	0.009	0.03	0.02
1979	0.016	0.02	0.018	0.01	0.0144	0.013	0.0068	0.0121	0.0033	0.006	0.014	0.0192
1980	0.0187	0.02	0.013	0.013	0.0095	0.00049	0.0035	0.0114	0.0164	0.0185	0.0212	0.0269
1981	0.0206	0.0216	0.0195	0.0149	0.0086	0.0032	0.0142	0.0196	0.0222	0.0187	0.0214	0.0259
1982	0.0241	0.0264	0.0169	0.0162	0.0168	0.0159	0.0125	0.0211	0.0189	0.0152	0.0207	0.0298
1983	0.0258	0.0224	0.0167	0.0086	0.00132	0.0075	0.0046	0.0134	0.0071	0.0168	0.0132	0.0159
1984	0.0193	0.0154	0.0165	0.0078	0.0075	0.0007	0.0058	0.0159	0.0116	0.0232	0.013	0.0162
1985	0.0153	0.0153	0.0154	0.0133	0.0083	0.0072	0.0049	0.0104	0	0	0	0
1986	0	0	0	0	0	0	0.0124	0	0	0	0.0066	0.0045
1987	0.0075	0.009	0.0207	0.0008	0	0	0	0	0	0	0	0
1988	0	0	0.0129	0.0009	0.0095	0	0	0	0	0	0	0.0106
1989	0.0106	0.042	0.0535	0	0	0	0	0	0	0	0	0
1990	0.031	0.053	0.0544	0.0058	0.0326	0	0	0	0	0	0.0429	0
1991	0.0142	0.0912	0.0284	0	0	0	0.039	0.0199	0.0009	0	0	0
1992	0.0073	0.0184	0.0068	0.0065	0.0065	0.008	0.0028	0.0062	0.0057	0.0029	0.0063	0.0081
1993	0.0102	ND	ND	ND	ND	ND	ND	ND	ND	ND	ND	ND

NI – No information available for discharges prior to October 1978

ND – No discharge; discharge from the impoundments was stopped on February 1, 1993.

Source: LANL 1998, ER ID 58841, Appendix D

The liquid and sludge from the two northern impoundments was sampled during four separate events in 1988 (DOE), 1991 (EM-8), 1992 (EM-8), and 1994/1995 (ER). Trace quantities of VOCs, low concentrations of SVOCs, and the following metals (max concentrations) were detected in the sludge samples from 1988, 1991, and 1992: Ag (5.1 mg/kg), As (4.8 mg/kg), Ba (52.4 mg/kg), Cd (3.1 mg/kg), Cr (17.7 mg/kg), Cu (303 mg/kg), Hg (1.1 mg/kg), Pb (44.8 mg/kg), Se (6.8 mg/kg), and Zn (578 mg/kg). Metals (max concentrations) detected in the water samples collected in 1991 and 1992 are: Ag (23 µg/L), As (6.8 µg/L), Ba (80 µg/L), Cd (4.5 µg/L), Cr (5.8 µg/L), Pb (3.1 µg/L), and Se (4.5 µg/L). The highest concentrations of radionuclides detected in sludge are present in the samples collected in 1988, the last year that the northern impoundments received industrial and radioactive liquid wastes. The highest concentrations were generally present in the sample collected in the northwestern impoundment near the influent pipe, where the initial settling occurred. Radionuclides detected (and ranges) in the 1988 sludge samples are: ^{7}Be (400-14,790 nCi/kg W), ^{109}Cd (1,060 nCi/kg W), ^{57}Co (238-5,740 nCi/kg W), ^{58}Co (43.7-1,610 nCi/kg W), ^{60}Co (61.8-1,060 nCi/kg W), ^{54}Mn (235-3,100 nCi/kg W), ^{56}Mn (15-540 nCi/kg W), ^{83}Rb (46.5-240 nCi/kg W), ^{75}Se (4.3-57.5 nCi/kg W), ^{46}Sc 1.8-5.3 nCi/kg W), ^{110}Ag (2.9-3.0 nCi/kg W), ^{22}Na (7.9-28.6 nCi/kg W), ^{88}Y (0.3-12.3 nCi/kg W), ^{65}Zn (2.5-154 nCi/kg W), and ^{88}Zr (1.1-1.8 nCi/kg W). Radionuclides (max concentrations) detected in water samples collected in 1991 are: ^{7}Be (0.85 nCi/L), ^{57}Co (0.346 nCi/L), ^{58}Co (0.095 nCi/L), ^{60}Co (0.096 nCi/L), ^{134}Cs (0.262 nCi/L), ^{154}Eu (0.99 nCi/L), ^{175}Ha (0.31 nCi/L), ^{54}Mn (0.116 nCi/L), ^{56}Mn (82.5 nCi/L), ^{83}Rb (0.198 nCi/L), and tritium (4.0 nCi/L). In 1992, the only rad sampling was for tritium in water collected from the northern impoundments: 2200 pCi/L in the northwestern impoundment and 5000 pCi/L in the

northeastern impoundment. (LANL 1998, ER ID 58841, Section 2.2.1.2 and Appendix E).

In 1994/1995, samples were collected from the sludge, clay liner, and underlying tuff from 17 locations in each of the northern impoundments and analyzed for metals, radionuclides (alpha and gamma spec, ^{90}Sr, tritium), SVOCs, VOCs, pesticides, herbicides, and PCBs. The northern impoundments were characterized by elevated concentrations of Al, Sb, Ba, Cd, Ca, Cr, Cu, Pb, Mg, Hg, Ni, Se, Ag, Na, Tl, Zn, acetone, PCBs, pesticides, methylene chloride, toluene, trichlorofluoromethane, ^{134}Cs, ^{57}Co, ^{60}Co, ^{54}Mn, ^{237}Np, ^{238}Pu, ^{239}Pu, ^{22}Na, ^{90}Sr and tritium. A detailed data report is presented LANL 1998, ER ID 58841, Appendix F.

In 1991, eight boreholes ranging in depth from 50 to 150 ft were drilled adjacent to the three impoundments to evaluate subsurface saturation and potential leakage. Samples from select intervals from select boreholes were analyzed for gravimetric moisture, tritium, VOC, SVOCs, and metals. Only tritium was detected at depth. The highest concentration of tritium (100nCi/L) was observed in borehole 53-5, located between the three impoundments, at a depth of 80 ft (TD = 100 ft). This borehole location coincides with the location of the unlined overflow ditch that served the northern impoundments prior to 1985 and may have discharged to Sandia Canyon. The other boreholes drilled within 50 ft of the impoundments all had tritium concentrations at depth that ranged from <0.1 to 10 nCi/L. Metals were detected at background concentrations, and VOCs and SVOCs were not detected. Gravimetric moisture content in the 50 ft boreholes (all in Tshirege 2b) was generally highest at depths of 5 to 10 ft (ranging from 8.8 to 20.8%) and showed a decreasing trend with depth. Gravimetric moisture content in borehole 53-5 (TD 100 ft in Tshirege 2a) and borehole 53-6 (located north of borehole 53-5 between the northern impoundments - TD 150 ft in Tshirege 1a) did not show a decreasing trend with depth, but fluctuated from 0% to 20% and measured 6.5% and 14.5% at their respective TDs (LANL 1998, ER ID 58841, Section 2.2.1.2 and Appendix E.

PRS 53-012(a) – Cooling tower outfall – NPDES 03A047 - discharges cooling tower blowdown from tower TA-53-60 into Los Alamos Canyon. Long term average and maximum flow is 4,000 and 13,000 gpd, respectively.

PRS 53-012(b) – Cooling tower outfall – NPDES 03A048 – discharges cooling tower blowdown from tower TA-53-62 into Los Alamos Canyon. Long term average and maximum flow is 22,000 and 112,000 gpd, respectively.

PRS 53-012(c) – Cooling tower outfall – NPDES 03A049 – discharges cooling tower blowdown from tower TA-53-64 and boiler blowdown and drainage from an air compressor via floor drains in the utility room of building TA-53-65 into Los Alamos Canyon. Long term average and maximum flow is 13,000 and 66,000 gpd, respectively.

General Information

Plutonium Isotope Discharges

"The LASL did not discharge any substantial quantities of ^{238}Pu until 1967 (^{239}Pu discharged prior to this date). No routine analyses were made on the differentiation between ^{238}Pu and ^{239}Pu until 1971 at which time about 80% of the plutonium was ^{238}Pu. This ratio had continued to increase until ^{238}Pu is now (written in 1973) about 95% of the total plutonium released." (Christenson, 1973, ER ID?)

NPDES 03A Category "Worst Case" Composite Data

LANL characterized the 03A outfalls as part of the NPDES permit application. The data below represent a composite sample from 36 outfalls (presented as a "worst case" scenario) and may serve as estimate for releases for 03A Category Outfalls.

Concentrations of Constituents in Cooling Tower Outfalls

Constituent	"Worst Case" Concentration (µg/L)
Barium	110
Manganese	50
Antimony	<50
Arsenic	40
Beryllium	<100
Cadmium	4
Chromium	260
Copper	100
Mercury	<0.2
Nickel	280
Selenium	<1
Silver	<10
Thallium	510
Zinc	71
Cyanide	33
Benzene	<5
Bromoform	<5
Carbon tetrachloride	<5
Chlorobenzene	<5
Chlorodibromomethane	<5
Chloroform	<5
Dichlorobromomethane	<5
1,1-Dichloroethane	<5
1,2-Dichloroethane	<5

Constituent	"Worst Case" Concentration (µg/L)
2,4-Dimethylphenol	<10
2,4-Dinitrophenol	<10
p-Chloro-m-methylphenol	<10
Pentachlorophenol	<10
Phenol	<10
2,4,6-Trichlorophenol	<10
Acenaphthene	<10
Anthracene	<10
Benzo(a)pyrene	<10
Bis (2-chloroethyl) ether	<10
Bis (2-chloroisopropyl) ether	<10
Bis (2-ethylhexyl) phthalate	<10
Butylbenzylphthalate	<10
2-Chloronaphthalene	<10
1,2-Dichlorobenzene	<10
Diethylphthalate	<10
Dimethylphthalate	<10
Di-n-butylphthalate	<10
2,4-Dinitrotoluene	<10
2,6-Dinitrotoluene	<10
Di-n-octylphthalate	<10
Fluoranthene	<10
Fluorene	<10
Hexachlorobenzene	<10

1,1-Dichloroethene	<5
1,2-Dichloropropane	<5
1,3-Dichloropropene	<5
Ethylbenzene	<5
Methylbromide	<10
Methylchloride	<10
Methylene chloride	<5
1,1,2,2-Tetrachloroethane	<5
Tetrachloroethylene	<5
Toluene	<5
1,2-trans dichloroethylene	<5
1,1,1-Trichloroethane	<5
1,1,2-Trichloroethane	<5
Trichloroethene	<5
Vinyl chloride	<10
2-Chlorophenol	<10
2,4-Dichlorophenol	<10

Hexachlorocyclopentadiene	<10
Hexachloroethane	<10
Isophorone	<10
Naphthalene	<10
Nitrobenznene	<10
N-Nitroso-di-N-propylamine	<10
N-Nitrosodiphenylamine	<10
Pyrene	<10
1,2,4-Trichloroebenzene	<10
Chlrodane	<0.25
p-p'-DDT	<0.06
p-p'-DDD	<0.08
alpha-Endosulfan	<0.05
beta-Endosulfan	<0.08
PCB-1242	<0.71
PCB-1254	<0.71
PCB-1260	<0.71

Source:. *RFI Work Plan for Operable Unit 1100*, LANL 1994, ER ID?, Table 5-16, p. 5-79.

REFERENCES

no author, no date. "Industrial Liquid Waste Treatment Facility" (No author, no date, ER ID 385)

no author, September 1970. "Standard Operating Procedures Bldg. DP-257 Waste Treatment Plant" (No author 1970, ER ID 422)

Christenson, C.W., November 29, 1972. "Tritium Analyses of Plant Effluent Samples," Los Alamos Scientific Laboratory Memorandum to Dean Meyer (H-1) from C.W. Christenson (H-7), Los Alamos, New Mexico. (Christenson, 1972, ER ID 425)

Christenson, C.W., November 8, 1973. "Nuclide Inventory Data," Los Alamos Scientific Laboratory Memo H7-CWC-437 to Harry Jordan (H-DO) from C.W. Christenson (H-7), Los Alamos, New Mexico. (Christenson 1973, ER ID?)

LANL (Los Alamos National Laboratory), May 1991. "TA-21 Operable Unit RFI Work Plan for Environmental Restoration," Vol. II, Los Alamos National Laboratory Report LA-UR-91-962, Los Alamos, New Mexico. (LANL 1991, ER ID 7529)

LANL (Los Alamos National Laboratory), May 1992. "RFI Work Plan for Operable Unit 1078," Los Alamos National Laboratory Report LA-UR-92-838, Los Alamos, New Mexico. (LANL 1992, ER ID 43454)

LANL (Los Alamos National Laboratory), May 1992. "RFI Work Plan for Operable Unit 1079," Los Alamos National Laboratory Report LA-UR-92-850, Los Alamos, New Mexico. (LANL 1992, ER ID 7668)

LANL (Los Alamos National Laboratory), May 1992. "RFI Work Plan for Operable Unit 1071," Los Alamos National Laboratory Report LA-UR-92-810, Los Alamos, New Mexico. (LANL 1992, ER ID 7667)

LANL (Los Alamos National Laboratory), June 1993. "RFI Work Plan for Operable Unit 1098," Los Alamos National Laboratory Report LA-UR-92-3825, Los Alamos, New Mexico. (LANL 1993, ER ID 21404)

LANL (Los Alamos National Laboratory), February 28, 1994. "Phase Report 1C, TA-21 Operable Unit RCRA Facility Investigation: Outfalls Investigation," Los Alamos National Laboratory Report LA-UR-94-228, Los Alamos, New Mexico. (LANL 1994, ER ID?)

LANL (Los Alamos National Laboratory), May 1994. "RFI Work Plan for Operable Unit 1136," Los Alamos National Laboratory Report LA-UR-94-1244, Los Alamos, New Mexico. (LANL 1994, ER ID ?)

LANL (Los Alamos National Laboratory), May 1994. "RFI Work Plan for Operable Unit 1100," Los Alamos National Laboratory Report LA-UR-94-1097, Los Alamos, New Mexico. (LANL 1994, ER ID 34756)

LANL (Los Alamos National Laboratory), September 10, 1996, "VCA Report for SWMU 0-030(a)", Los Alamos National Laboratory Report LA-UR-96-3203, Los Alamos, New Mexico. (LANL 1996, ER ID?)

LANL (Los Alamos National Laboratory), July 20, 1998, "RFI Report for PRS 0-027", Los Alamos National Laboratory Report ?, Los Alamos, New Mexico. (LANL 1998, ER ID?)

LANL (Los Alamos National Laboratory), June 1998. "RFI Work Plan and SAP for Potential Release Sites 53-002(a) 53-002(b)," Los Alamos National Laboratory Report LA-UR-98-2547, Los Alamos, New Mexico. (LANL 1998, ER ID 58841)

Miller, E.L, July 30, 1971. "Effluent from Plant Cooling Towers," Los Alamos Scientific Laboratory Memorandum to C. Christenson (H-7) from E.L. Miller (ENG-4), Los Alamos, New Mexico. (Miller 1971, ER ID 3853)

Nyhan, J.W., September 28, 1990. "RCRA Facility Investigation Task, SWMU Descriptions and Identifications of Data

Needs: TA-21 Surface Units Aggregate at Los, Alamos, NM," draft report prepared for the Environmental Science Group, Los Alamos National Laboratory, Los Alamos, New Mexico. (Nyhan 1990, ER ID 12605)

Purtymun, W. D., 1975. "Geohydrology of the Pajarito Plateau with Reference to Quality of Water, 1949–1972," Los Alamos Scientific Laboratory Informal Report LA-5744, Los Alamos, New Mexico. (Purtymun 1975, ER ID 11787)

SAIC (Science Applications International Corporation, August 7, 1998, "Radioactive Waste Releases in the TA-21-011(k) Outfall into DP Canyon," Los Alamos, New Mexico. (SAIC, 1998, ER ID 58719)

Whipple, H.O., April 10, 1970. "Radioactive Effluents and Releases," Los Alamos Scientific Laboratory Memorandum to H. Jack Blackwell (LAAO) from H.O. Whipple (H-Division), Los Alamos, New Mexico. (Whipple 1970, ER ID 8750)